Volume II.E

Midwestern Regional Carbon Sequestration Partnership (MRCSP) Phase III (Development Phase)

InSAR Monitoring to Evaluate Surface Changes with CO_2 Storage in a Depleted Oil Field in Northern Michigan

Prepared by:

Battelle
505 King Avenue
Columbus, Ohio 43201

Principal Investigator: Dr. Neeraj Gupta

Authors: Matthew Place, Marie-Josée Banwell, Giacomo Falorni, Neeraj Gupta

Submitted to:

The U.S. Department of Energy, National Energy Technology Laboratory
Program Manager: Andrea McNemar

DOE MRCSP Project #DE-FC26-05NT42589

September 2020

Notice

This report was prepared by Battelle as an account of work sponsored by an agency of the United States Government and other project sponsors, including Core Energy, LLC and The Ohio Development Services Agency. Neither the United States Government, nor any agency thereof, nor any of their employees, nor Battelle and other cosponsors, makes any warranty, express or implied, or assumes any liability or responsibility for the accuracy, completeness, or usefulness of any information, apparatus, product, or process disclosed, or represents that its use would not infringe privately owned rights. Reference herein to any specific commercial product, process, or service by trade name, trademark, manufacturer, or otherwise does not necessarily constitute or imply its endorsement, recommendations, or favoring by the United States Government or any agency thereof. The views and the opinions of authors expressed herein do not necessarily state or reflect those of the United States Government or any agency thereof.

Battelle does not engage in research for advertising, sales promotion, or endorsement of our clients' interests including raising investment capital or recommending investments decisions, or other publicity purposes, or for any use in litigation.

Battelle endeavors at all times to produce work of the highest quality, consistent with our contract commitments. However, because of the research and/or experimental nature of this work the client undertakes the sole responsibility for the consequence of any use or misuse of, or inability to use, any information, apparatus, process or result obtained from Battelle, and Battelle, its employees, officers, or Trustees have no legal liability for the accuracy, adequacy, or efficacy thereof.

Acknowledgements

Sponsorships - This report is part of a series of reports prepared under the Midwestern Regional Carbon Sequestration Partnership (MRCSP) Phase III (Development Phase). This report details the results of the InSAR monitoring activity used to determine the effects of CO_2 injection into the Dover 33 reef on potential deformation of ground surface. The primary funding for the MRCSP program is from the US Department of Energy's National Energy Technology Laboratory (NETL) under DOE project number DE-FC26-05NT42589 with Ms. Andrea McNemar as the DOE project manager. The past DOE project managers for MRCSP include Dawn Deel, and Lynn Brickett.

The large-scale test also received significant in-kind cost share from Core Energy, LLC, who also provided access to the field test site and related data. Overall MRCSP program has also been supported by the Ohio Coal Development Office in the Ohio Development Services Agency under various grants (CDO D-10-7, CDO-D-13-22, CDO-D-D-13-24, and CDO-D-15-08) with Mr. Greg Payne as the OCDO project manager. Finally, a number of industry sponsors and technical team members from State Geological Surveys and universities have supported MRCSP through cash and in-kind contributions over the years.

Program Leadership – During the MRCSP Phase III project period, several Battelle staff and external collaborators contributed to the successful completion of the program through their efforts in field work, geological data analysis and interpretation, and/or reporting. MRCSP principal investigator is Dr. Neeraj Gupta. The project managers have included David Ball, Darrell Paul, Jacqueline Gerst, Caitlin McNeil, and Rebecca Wessinger with support from Andrew Burchwell.

Principal Investigator: Neeraj Gupta (614-424-3820/gupta@battelle.org)

Report Authors and Principal Technical Contributors – Matthew Place (Battelle), Marie-Josée Banwell (TRE Canada), Giacomo Falorni (TRE Canada), Neeraj Gupta (Battelle)

Other Technical Contributors – Vicky Hsiao (TRE Canada), Andrew Higgs (TRE Canada)

Table of Contents

List of Figures

Page

Acronyms and Abbreviations

ACR	Artificial corner reflectors
AOI	Area of interest
BHP	Bottom hole pressure
CCS	Carbon capture and storage
CCUS	Carbon capture, utilization, and storage
CO_2	Carbon dioxide
CSK	COSMO-Skymed
DS	Distributed scatterers
ERS	European Remote Sensing
GIS	Geographic Information System
InSAR	Interferometric Synthetic Aperture Radar
LOS	Line-of-sight
mm	Millimeters
MRCSP	Midwest Regional Carbon Sequestration Program
NETL	National Energy Technology Laboratory
PS	Permanent scatterers
psi	Pounds per square inch
yr	Year

1.0 Background and Objectives

Battelle evaluated the potential use of Interferometric Synthetic Aperture Radar (InSAR) for monitoring the outcome of injected CO_2 at the Dover 33 reef near Gaylord, Michigan. InSAR is a satellite-based technology that provides high-precision information on the movement of ground surface in areas with high radar coherence (e.g., roads, buildings, bare soils). Depending on the setting, this technique may provide a useful tool for characterizing reservoirs by measuring surface deformations from activities such as brine water disposal; production of water, oil, and/or gas; and carbon capture, utilization, and storage (CCUS).

The InSAR data package includes three main sets of data: (1) Geographic Information System (GIS) spatial data including displacement rates, cumulative displacements, and standard deviations); (2) time series graphs of measured points used to calculate displacement rates with linear regressions; and (3) database of shapefiles used to create the maps (Figure 1-1). In addition to the vendor (TRE Canada) supplied data and analysis, Battelle performed its own statistical analysis of the data.

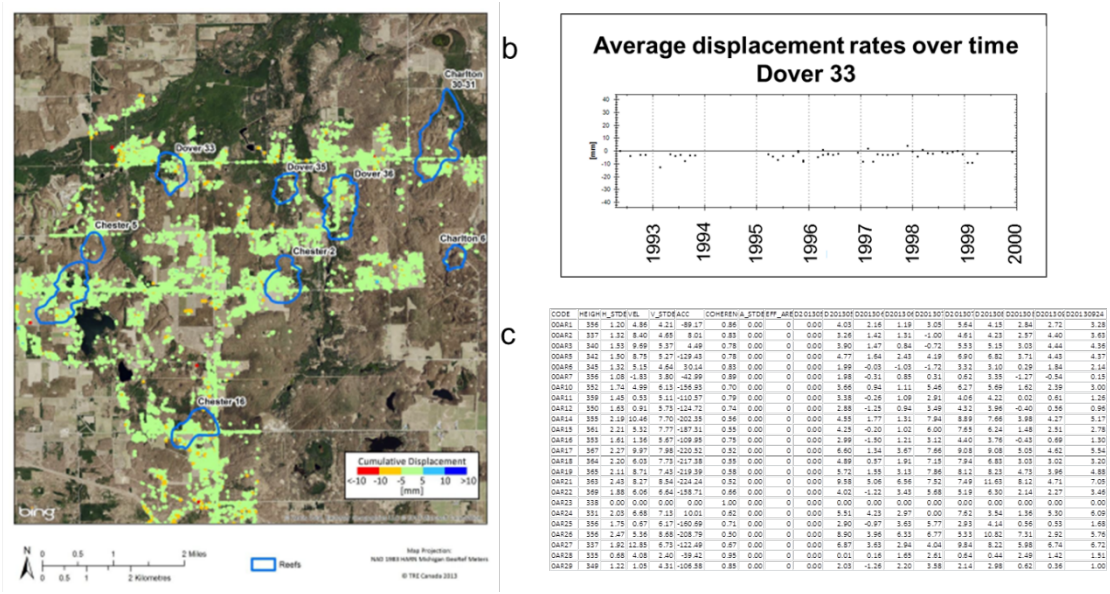

Figure 1-1. InSAR data packages provided by TRE Canada include (a) GIS spatial data, (b) time series graphs of measured points, and (c) Shapefiles used to create the maps.

InSAR technology has been used to monitor small-scale surface-level changes in response to the injection of CO_2 in the subsurface at other carbon sequestration test sites. The most prominent example is the In Salah project in Algeria, in which an injected mass of 3 million tons of carbon dioxide produced a measurable surface displacement of approximately 5 millimeters (mm)/year (yr). Battelle investigated the applicability of InSAR in Northern Michigan, which consists of agricultural areas and forests, to investigate any quantifiable, small-scale, surface-level changes related to the injection of CO_2 into Silurian-age (Niagaran) reef structures.

This research was conducted because remote sensing technologies for monitoring land surface deformation can be a cost-effective method to demonstrate long-term geologic storage security. Where it can be applied, InSAR may become one of the essential methods for monitoring commercial-scale CO_2 injection efforts by providing large-scale snapshots of the surface response to elevated pressure over time, including inaccessible areas. This large-scale test provides a unique opportunity to gain knowledge

and experience in applying InSAR for CCUS monitoring, necessary to build capacity for future commercial-scale deployment.

The attractiveness of InSAR as a monitoring technology stems from:

- Because of InSAR's ability to cover a large area remotely, this technology could be a cost-effective method to demonstrate security;
- The results of this test will add to the collective knowledge about the capabilities of this technology;
- The results will also add to the collective knowledge about the surface responses to CO_2 injection (in this case, the expected surface response was none). The In Salah project case study had a measurable response to injection because there was an unidentified fracture, which was not present here.

Battelle conducted surface deformation monitoring and analysis for the Dover 33 reef to meet the following objectives:

- Contributing to the understanding of the CO_2 migration through the reservoir and how injection operations interact with the rest of the geologic column;
- Assessing technology performance and deploy adaptive methods, such as artificial corner reflectors (ACRs), to address snow coverage, vegetation, topography; and
- Building knowledge and experience in this potentially practical, cost-effective monitoring approach for future commercial-scale applications in similar settings.

2.0 Field Implementation

Deformation monitoring and analysis was performed for the late stage (Dover 33) reef. ACRs were used to monitor local deformation in areas with low radar coherence (e.g., areas with dense vegetation coverage) and to mitigate for snow coverage. InSAR methods work best in environments with low topographic relief, sparse or low-lying vegetation, and minimal changes to the land cover over time. Adaptive methods, such as ACRs can be deployed where these conditions are not met to improve the quality of the data produced. The technical approach of the study included the following major activities:

1. Historical deformation study;
2. Baseline monitoring;
3. ACR layout, construction and installation; and
4. Deformation monitoring and analysis in response to CO_2 injection.

2.1 Historical Deformation Study

The purpose of the historical deformation study was to determine if large-scale ground movements could be detected over an 80 square kilometer (30 square mile) area of interest (AOI) that encompasses the Dover 33 reef and other reefs owned by Core Energy, as well as a nearby natural gas storage field (Figure 2-1). TRE Canada completed the historical study using 60 images collected by the European Space Agency's European Remote Sensing (ERS) satellite between 1992 to 2000. The ERS mission was launched in 1992 and InSAR data was collected until 2000, providing a comprehensive, multiyear record of satellite data. TRE procured and processed the 60 SAR images with its proprietary SqueeSAR algorithm over a period of 6 weeks, with 51 of the 60 satellite images being usable for the analysis. The historical report is included in Appendix A.

The data processing led to a density of 33 measurement points per square mile, which is in the lower range of expected values. This relatively low density was likely caused by the challenging ground conditions, the low quality of the data set, including gaps in imagery, and the low resolution of older satellite imagery. However, the conditions were suitable for the use of advanced processing algorithms such as SqueeSAR to monitor local deformations in areas with high radar coherence (e.g., roads, buildings, bare soils) that provided sources of stable permanent scatterers (PS) and distributed scatterers (DS).

The results obtained from the historical analysis of the ERS imagery were used to measure deformation over the time range of interest and provide an indication of the natural reflectively of the area (Figure 2-1). Each point corresponds to a PS or DS target and is color-coded according to its displacement. Figure 2-1 indicates that most points throughout the AOI displayed little or no displacement over the period of analysis. No significantly strong ground deformation trends were visible (cumulative deformation was within 10 mm) at the majority of targets and an average surface deformation rate of -1.2 ± 0.5 mm/yr was identified for the AOI. The cause of this deformation is unknown but believed to be natural and the result of weather-related events, such as frost heaving and thawing. The line-of-sight (LOS) displacement rates for Dover 33, expressed in millimeters per year (mm/yr), are presented in Figure 2-2, and indicate no apparent differences in deformation between the on- and off-reef points. The low standard deviation of 0.5 mm/yr is due to the large number of images used in the data processing. Displacement values are calculated from a linear regression of the ground movement measured over the entire period covered by the satellite images (Figure 2-3).

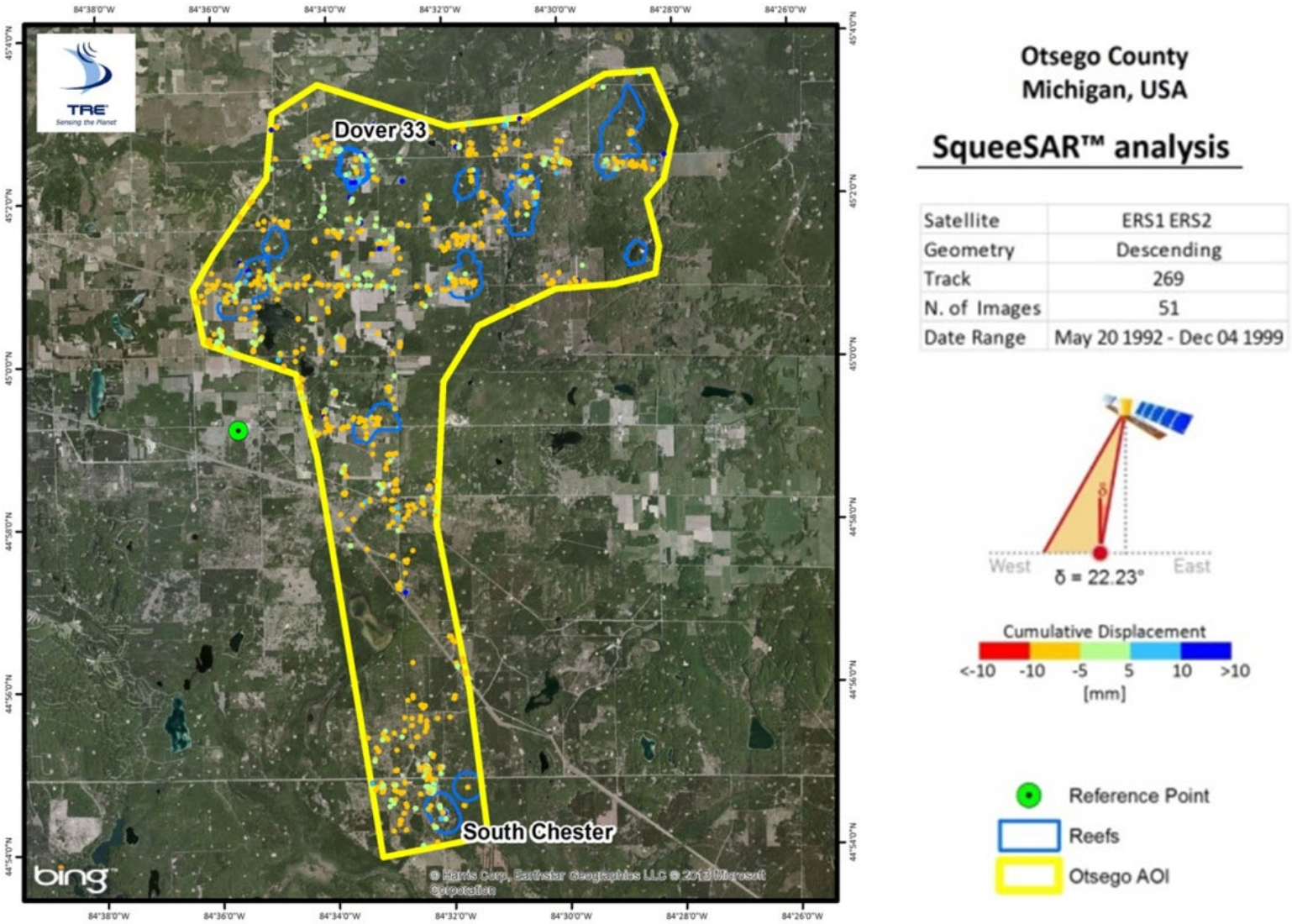

Figure 2-1. Example GIS map showing the AOI, cumulative displacement measured for the AOI using historical satellite imagery from 1992 through 1999. The data displays a relatively low density of measurement points (33 per mi2).

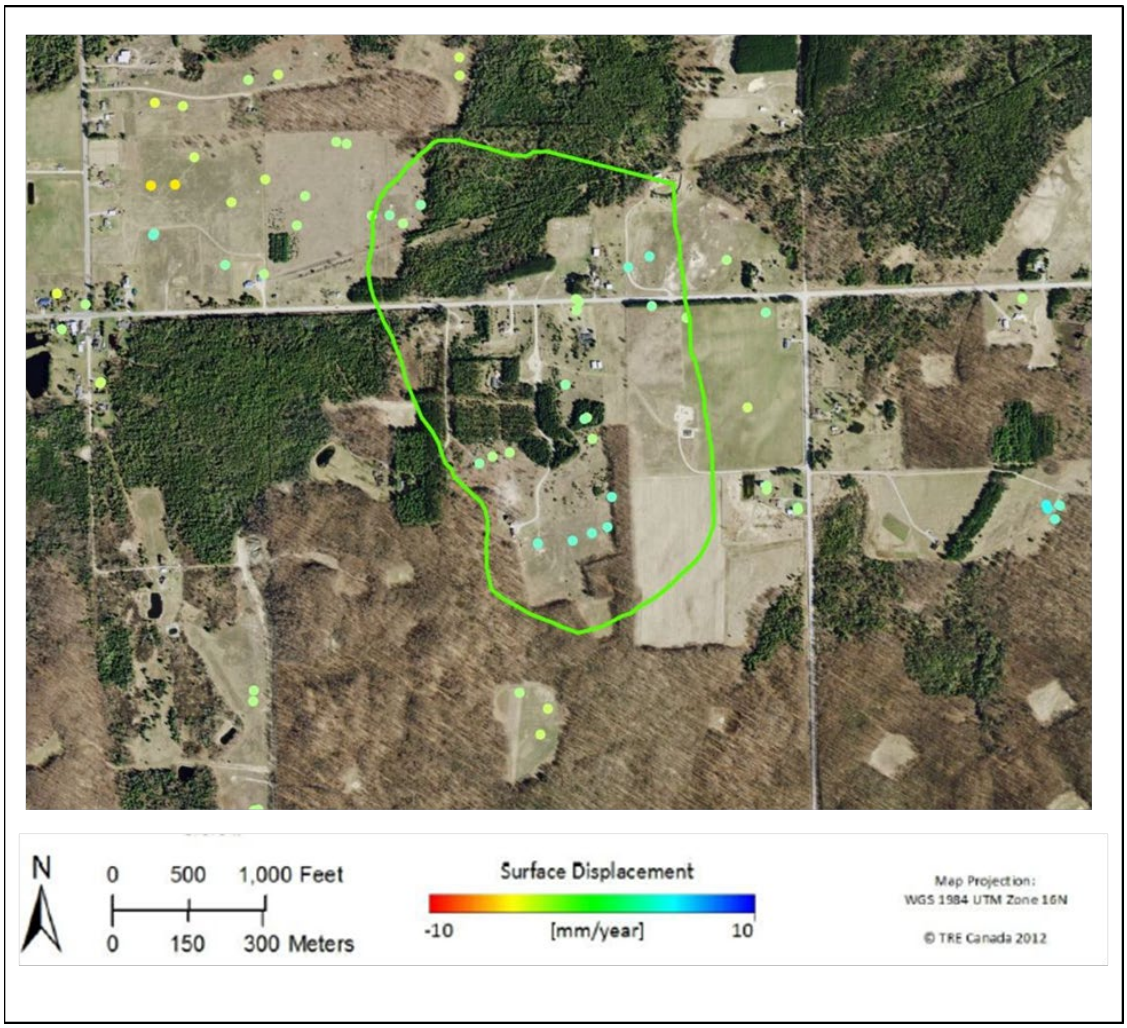

Figure 2-2. Example GIS map showing surface displacement rates in terms of mm/yr during the historical monitoring period for Dover 33.

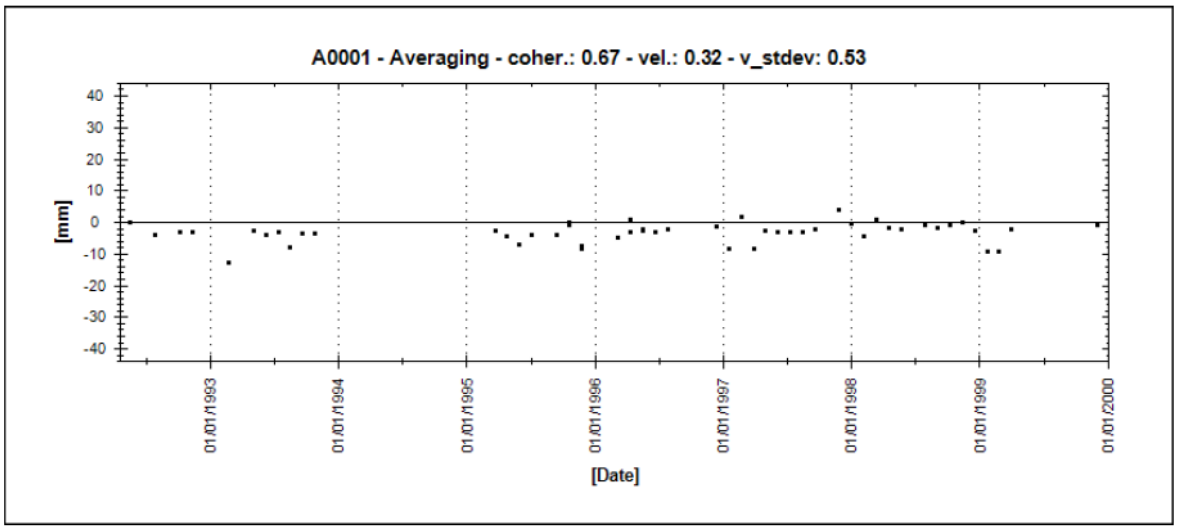

Figure 2-3. Example time series graph averaging all measurement points identified over the Dover 33 reef.

The historical analysis indicated there was a mild seasonal component present over part of this area (typified by the appearance of cyclical deformation patterns). Therefore, it was expected that similar patterns would develop over time for ongoing monitoring after two years of data have been collected. TRE indicated it would be possible to normalize the data for seasonal effects, and any statistically significant movement related to operations could then be isolated. The historical deformation analysis increased confidence in the ability of the technology to assess land surface deformation in this forested and agricultural area.

2.2 Baseline Monitoring

The baseline analysis was conducted on the first six months of radar imagery acquired from the COSMO-Skymed (CSK) constellation of satellites from April 22, 2012 through October 23, 2012. A total of 22 satellite images were obtained (a minimum of 15 images is required to reach a statistical robustness of results). The nature of the terrain, with low wooded slopes, farmed fields, and open areas, provided a reasonable density of natural reflectors. The SqueeSAR processing algorithm provided a density of 545 measurement points per square mile (211 measurement points per square kilometer) (Figure 2-4). Buildings and other man-made structures, as well as natural features such as exposed ground, are likely sources of stable PS and DS targets. The baseline report is included in Appendix B.

The LOS displacement rates for the AOI and Dover 33, expressed in mm/yr, are presented in Figure 2-4 and Figure 2-5. Each point corresponds to a PS or DS target and is color-coded according to its annual rate of movement. Average displacement values are calculated from a linear regression of the ground movement measured over the entire period covered by the satellite images. Figure 2-6 presents an example of a time series plot of the surface deformation over the Dover 33 reef during the baseline monitoring period.

The results indicate the 80 square kilometer AOI is predominantly stable with over 90% of the measurement points showing minimal deformation (displacement less than 5 mm) and an average surface deformation rate of -1.1 mm/yr relative to the reference point, which is outside the AOI. However, there are areas that display mild subsidence. The lower precision compared to the historical analysis is due to the small number of images. A zone of subsidence was observed in the area immediately north of

the South Chester 15 gas storage field (Figure 2-4). Field observations revealed this zone was clear cut of trees just before or during the baseline monitoring period.

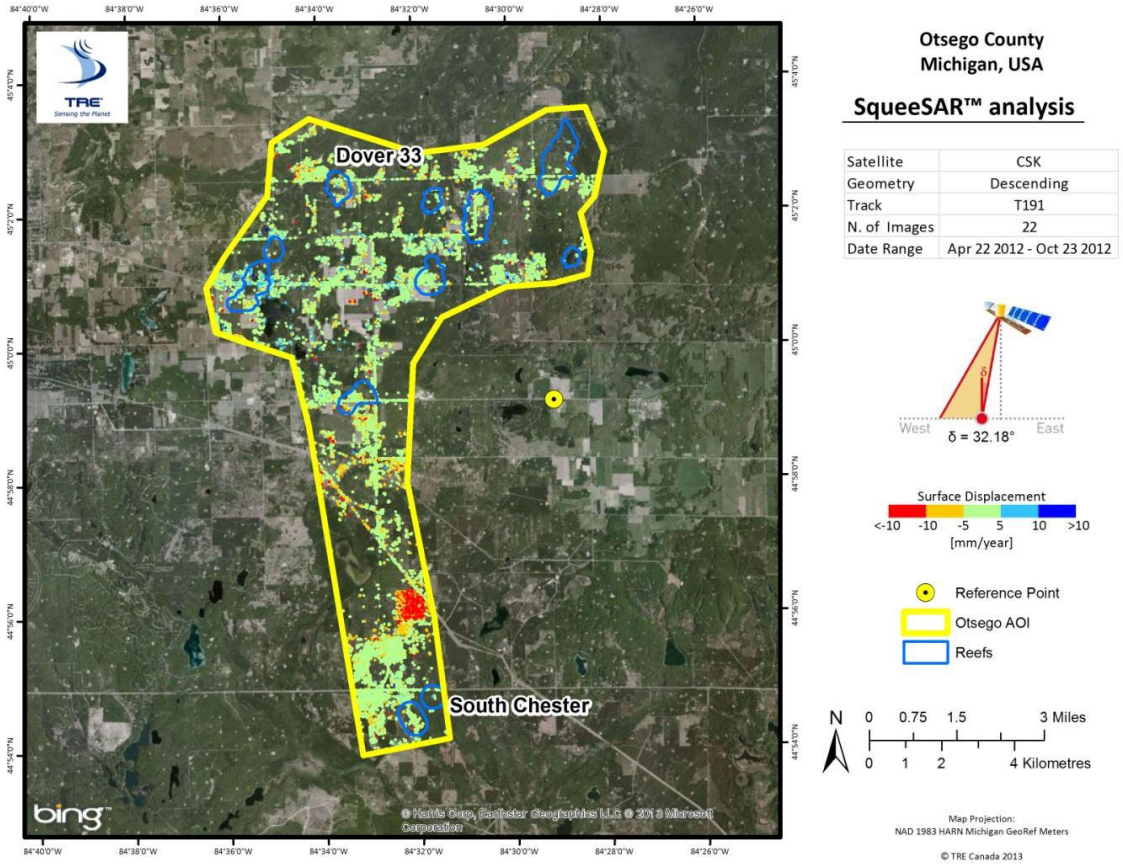

Figure 2-4. Example GIS map showing surface displacement rates in mm/yr during the baseline monitoring period for 80 km² AOI. This figure displays the higher density of measurement points (545 per mi² compared to 33 per mi²) between the baseline and historical monitoring periods.

Baseline displacement results over the Dover 33 reef and surrounding area are presented in Figure 2-5. The baseline monitoring around the Dover 33 reef indicates nearly all of the measurement points remained relatively stable with a cumulative displacement of ±5 mm over the monitoring period. In addition, there does not appear to be a difference in cumulative displacement between measurement points located over the reef compared to measurement points located off the reef. Finally, there does not appear to be a spatial trend to the data (i.e., greater displacement toward the center of the reef and decreasing away from this location). It appears that measurement points with greater displacement are surrounded by points with little to no displacement.

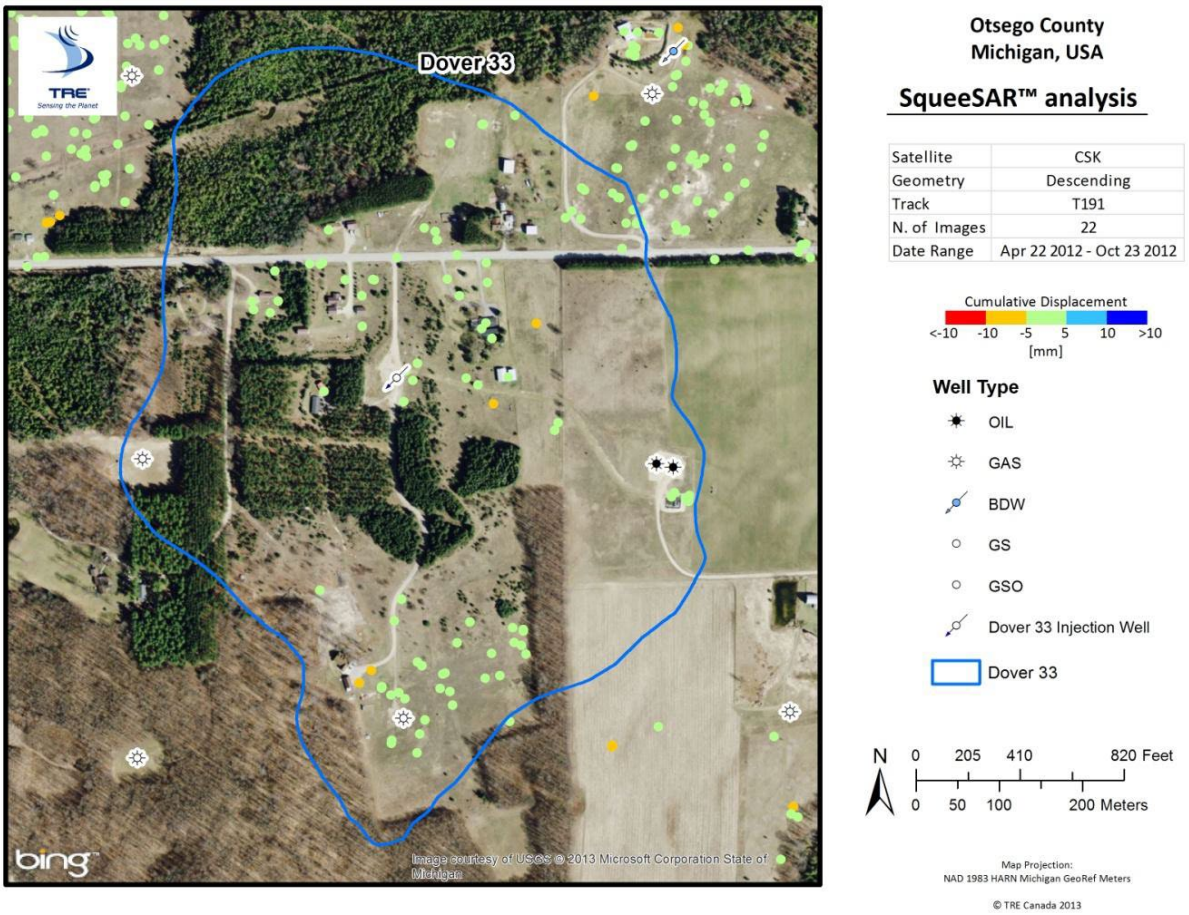

Figure 2-5. Example GIS map showing surface displacement rates in mm/yr during the baseline monitoring period for Dover 33. There are no apparent differences between points located "on" and "off" reef.

Figure 2-6 displays the average displacement values for all points over the Dover 33 reef relative to the reference point (outside the AOI). The average data indicates there was a small amount of subsidence (-2 mm) over the baseline monitoring period, which is within the standard deviation of the data (±3.7 mm).

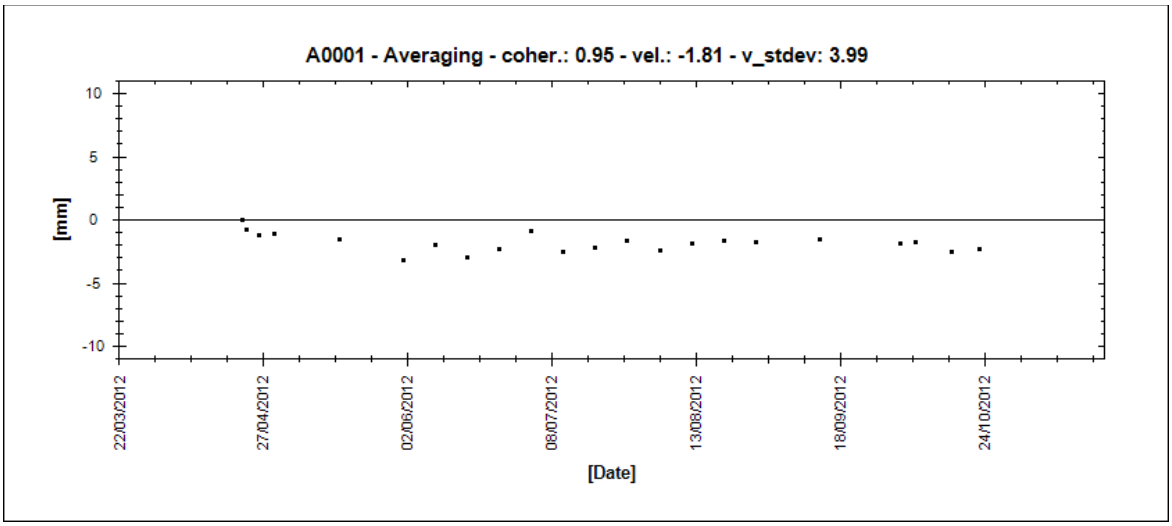

Figure 2-6. Example time series graph during the baseline monitoring period, averaging all measurement points identified over the Dover 33 reef. Average displacement values are calculated from a linear regression (vel). The precision is determined from the standard deviation (v-stdev).

2.3 ACR Design, Construction, and Installation

ACRs were used around the Dover 33 reef to provide measurement points in areas of low radar reflectivity. ACR's are aluminum structures fixed to the ground to reflect satellite signals (Figure 2-7). Installation involves an auger system to place the steel pipes into the ground below the frost line to minimize the effects of frost heaving and other ground surface movements on the deformation data. The ACRs were covered with a durable cloth to keep snow and other debris off the reflectors so they function year-round. The ACRs were installed after the baseline monitoring period and before long-term injection began at Dover 33.

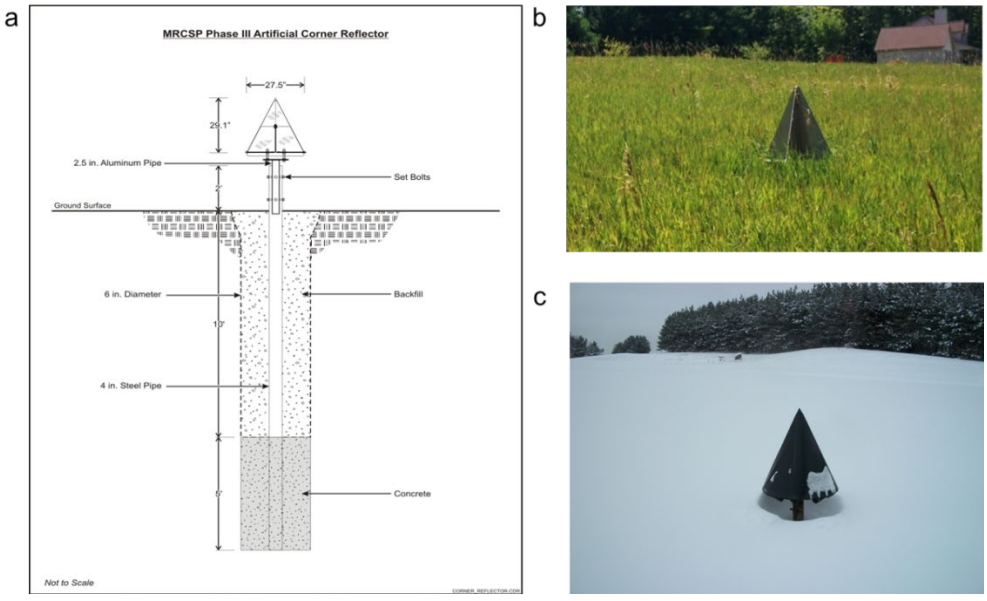

Figure 2-7. a) ACR schematic diagram; b) ACR without the cone; and c) ACR covered with fabric

As part of the baseline monitoring, a single CSK satellite image was collected over the AOI to determine areas of high natural reflectivity and to more accurately guide the optimal location of the ACRs. The following factors were considered:

- keep the number of ACRs to a minimum, while achieving adequate coverage across the project site;
- avoid existing substantial infrastructure, such as buildings, as these provide measurement points and would mask the ACR due to extraneous reflective radar noise;
- have minimal impact on landowner activities or farming operations;
- avoid heavily wooded areas; and
- locate ACRs near field boundaries, roads, and wellheads.

Several working sessions took place to complete the final design layout for the ACRs and develop detailed installation instructions. TRE Canada provided a set of PDF drawings to Battelle, which were used by a machine shop to construct the ACRs. They are designed to be installed on site with minimum instruction, using standard field equipment and tools. The design features low visual impact and requires minimal maintenance. Core Energy was responsible for contacting the landowners for access and permission, as well as the installation of the ACRs. Figure 2-8 depicts images from the installation and orientation of the reflectors.

Figure 2-8. Photographs documenting the installation of the ACRs

The timeline of ACR installation is presented in Figure 2-9. The permitting and installation of 29 ACRs was completed on March 29, 2013. TRE Canada performed a visibility check on April 5, 2013 and reported that eight ACRs had low reflectivity values and five were not visible. The possible reasons given were shadowing by trees or incorrect orientation of the ACRs. Battelle re-orientated these ACRs on April 24 (Figure 2-8). On May 27, a second visibility check indicated that some reflectors (ACRs 4, 8, 9, 13, and 20) were blocked or partially blocked by trees. Battelle worked with Core Energy to move ACR 8 and ACR 20 on July 7 to position them away from trees and increase visibility (Figure 2-10). ACRs 4, 9 and 13 were

not moved because no better locations were nearby. Following the relocation effort, TRE Canada performed a third visibility check on August 28, which showed the relocations of ACR 8 and 20 were successful. However, ACR 4 was no longer visible, likely due to growth of vegetation around this reflector. Thus, 26 of the 29 ACRs are usable for this study. Of the 29 ACRs installed at the study area, 13 ACRs were placed over the Dover 33 reef and the remaining 16 ACRs were positioned in the surrounding area to extend the artificial reflector network. Reflector #28 was selected to be the reference point for the ACRs and was located approximately 2,547 feet northeast of the injection well for the reef.

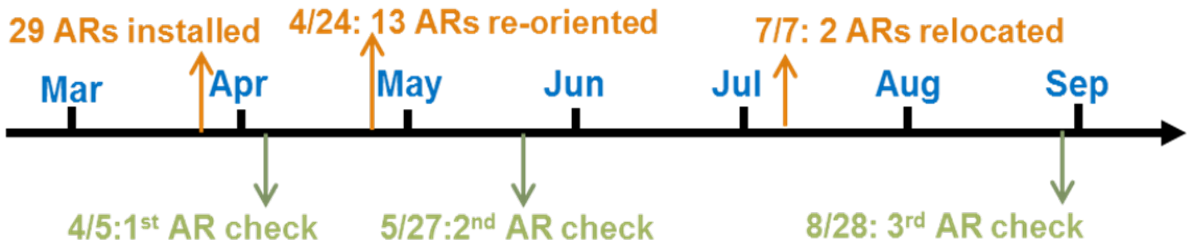

Figure 2-9. Timeline of ACR installation in 2013

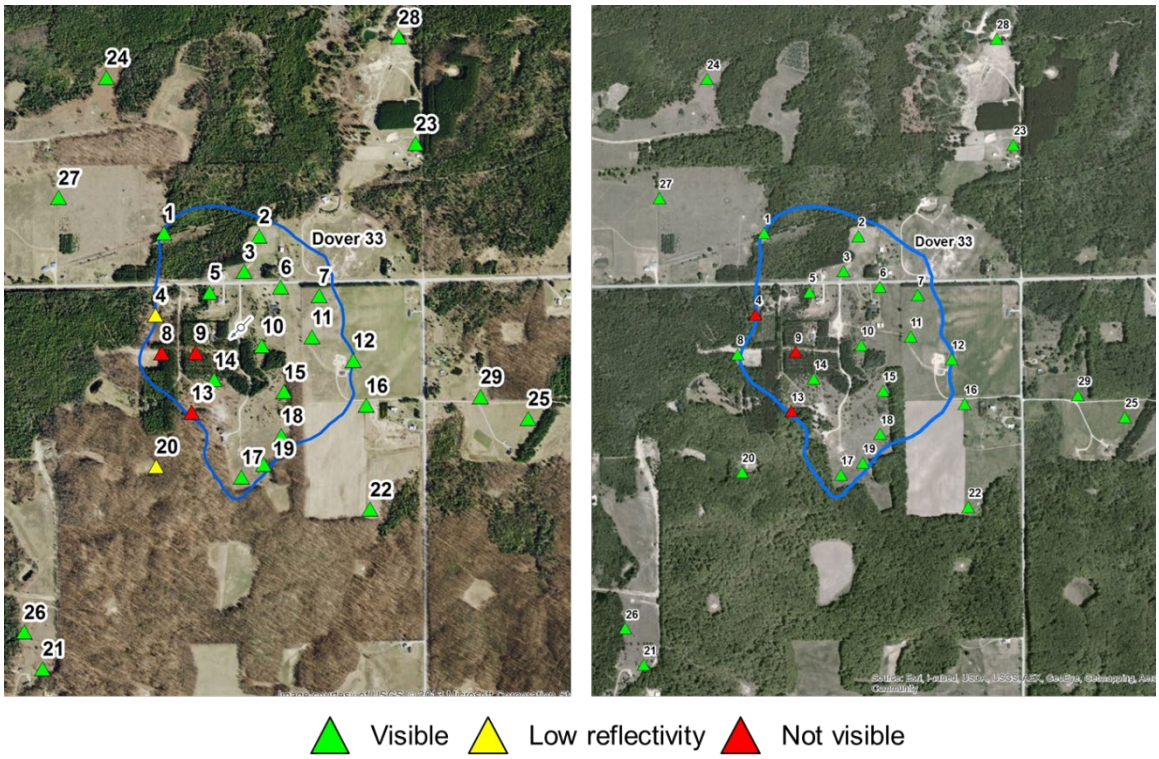

Figure 2-10. a) Results of the second visibility check following reorientation; and b) results of the third visibility check following relocation of ACR 8 and 20.

2.4 Long-Term Monitoring

While the focus of the study was the Dover 33 reef, the AOI covered a broader area in order to compare data over the Dover 33 reef with regional trends and with other reefs. The radar imagery available for the analysis consisted of 76 images acquired between April 22, 2012 and March 22, 2015. All images were acquired by CSK from a descending orbit.

Continuous CO_2 injection into the Dover 33 reef under the Midwest Regional Carbon Sequestration Program (MRCSP) began in March 2013 and was halted in August 2014 after reaching a bottom hole pressure (BHP) of approximately 3,300 pounds per square inch (psi) in the Lawnichak-Myszkier (L-M) 1-33 injection well. Ground surface movement trends across the entire AOI (including the Dover 33 reef) were measured both before and during CO_2 injection, using natural radar targets and 26 ACRs. Satellite imagery was processed in two steps for the current analysis. One processing effort comprised the full stack of images (full data set) from the start of satellite image acquisitions until the end of March 2015, while the second processing effort was performed on all images acquired after the start of CO_2 injection (co-injection data set).

The AOI was updated from 80 to 81 square kilometers (31 to 32 square miles) to include an additional reef (Charlton 19) located in the northeastern portion of the previous AOI (Figure 2-11). Battelle contemplated adding this new reef to the detailed monitoring program; however, timing of the new reef flood did not fit the program, so the monitoring analysis was ultimately limited to the Dover 33 reef. While the environment is predominantly non-urban, there are structures in the area related to oil and gas infrastructure, housing, roads and other buildings that provide reasonable reflectors. Measurement points are often identified from these man-made features, as well as from cleared or sparsely vegetated areas. Forested regions and agricultural areas are more challenging for InSAR as their reflectivity changes over time. The final long-term monitoring report is included in Appendix C.

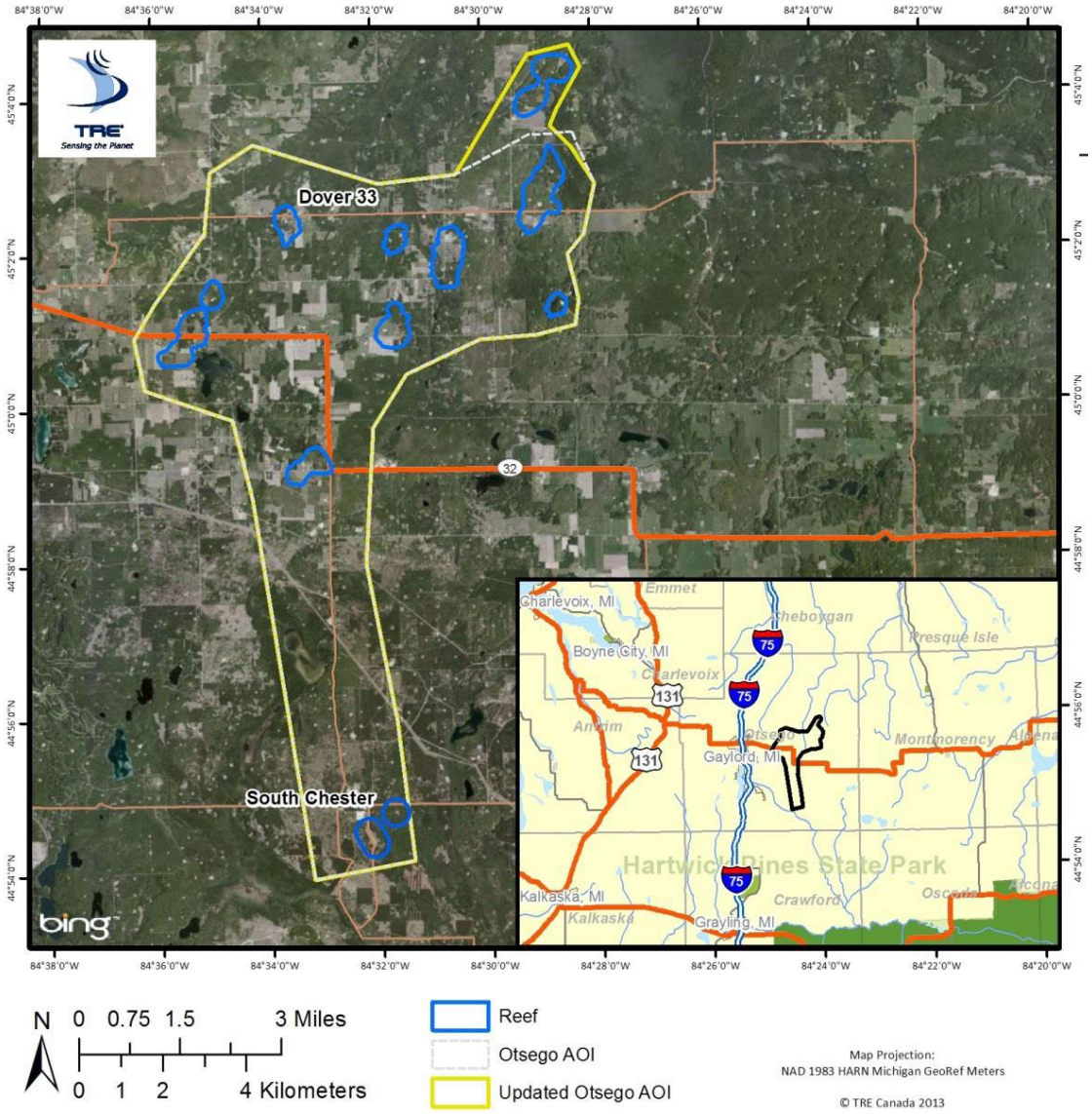

Figure 2-11. Map of the revised AOI showing the inclusion of the Charlton 19 reef in the northeast portion of the area.

Figure 2-12 displays the cumulative displacement measured during the 35-month monitoring period (full data set) for the entire AOI. Cumulative displacement amounts across the AOI during the full data set monitoring period were between -60.5 to 50.7 mm, and slight uplift was observed over the entire AOI, with an average uplift of 1.2 mm. These relatively large displacement values appeared at individual points and were very localized movements. However, a few areas of subsidence were detected (mostly outside the reef structures).

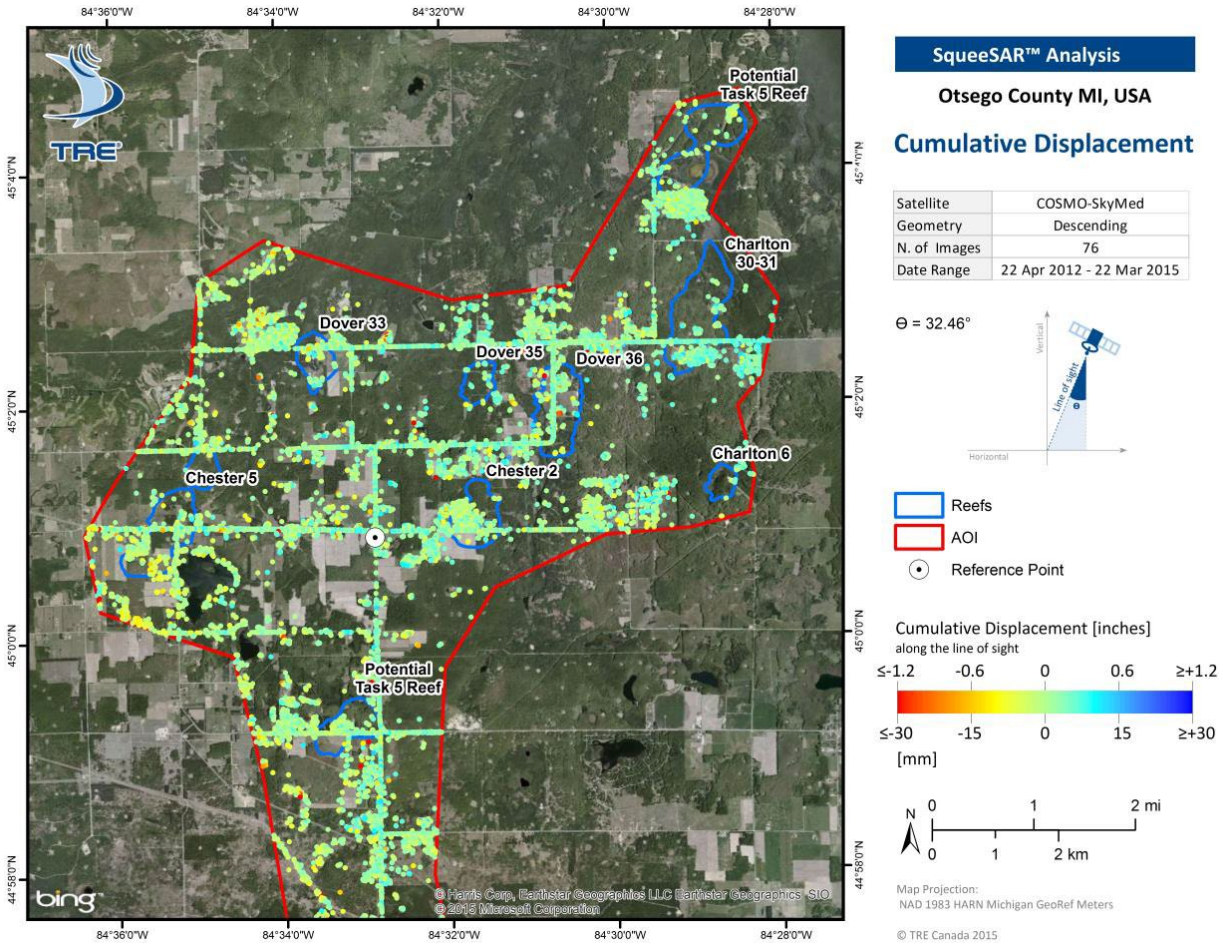

Figure 2-12. Cumulative deformation, expressed in mm between April 22, 2012 and March 22, 2015.

The LOS displacement rates over the entire AOI, expressed in millimeters per year (mm/yr), are presented in Figure 2-13 and Figure 2-14 for the full data and co-injection data, respectively. Each point corresponds to a PS or a DS and is color-coded according to its annual rate of movement. Average displacement values are calculated from a linear regression of the ground movement measured relative to the reference point over each measurement period. Measurements should be interpreted by accounting for the associated standard deviations.

For the full data set, an average surface deformation rate of 0.04 ±0.4 mm/yr was identified within the nine reefs, compared to -0.2 ±0.4 mm/yr for the entire AOI (Figure 2-13). Maximum values ranged from -20.0 to +16.7 mm/yr over the reefs and from -21.4 to +16.7 mm/yr over the entire AOI.

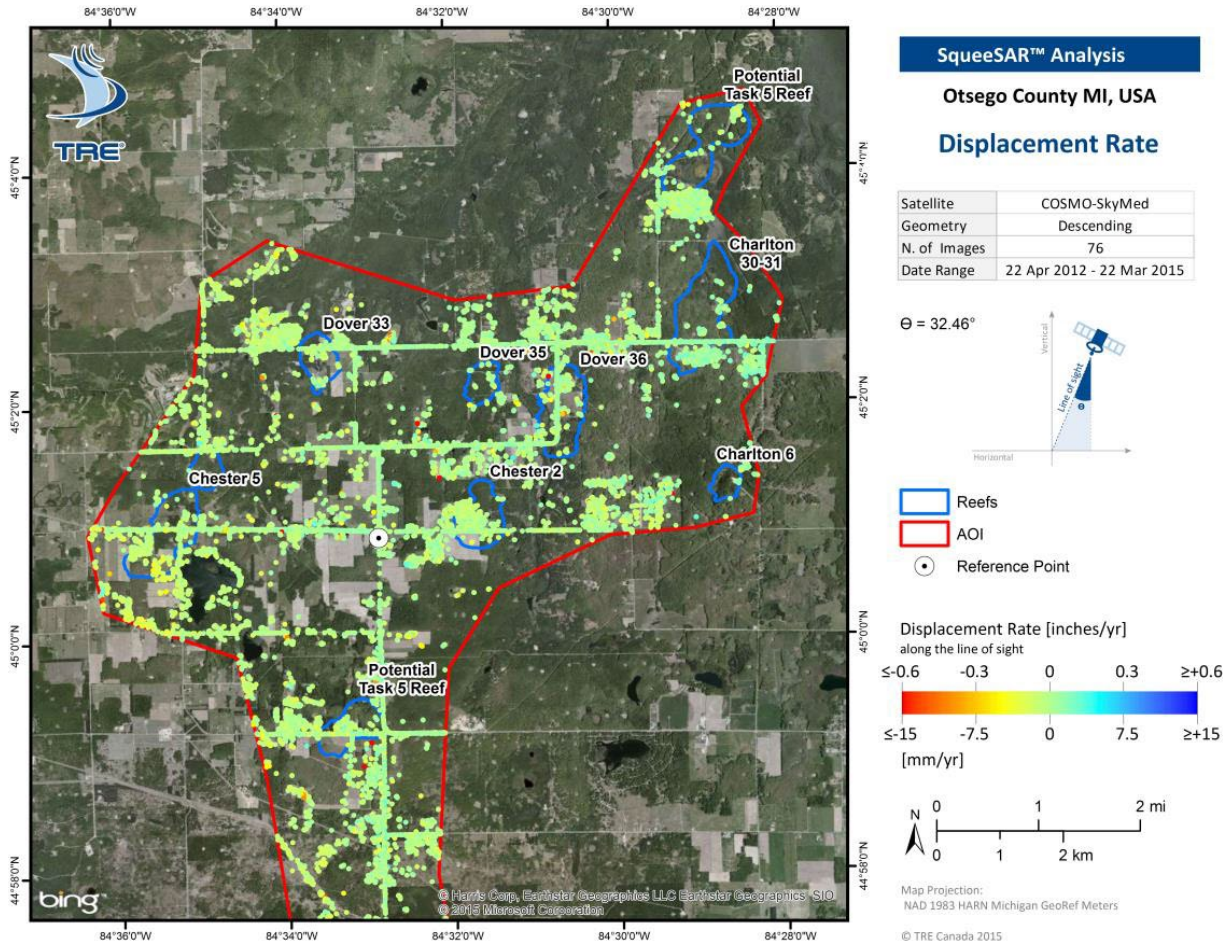

Figure 2-13. Deformation rates, expressed in mm/yr between April 22, 2012 and March 22, 2015.

For the co-injection data period, an average surface deformation rate of 1.0 ±0.9 mm/yr was identified within the nine reefs with a range of -16.6 mm/yr to +5.0 mm/yr (Figure 2-14). In the remainder of the AOI, an average surface deformation rate of 0.3 ±0.9 mm/yr was obtained, with rates ranging from -16.6 mm/yr to +15.8 mm/yr.

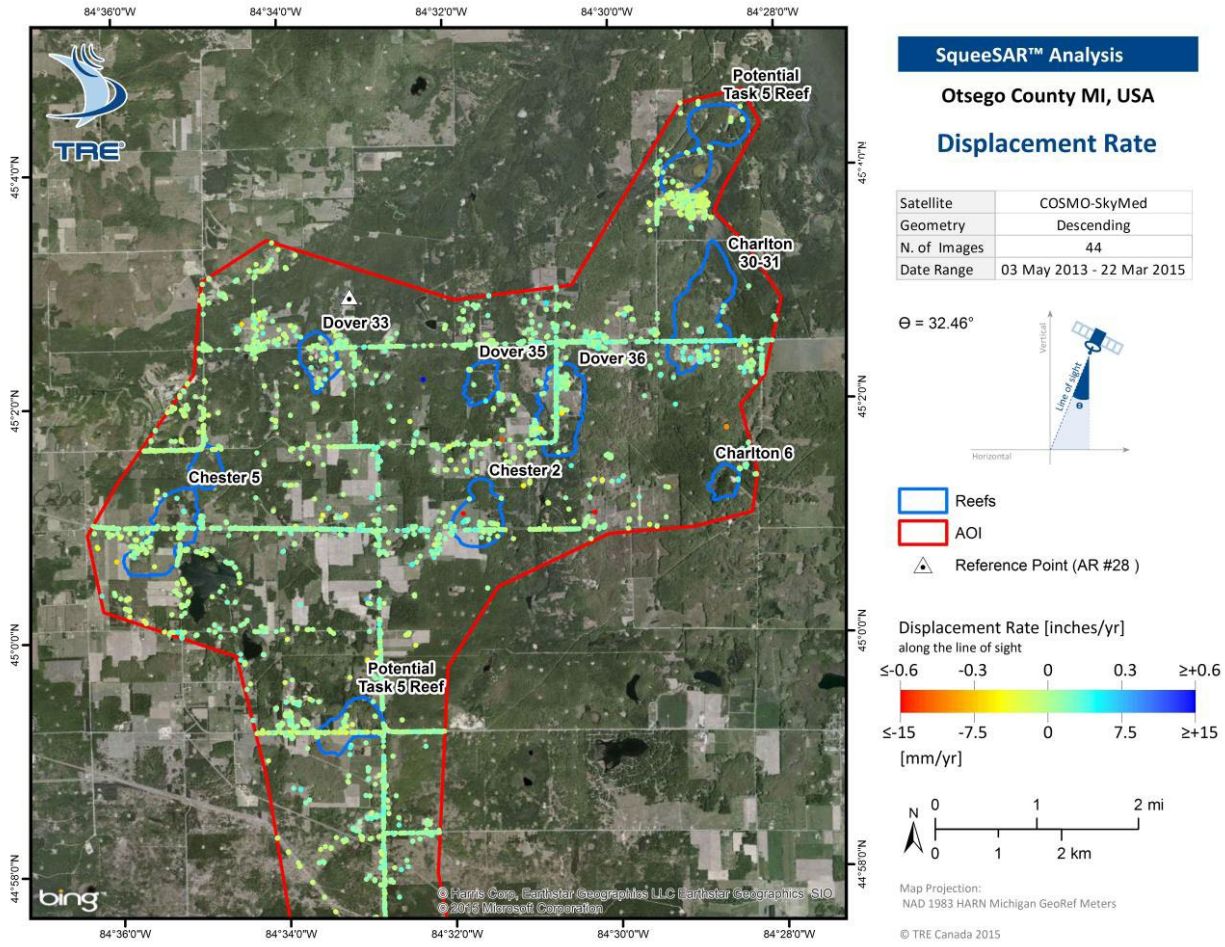

Figure 2-14. Deformation rates over the AOI, expressed in mm/yr, during the co-injection monitoring period (May 3, 2013 through March 22, 2015).

Surface deformation near the Dover 33 reef was measured using natural radar reflectors and ACRs installed in 2013, leading to 111 measurement points around the reef. Each point on the map corresponds to a PS or DS and is color-coded according to its annual rate of movement. Ground deformation rates from natural radar targets over the Dover 33 reef in the full data set showed little movement, with average rates of -0.3 mm/yr (Figure 2-15). A cumulative displacement of 0.7 mm was measured by the natural reflectors over the full data set and 1.2 mm during the CO_2 injection phase.

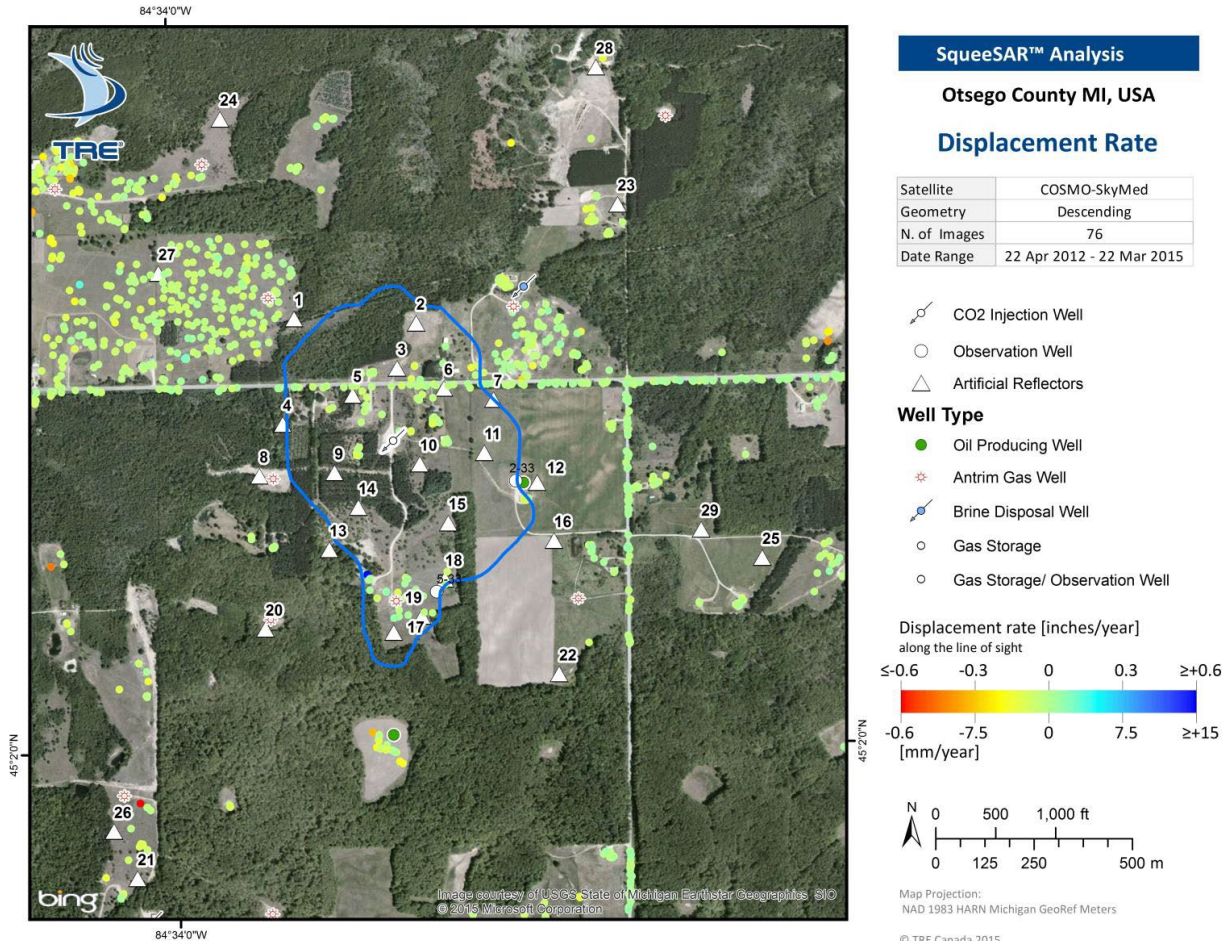

Figure 2-15. Displacement results from the full data set over the Dover 33 reef.

A total of 44 images were collected and processed for the ACR analysis between May 03, 2013 and March 22, 2015. Displacement rates over Dover 33 were between -0.1 mm/yr and +3.9 mm/yr. An average deformation rate of 1.1 mm/yr was obtained from the ACRs over Dover 33, while the average for all ACRs outside the reef was 0.01 mm/yr (Figure 2-16). The results indicate the reflectors within and outside of Dover 33 are mainly stable.

Displacement rates of all ACRs are minimal, ranging from -1.5 mm/yr to +3.9 mm/yr, with an average of +0.4 mm/yr. The five ACRs closest to the injection well were ACR 3, 5, 6, 10, and 14, and have displacement rates ranging from +0.2 to +2.4 mm/yr. Some of the fluctuations in the ACRs across the area are believed to be weather-related and due to snowfall in winter. These trends are visible in the time series analyses of the ACR data (ACR 14, 15, 20, 26), but no ground deformation trend related to CO_2 injection operations is observed in the ACR results. A +3 mm uplift is observed in the ACRs between November 2014 to February 2015, but this uplift is also noted across the entire AOI and is likely unrelated to injection activities and probably caused by a natural event, such as frost heaving.

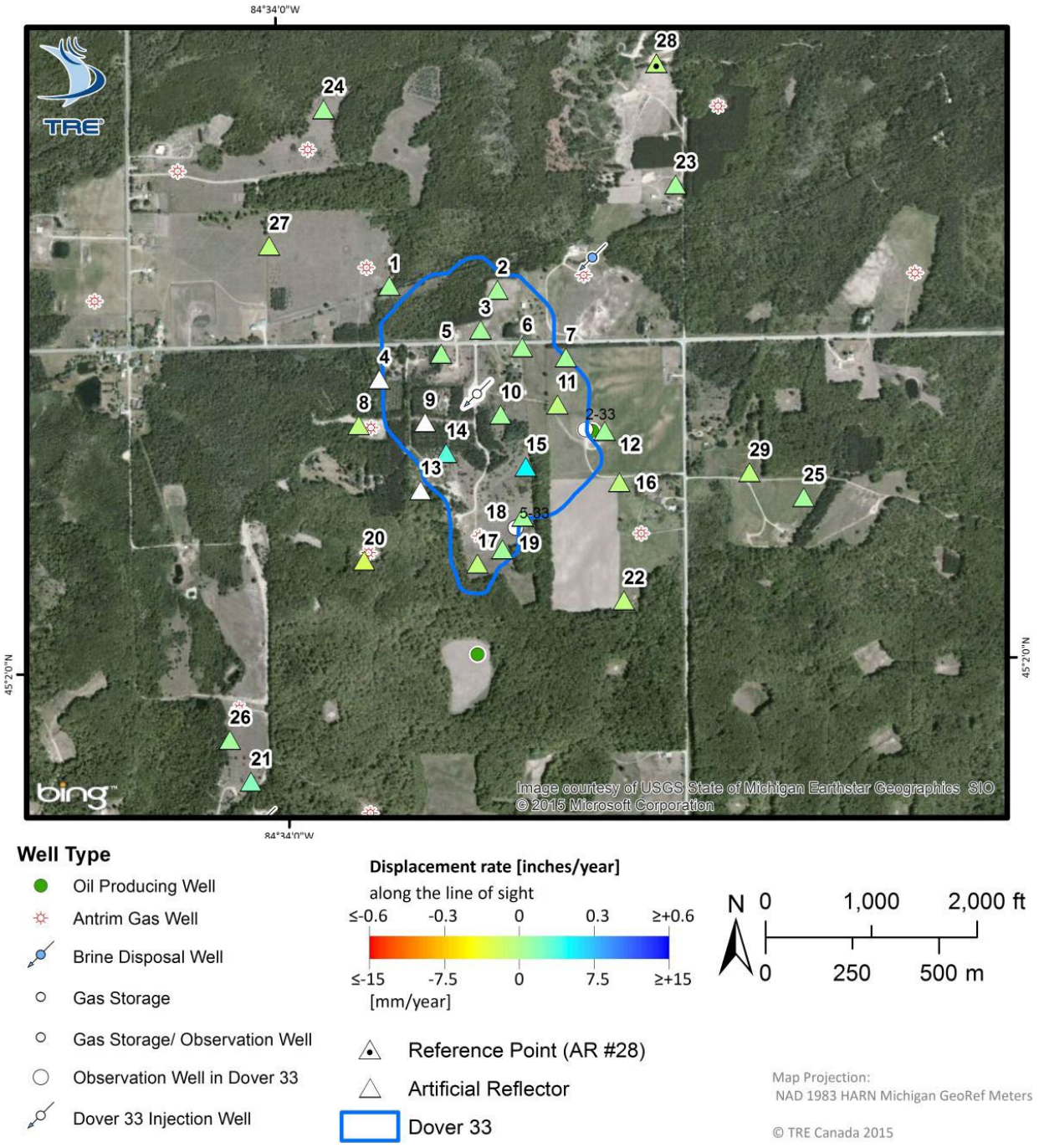

Figure 2-16. Displacement results obtained for all ACRs installed at the Dover 33 site. Three ARs (shown in white) are not included in the present analysis, as they were not visible to the satellite.

A comparison between the surface deformation and the reservoir pressure was performed to determine if there was a correlation between deformation and pressure. The reservoir pressure increased from approximately 800 psi to over 3,300 psi with the injection of 244,000 tons of CO_2, but the ground deformation measured with the ACRs and natural reflectors remained within ±5 mm and no discernable correlation between surface deformation and reservoir pressure was determined (Figure 2-17).

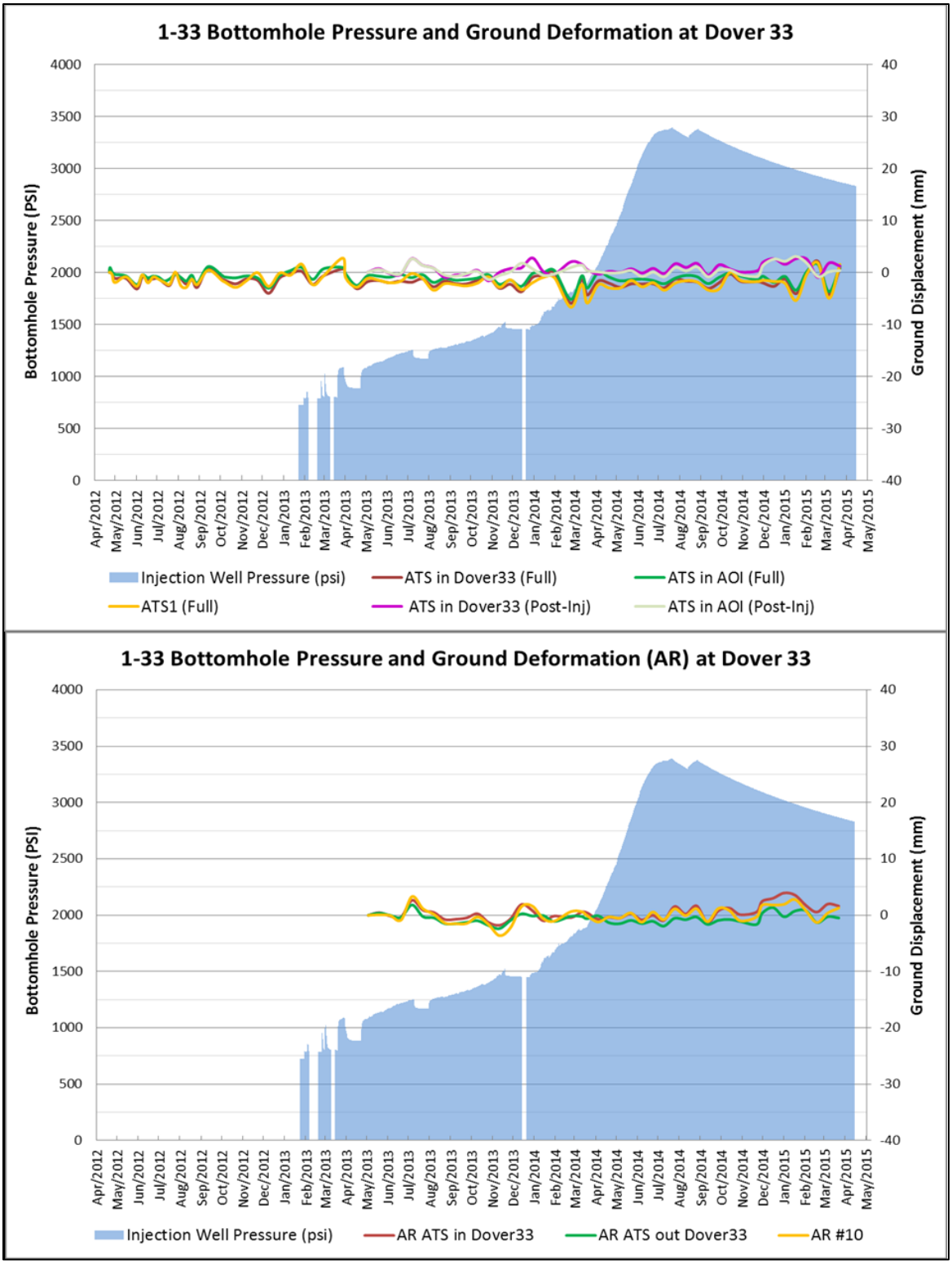

Figure 2-17. BHP and ground deformation results obtained at Dover 33. The top panel represents ground deformation from natural radar targets, while the bottom panel shows ground deformation results obtained from the ACRs for both the full and co-injection data.

3.0 Conclusions

InSAR was used to monitor ground surface deformation over the Dover 33 reef during carbon capture and storage (CCS) operations in three stages. An initial historical analysis covering the timeframe of 1992 to 1999 using the ERS satellite provided an overview of natural ground deformation over the 83 km^2 AOI. A second analysis provided a baseline monitoring over a period of six months (April 2012 to October 2012) prior to the start of CO_2 injection into the Dover 33 reef. While this analysis focused on the Dover 33 reef, ground deformation data were collected from the entire AOI. Further processing provided ground deformation measurements during the Dover 33 CO_2 injection with 16-day satellite revisit data from April 2012 to March 2015. A total of 29 ACRs were installed in 2013 to supplement the distribution of natural measurement points within and around the Dover 33 reef.

The results of the current monitoring analysis indicate there was no discernible ground surface response to CO_2 injection into the Dover 33 reef, either from natural radar targets or artificial reflectors. Deformation trends remain similar to those observed in the baseline results. This was confirmed both in the spatial domain (Dover 33 vs AOI) and the temporal domain (co-injection vs full processing data sets). Finally, no correlations were observed in the comparison of ground deformation against the reservoir pressure and injected CO_2 volume. The small degree deformation observed during the monitoring is generally localized to single monitoring locations and believed to be the result of natural events, such as freeze/thaw cycles or near surface aquifer drawdown/recharge.

The ACRs exhibited average displacement values of 1.1 mm/yr over the Dover 33 reef and 0.01 mm/yr outside the reef. However, no clear ground deformation in response to the CO_2 injection was observed when comparing the deformation data to the CO_2 injection and reservoir pressure data. Further, the geomechanical study predicted that no surface deformation would be anticipated as the result of the mass of CO_2 injected into the Dover 33 reef. The signature of the ground movement observed at the In Salah project in Algeria was contrasted with the lack of uplift observed at the Dover 33 reef. The comparison highlights the completely different behavior of ground surface response between the two sites.

Appendix A.

Historical Analysis

TRE®
Sensing the Planet

Historical InSAR Analysis

InSAR Analysis of Historic Ground Movement occurring between 1992 - 1999 over Otsego County, Michigan

Submitted to:
Lydia Cumming
Battelle
505 King Avenue
Columbus, Ohio 43201

Prepared by:
TRE Canada Inc.
Doc. Ref.: JO12-3008-REP1.0

24 October 2012

Prepared by:	Jessica Morgan GIS Analyst TRE Canada Inc.	_____ (signature)
	Vicky Hsiao GIS Analyst TRE Canada Inc.	_____ (signature)
Approved by:	Giacomo Falorni Operations Manager TRE Canada Inc.	_____ (signature)

Executive Summary

This report describes the approach and results of the InSAR analysis carried out to measure ground movement over reefs within Otsego County, Michigan between 1992 and 1999. The results provide an overview of ground movement during this time period.

The following points summarize the key findings of this analysis:

- Most of the reefs and surrounding areas were observed to be stable. Mild subsidence was observed at the Chester 5, 15, 16 and South Chester reefs, whereas slight uplift was observed in several measurement points identified within the Dover 33 reef.
- Time series of deformation extracted from several features within the results provide additional insight into ground movement occurring over multiple spatial scales.
- Surface displacement results over the South Chester gas storage field were compared to historic operations information for this site; however, no correlations could be established.
- Some of the measurement points were observed to contain a faint seasonal component, including several points within the South Chester field.

The deliverables for this stage of the project include the present report, which describes the results of the data processing, and a CD containing the displacement data. New imagery is currently being acquired for the ongoing monitoring of the site using the Cosmo-SkyMed constellation of satellites.

Table Of Contents

1 Background

The Battelle Memorial Institute (Battelle) is an independent research and development organization that is currently heading the Mid-West Regional Carbon Sequestration Partnership (MRCSP). The MRCSP is focused on the investigation of the geological suitability of the north-west United States for carbon sequestration, as part of a larger Department of Environment strategy for developing CO_2 mitigation strategies. Now entering the development phase of this research project, the Dover reef (a depleted reservoir) in Otsego County in the northern Michigan Basin has been selected as a site for carbon sequestration over a period of ten years.

As part of a comprehensive monitoring program being implemented during the sequestration process, InSAR is being used to map surface response to CO_2 injection and migration throughout the reservoir. TRE Canada Inc. (TRE) has been contracted by Battelle to perform both a historic InSAR analysis of ground movement at this site, as well as provide ongoing InSAR monitoring. This report details the results of the present analysis, with an objective to assess the density and distribution of measurement points, and to identify any historic surface movement over gas storage operations. An archive dataset acquired by the ERS satellite between 1992 and 1999 was processed for this purpose using TRE's proprietary SqueeSAR™ algorithm.

2 Overview of the Area of Interest

The area of interest (AOI) as indicated by Battelle has a surface area of 31 square miles (80 square kilometers) and is located east of Gaylord, Michigan in between Lake Michigan and Lake Huron (Figure 1). The majority of the AOI consists of cleared areas, active agriculture and forested regions. While the area is located in a predominantly non-urban environment, there are several man-made objects in the area related to oil and gas operations, houses, roads and other buildings. Measurement points can often be identified from these man-made features, as well as from cleared or sparsely vegetated areas. Forested regions and agricultural areas are more challenging for InSAR as their associated reflectivity change over time.

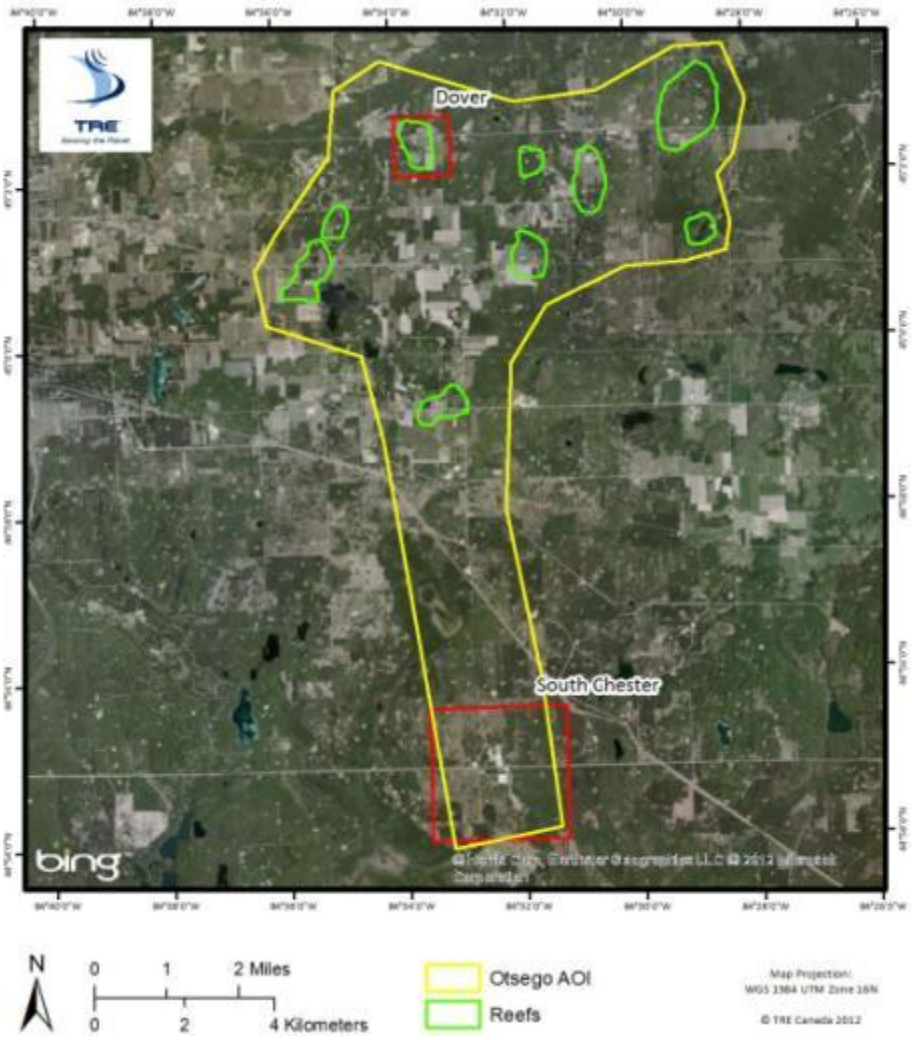

Figure 1: The Area of Interest (AOI) for Otsego County, Michigan as indicated by Battelle.

It is important to consider that the results of the historic analysis shown in Figure 1 are overlain on modern background optical imagery (2012) in all figures included in this report, and conditions may have changed between the period covered by the data set (1992 to 1999) and 2012. Furthermore, while man-made features provide ideal targets for InSAR measurement points, the feature must be present throughout the entire length of the analysis in order to be identified. Similarly, several areas within this region have been cleared of vegetation since the historic analysis, meaning some areas that look favorable for InSAR based on the current imagery may not have been ideal in a historical context.

3 Radar Data

The archive radar imagery utilized for this analysis consists of 51 images acquired between 20 May 1992 - 04 December 1999 (Table 1). All images in this stack were acquired from Track 269 in a descending orbit (meaning the satellite is travelling from north to south and imaging to the east).

While the complete archive data set comprised 60 images over this site, nine were not included in the data processing as they did not meet the requirements for InSAR processing. Individual images were removed due to excessive snow cover, and for orbital acquisition parameters outside the acceptable limits. The removal of these images improved the quality of the processing and increased the density of the measurement points.

Further information on InSAR is described in Appendix 2 and 3.

ERS Archive Data					
1	5/20/1992	**18**	10/21/1995	**35**	8/16/1997
2	7/29/1992	**19**	11/24/1995	**36**	9/20/1997
3	10/7/1992	**20**	11/25/1995	**37**	11/29/1997
4	11/11/1992	**21**	3/9/1996	**38**	1/3/1998
5	2/24/1993	**22**	4/12/1996	**39**	2/7/1998
6	5/5/1993	**23**	4/13/1996	**40**	3/14/1998
7	6/9/1993	**24**	5/17/1996	**41**	4/18/1998
8	7/14/1993	**25**	5/18/1996	**42**	5/23/1998
9	8/18/1993	**26**	6/22/1996	**43**	8/1/1998
10	9/22/1993	**27**	7/27/1996	**44**	9/5/1998
11	10/27/1993	**28**	12/14/1996	**45**	10/10/1998
12	3/24/1995	**29**	1/18/1997	**46**	11/14/1998
13	4/28/1995	**30**	2/22/1997	**47**	12/19/1998
14	6/2/1995	**31**	3/29/1997	**48**	1/23/1999
15	7/7/1995	**32**	5/3/1997	**49**	2/27/1999
16	9/15/1995	**33**	6/7/1997	**50**	4/3/1999
17	10/20/1995	**34**	7/12/1997	**51**	12/4/1999

Table 1: Dates of the ERS archive imagery used in the historical analysis over Battelle AOI.

4 Reference Point

SqueeSAR is a differential technique, meaning displacement is measured compared to a reference point that is assumed to be stable. The reference point used for the historical analysis is shown in Figure 2. This point was selected using an optimization procedure which maximizes the quality of the results based on a suite of radar parameters including high coherence, low standard deviation values and low variability of movement over time.

It was originally proposed that different reference points be used for the Dover and Chester fields. However, when taking into consideration the characteristics of the historic results, it was decided that one reference point (located outside of the AOI) would provide the highest quality results. Reference point coordinates for the current analysis are listed in Appendix 1.

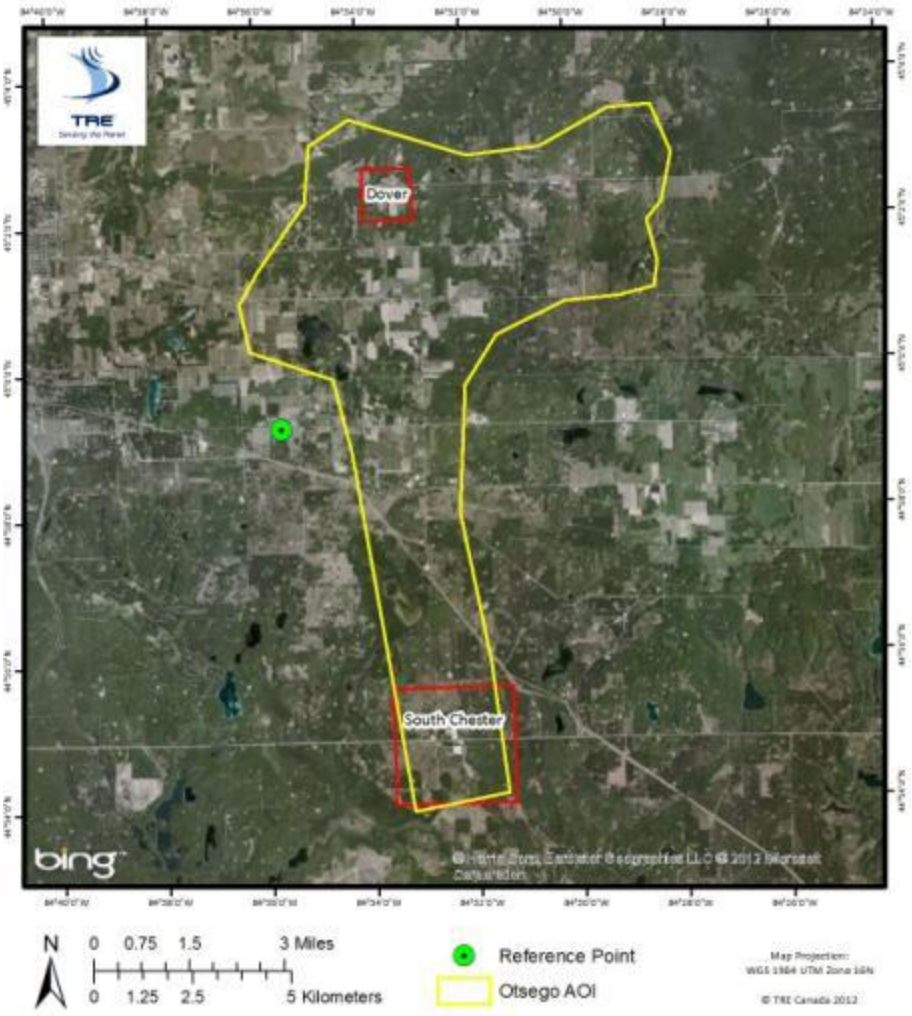

Figure 2: The location of the reference point used for the ERS data set.

5 Results of the SqueeSAR Analysis

5.1 Displacement Rate

The line-of-sight (LOS) displacement rates, expressed in millimetres per year (mm/yr), as detected from the processing of the dataset (Figure 3). Each point corresponds to a Permanent Scatterer (PS) or a Distributed Scatterer (DS), and is color-coded according to its annual rate of movement. Average displacement values are calculated from a linear regression of the ground movement measured over the entire period covered by the satellite images. Detailed information on ground motion is also provided by means of displacement time series, which are provided for each PS and DS.

Although several clusters of points indicating mild uplift or subsidence were observed within the results, surface displacement rates between 1992 and 1999 were generally stable. Average displacement rates illustrate only one aspect of surface deformation, whereas the time series of the results can provide more insight and are examined in further detail in section 6.2 to illustrate cyclical movement patterns and other variations in the ground surface over time.

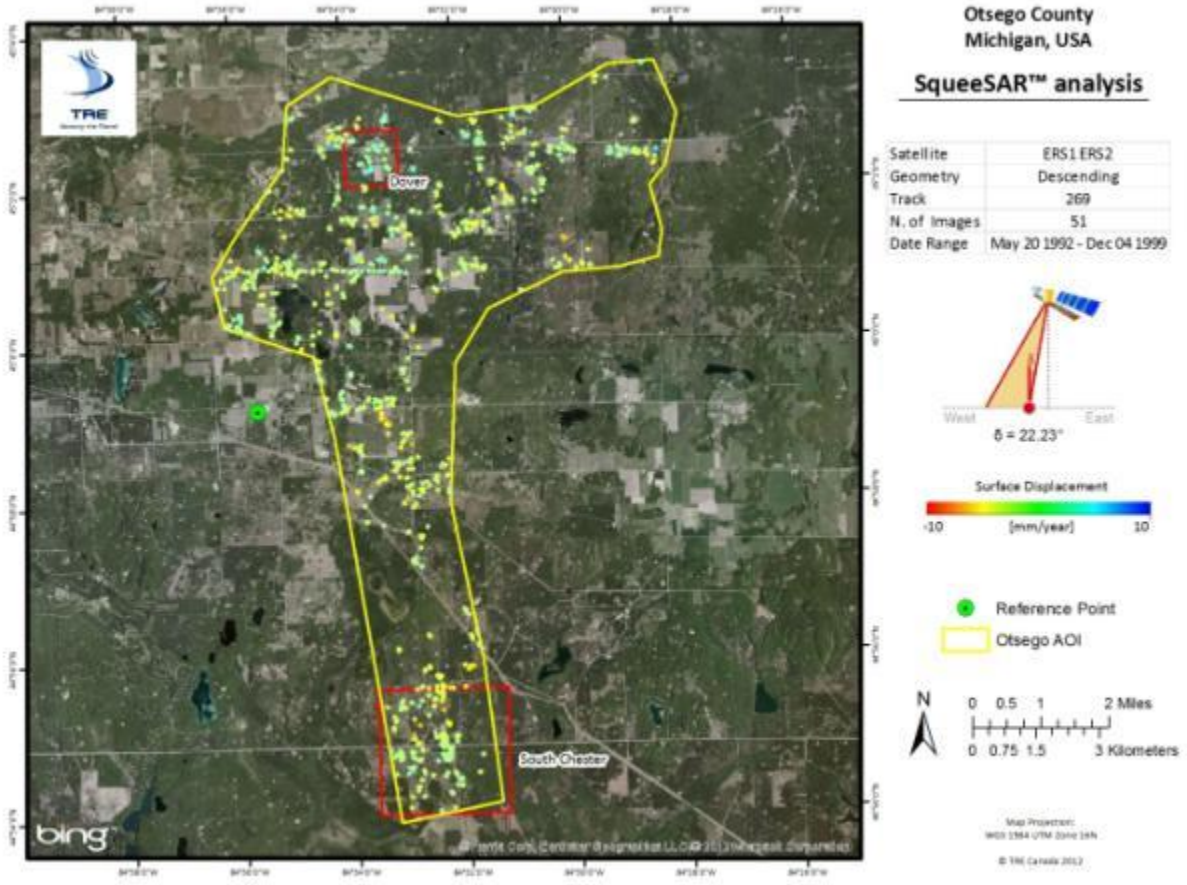

Figure 3: Historical deformation rates, expressed in millimetres per year.

5.2 Displacement Rate Standard Deviation

The standard deviation of the surface displacement data characterizes the error of the measurements (Figure 4). The displacement rate for a given point should be read in the form of *Displacement Rate ± Standard Deviation*. Areas impacted by higher standard deviations indicate a greater variability in measured displacement.

Standard deviation values are low throughout the AOI. In general, the precision of estimated displacement rates did not vary considerably over different features or land cover types. The average confidence interval associated with the measured displacement rates is 0.51 mm/year.

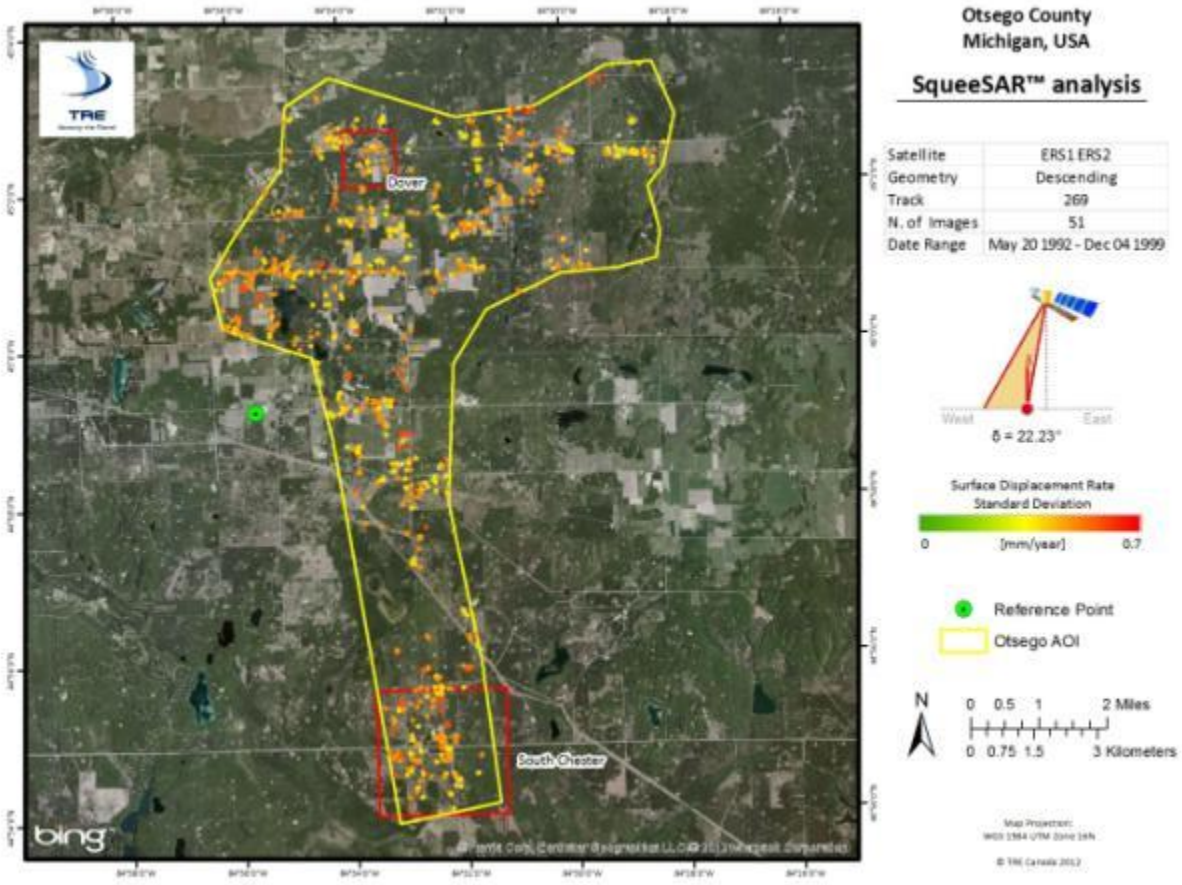

Figure 4: Standard deviation of the historical displacement rates, expressed in millimetres per year.

5.3 Acceleration

Measurement point acceleration values (Figure 5) can be used to identify non-linear trends in the deformation time series. Acceleration is used to identify areas where the deformation rate is increasing or decreasing over time. Negative accelerations are marked in red and indicate either an increase in downward movement rates, or a decrease in uplift. Positive accelerations are blue and indicate either an increase in the rate of uplift or a decrease in the rate of subsidence.

Acceleration rates are low throughout the AOI, which is fairly typical of areas where minimal deformation has occurred. In general, acceleration values are slightly negative around the Chester field, indicating that the rate of negative displacement at this site was increasing slightly towards the end of the analysis. In contrast, the acceleration rates at the Dover site are slightly positive.

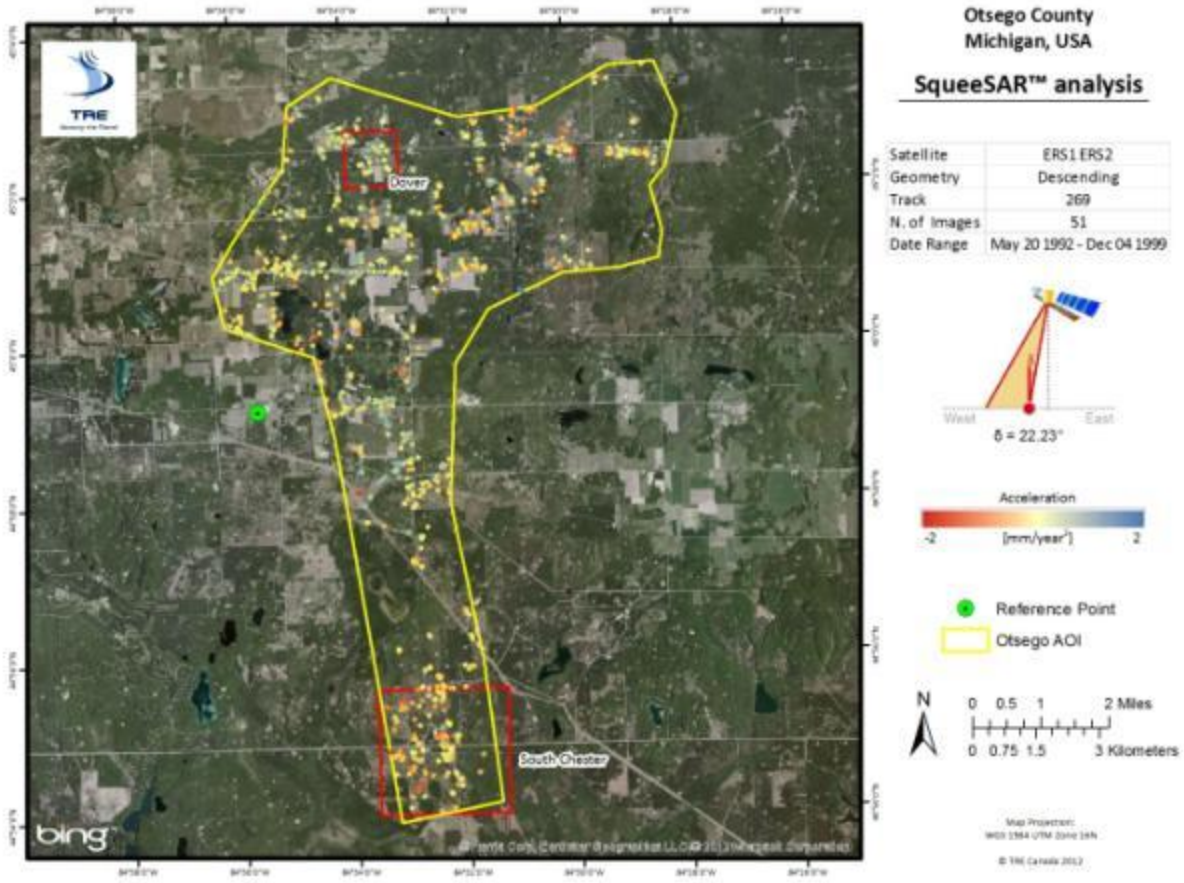

Figure 5: Historical acceleration values, expressed in millimetres per year squared.

6 Observations

6.1 Overview of Ground Deformation

No strong deformation trends are visible within the historic results; however, there are several areas which exhibit mild subsidence or uplift. The focus of the present analysis was placed on the areas within, and immediately surrounding the Dover 33 and South Chester fields and other reefs. In general, many of the measurement points identified within the Dover site demonstrated stability or mild uplift, whereas the majority of the points located in the Chester field were subsiding. The range of displacement rates identified throughout the AOI spanned from a maximum of 2 mm/year (identified from a measurement point located in the Dover field) to a minimum of -6 mm/year (identified from a measurement point located in the Chester field).

An analysis of the data time series indicates that there is a mild seasonal component in some of the measurement points identified in this area. Seasonal movement is typified by the appearance of cyclical (undulating) movement within the time series, which is most commonly caused by seasonal changes in temperature, soil moisture content or ground water levels. However, in the case of the Chester site, it may be possible that cyclical fluctuations are related to the seasonal storage and extraction of gas. A brief comparison of historic operations data and ground movement is detailed in Section 6.3.

6.2 Features of Interest

In order to better highlight movement occurring within the Otsego AOI, group time series were created to illustrate displacement trends over specific areas. Group times series are generated by averaging the ground movement measured by all points contained within a specified area. Displacement results over the nine reefs located across the northern portion of the AOI are shown in Figure 6, below. Group time series for each reef are displayed in Figure 7 to Figure 14, inclusive.

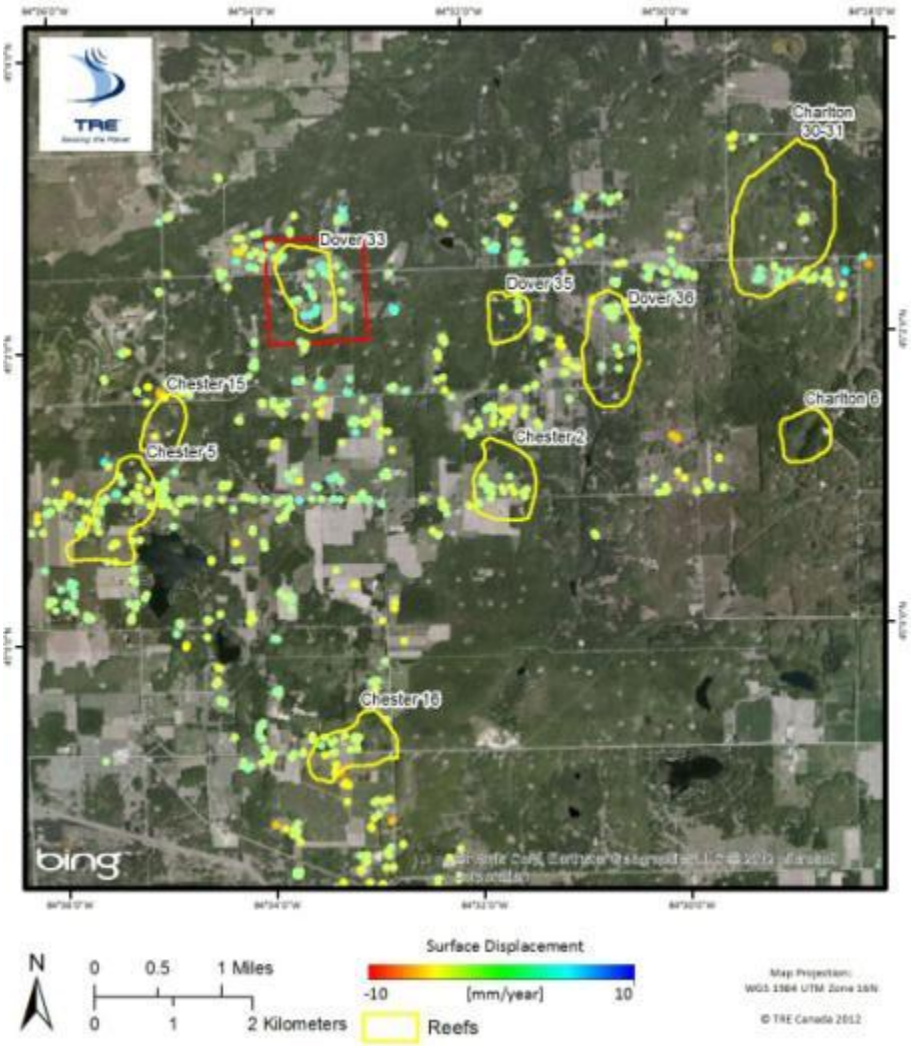

Figure 6: Historic surface displacement results over the nine reefs located in the Otsego AOI.

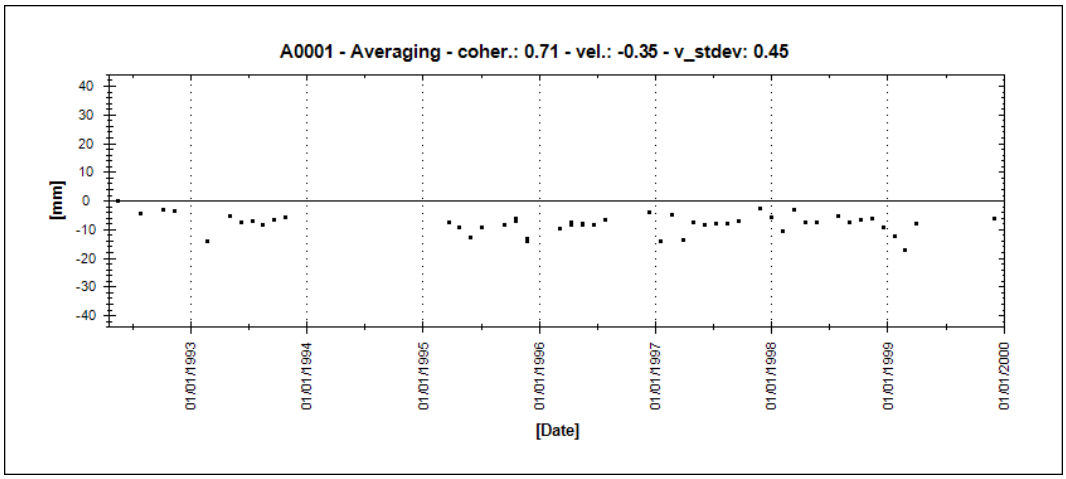

Figure 7: Average time series of all measurement points identified over the Charlton 30-31 reef.

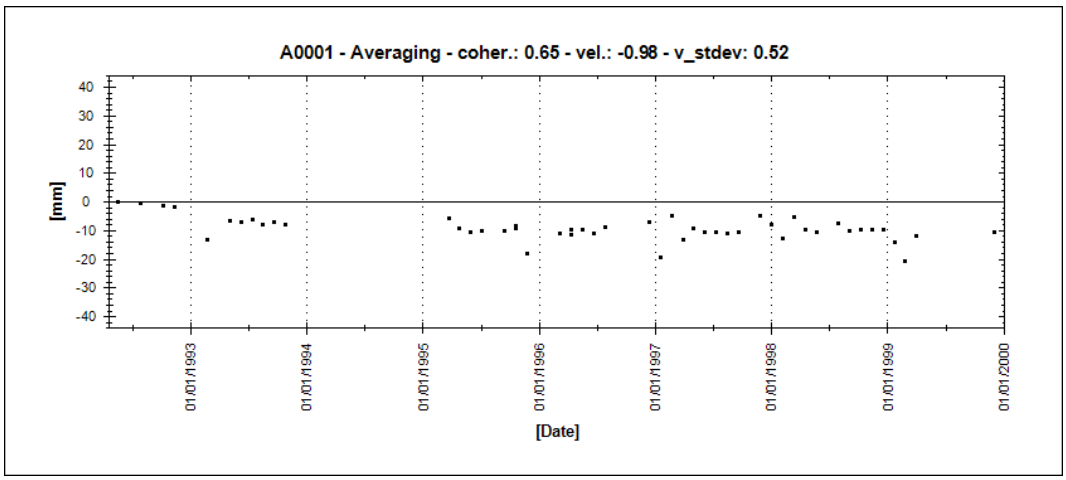

Figure 8: Average time series of all measurement points identified over the Chester 2 reef.

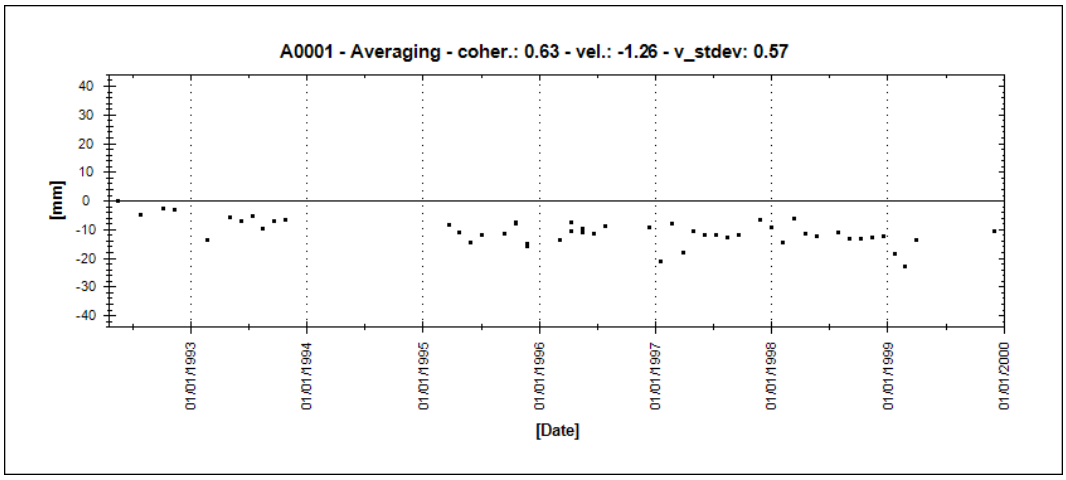

Figure 9: Average time series of all measurement points identified over the Chester 5 reef.

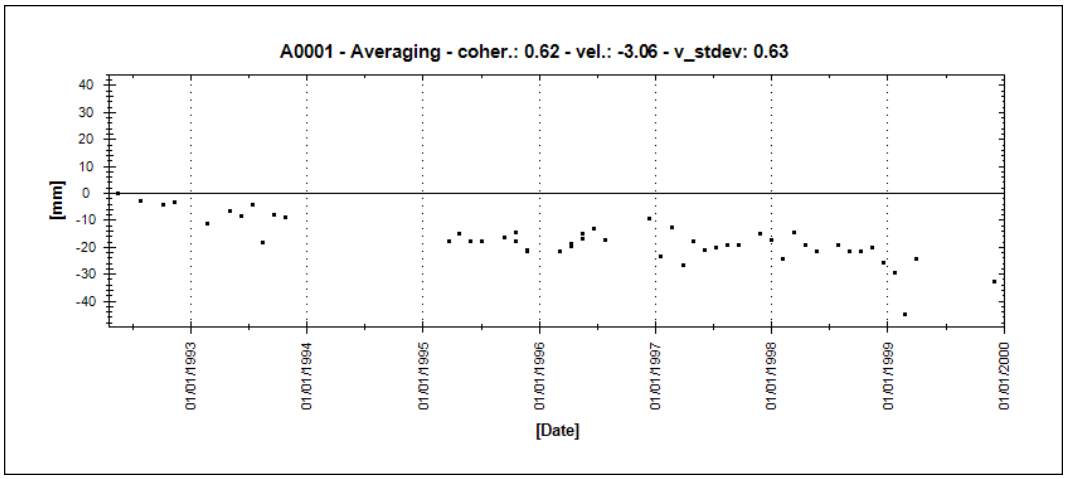

Figure 10: Average time series of all measurement points identified over the Chester 15 reef.

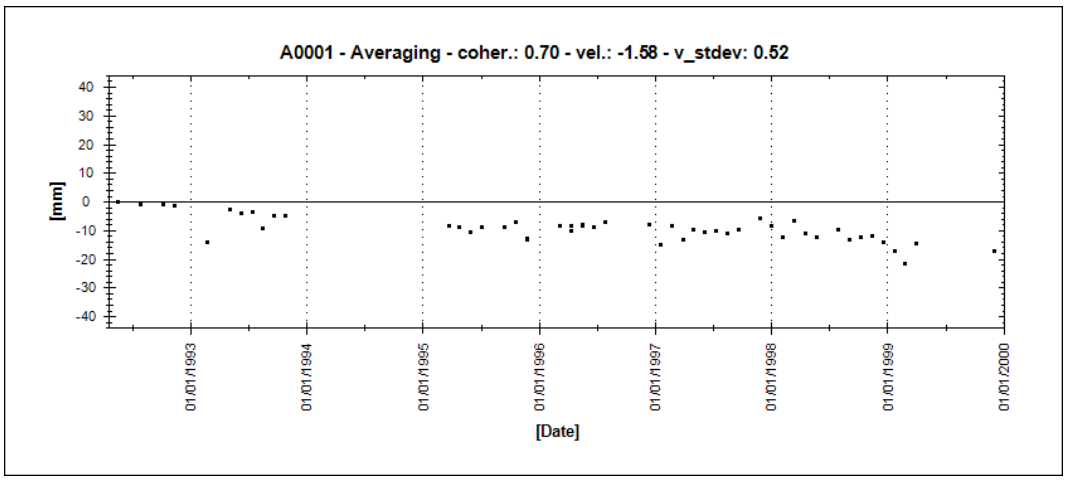

Figure 11: Average time series of all measurement points identified over the Chester 16 reef.

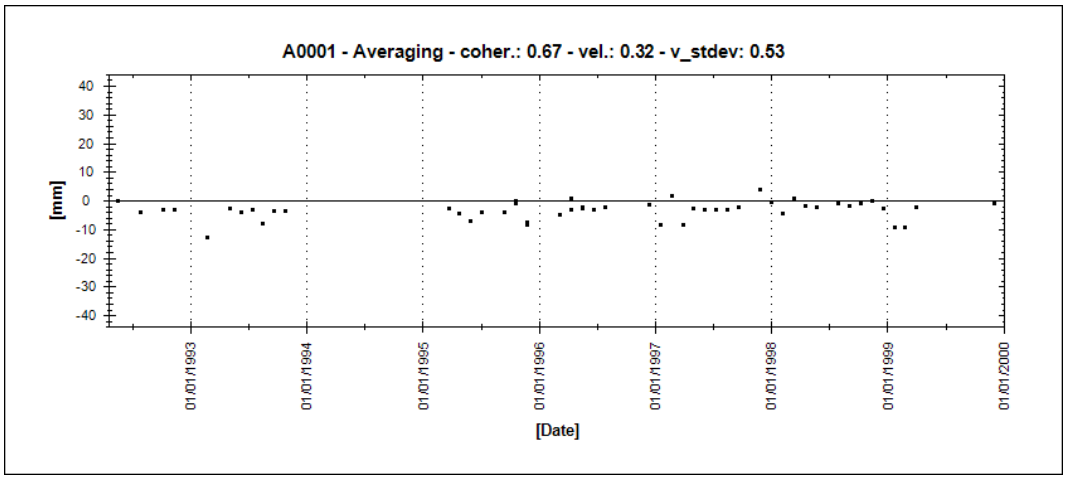

Figure 12: Average time series of all measurement points identified over the Dover 33 reef.

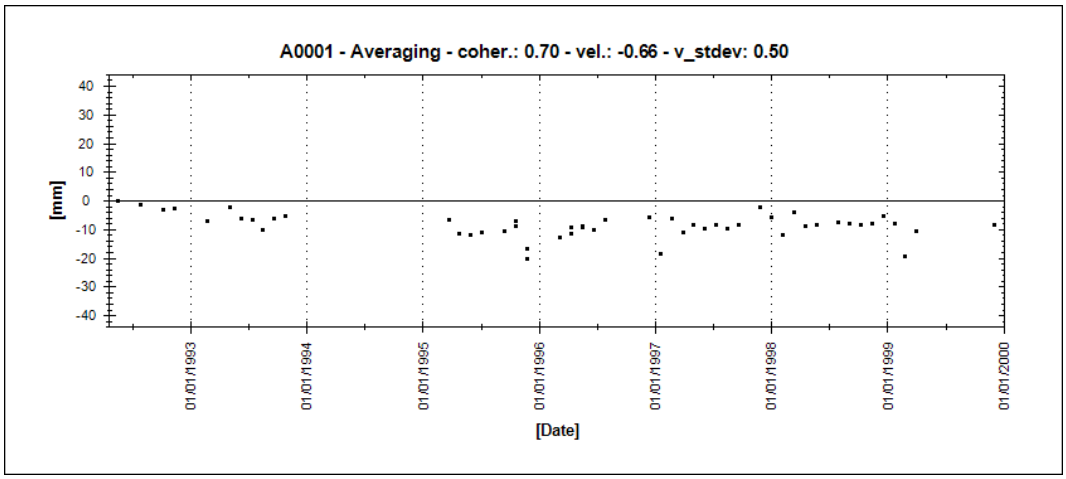

Figure 13: Average time series of all measurement points identified over the Dover 35 reef.

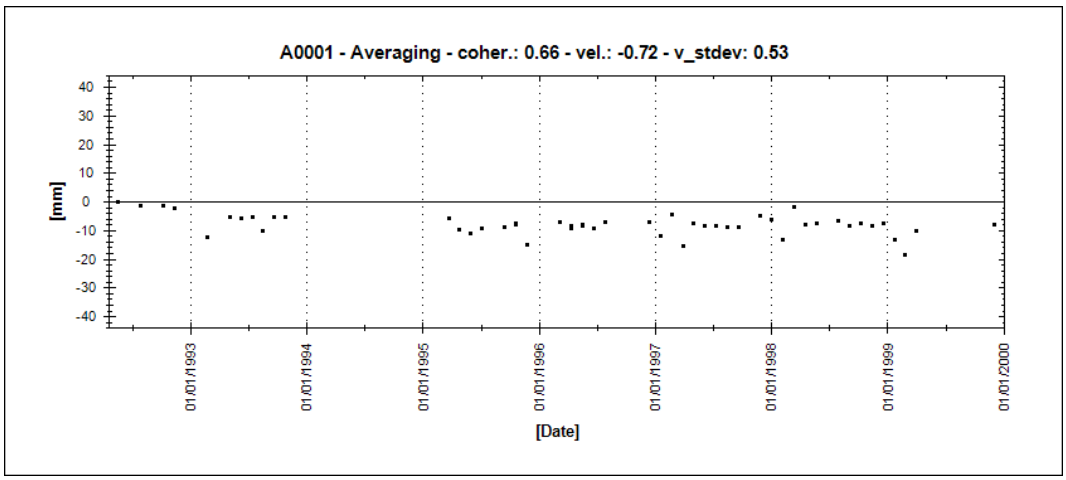

Figure 14: Average time series of all measurement points identified over the Dover 36 reef.

6.2.1 Dover Field

Figure 15 shows the displacement results obtained over the Dover field and surrounding area within four defined regions. The group time series for Zone 1, 2 and 4 indicate mild surface uplift (Figure 16, Figure 17 and Figure 19), while the results within the area labeled Zone 3 exhibited substantial subsidence (nearly 40 mm over seven years, Figure 18). Mild uplift can also be observed within the average time series generated using measurement points identified over the entire reef (Figure 12).

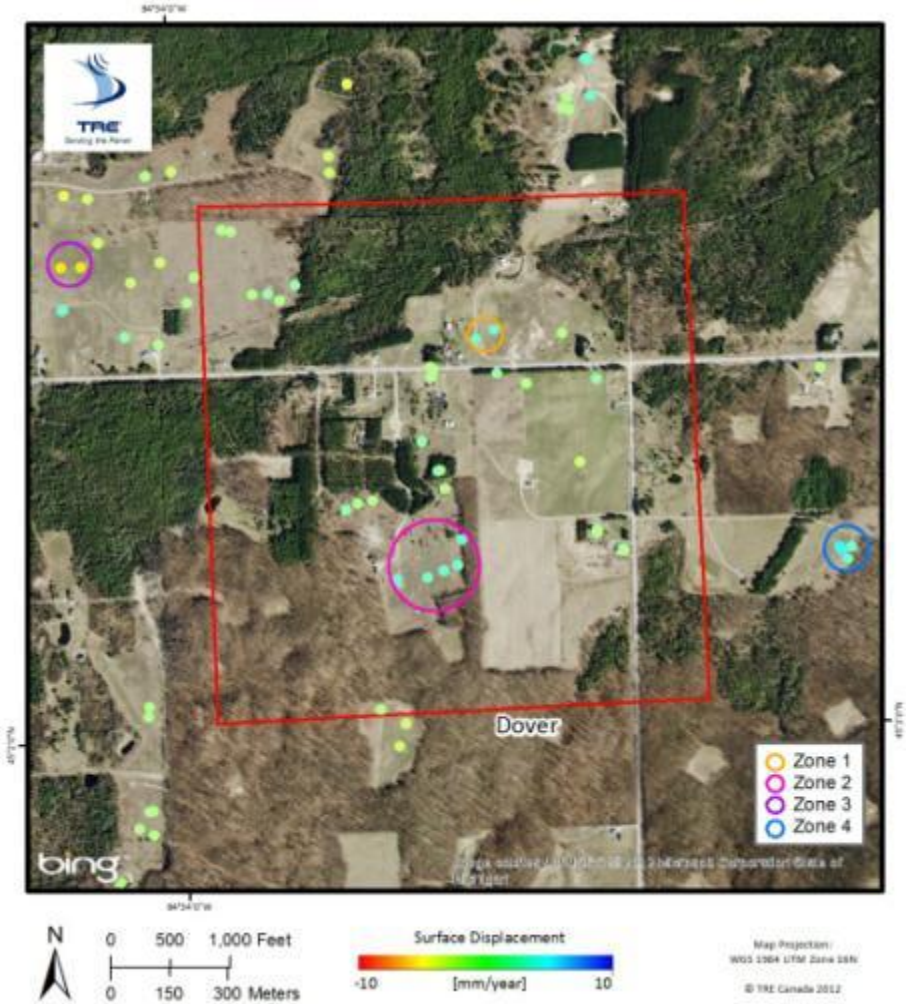

Figure 15: Displacement results obtained over the Dover field with four defined zones of deformation.

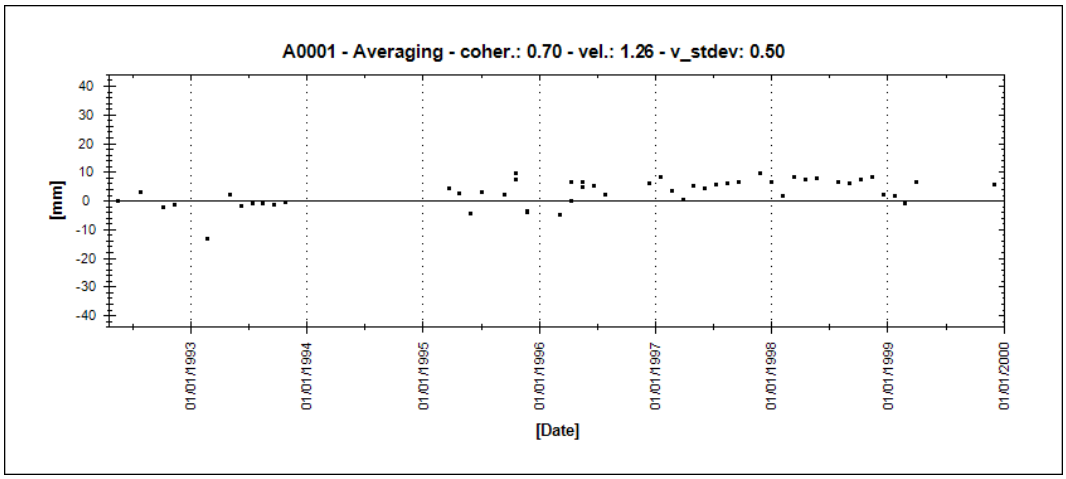

Figure 16: Average time series of measurement points identified within the area labeled Zone 1 in Figure 15.

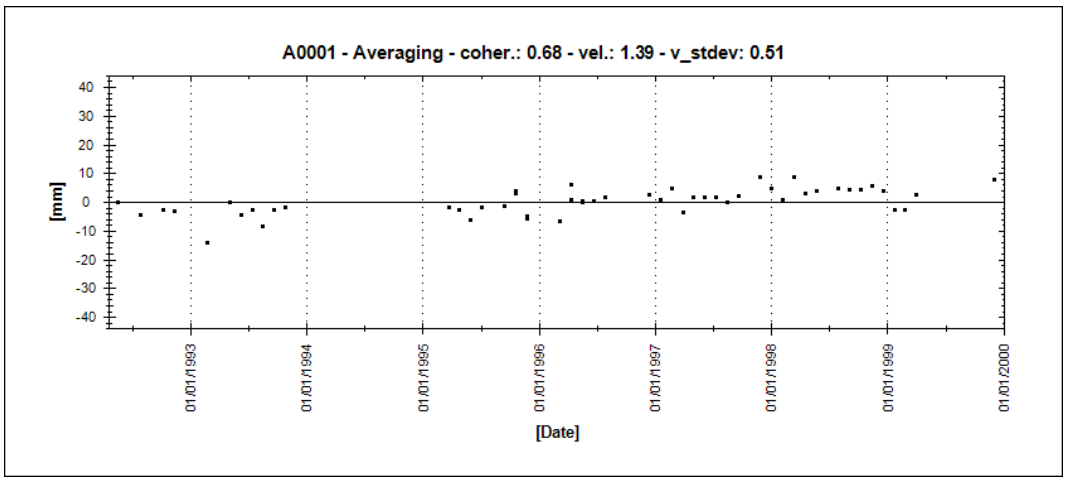

Figure 17: Average time series of measurement points identified within the area labeled Zone 2 in Figure 15.

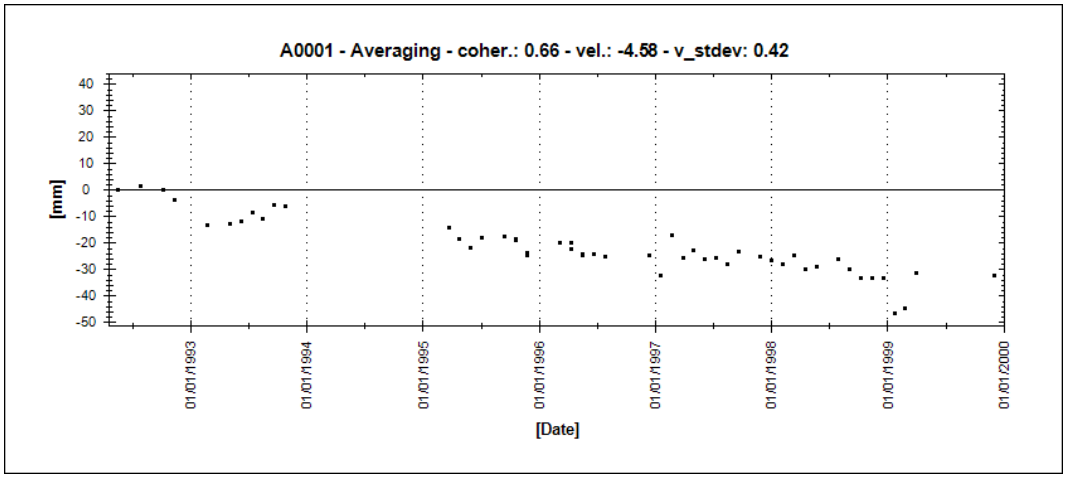

Figure 18: Average time series of measurement points identified within the area labeled Zone 3 in Figure 15.

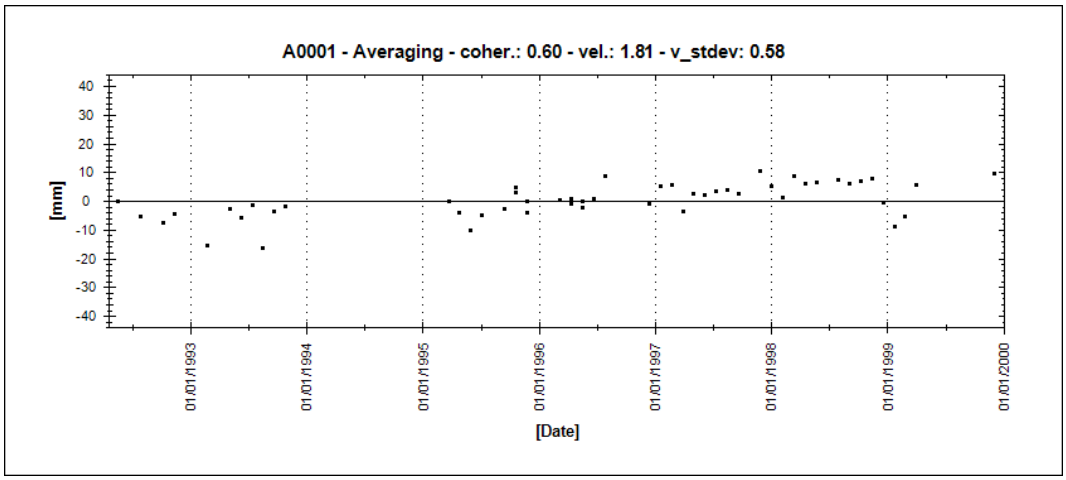

Figure 19: Average time series of measurement points identified within the area labeled Zone 4 in Figure 15.

6.2.2 South Chester Field

Several areas of displacement were also highlighted over the South Chester field (Figure 20). All three areas demonstrated subsidence over the course of the analysis (Figure 21, Figure 22 and Figure 23). The average time series of all points identified within the South Chester field also exhibit subsidence (Figure 24). All group time series appear to exhibit a slightly higher degree of cyclical movement than the results obtained over the Dover reef (Section 6.2.1). It is possible that this pattern may be correlated to seasonal gas storage operations undertaken during this time. Total deformation measured during the historical analysis was significantly larger over the cleared fields (-30 to -40 mm), than movement detected over the structures located in Zone 3 (-10 mm).

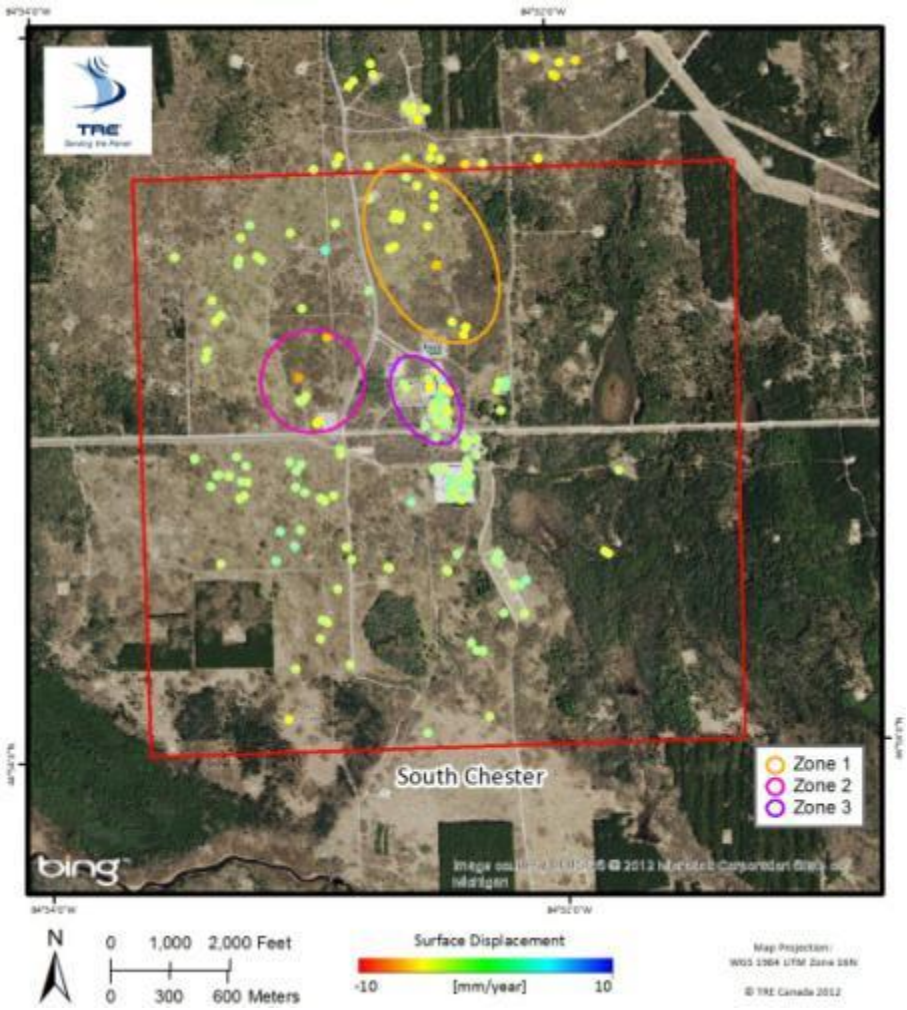

Figure 20: Displacement results obtained over the Chester field with three defined zones of deformation.

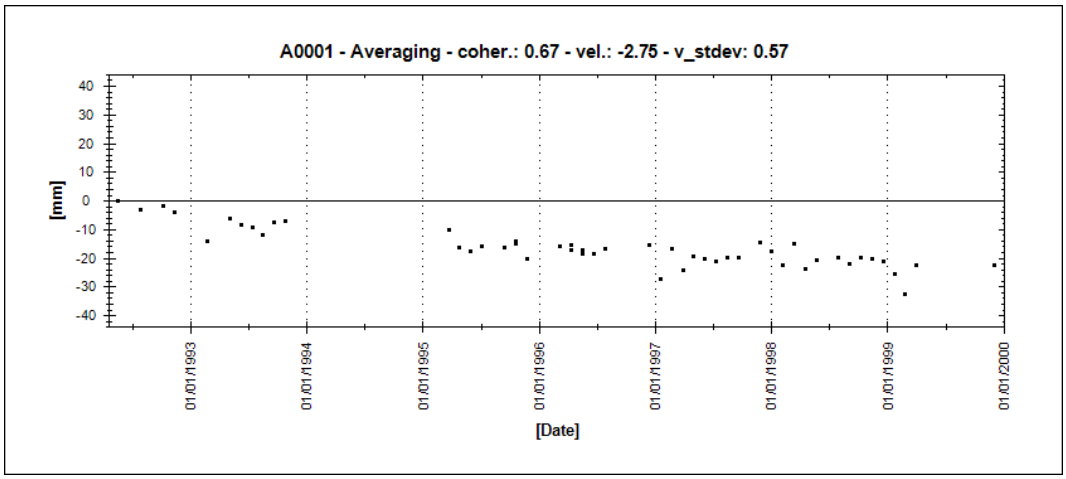

Figure 21: Average time series of measurement points identified within the area labeled Zone 1 in Figure 20.

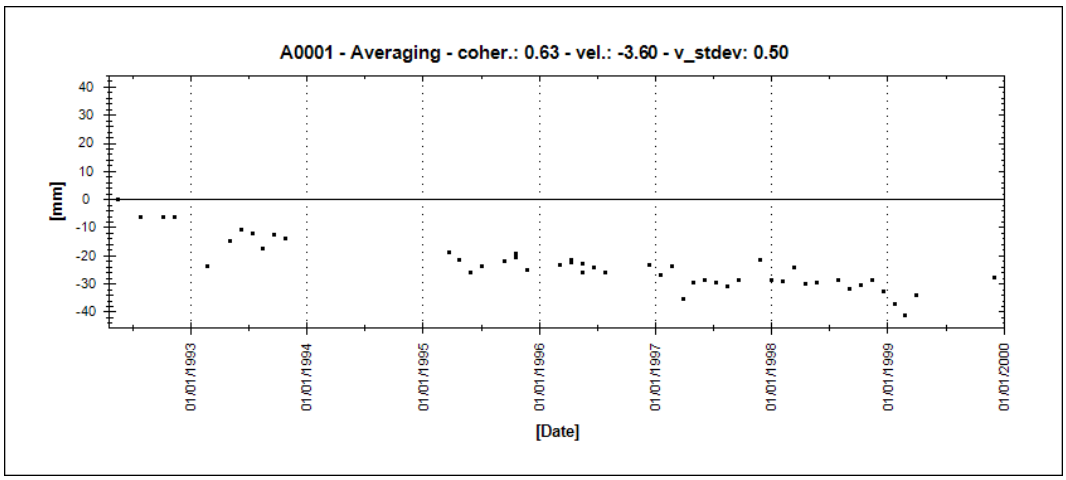

Figure 22: Average time series of measurement points identified within the area labeled Zone 2 in Figure 20.

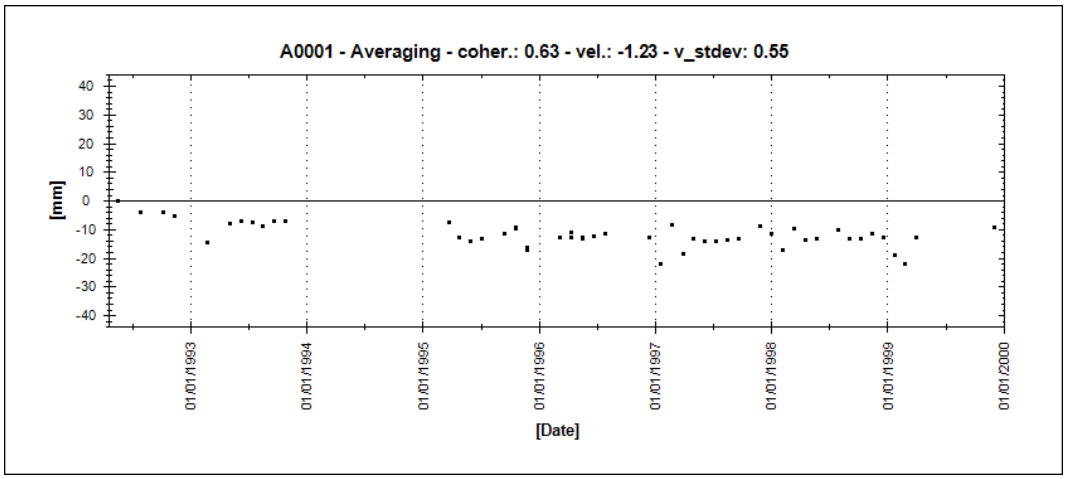

Figure 23: Average time series of measurement points identified within the area labeled Zone 3 in Figure 20.

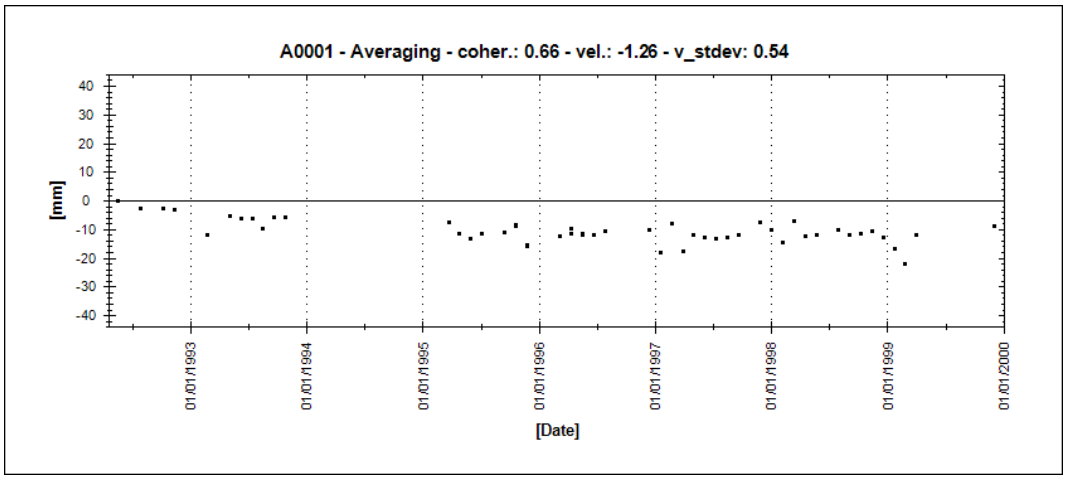

Figure 24: Average time series of all measurement points identified within the South Chester field (red square in Figure 20).

While InSAR is well suited for the identification of general movement patterns occurring over large areas, the precision of this technique and the ability to identify movement from individual features also enables results to be used for localized analyses over fine spatial scales. For instance, Figure 25 below, shows results obtained over a building within the Chester field. Average time series from buildings within this area are shown in Figure 26 and Figure 27.

Figure 25: Deformation results over a local area within the Chester field.

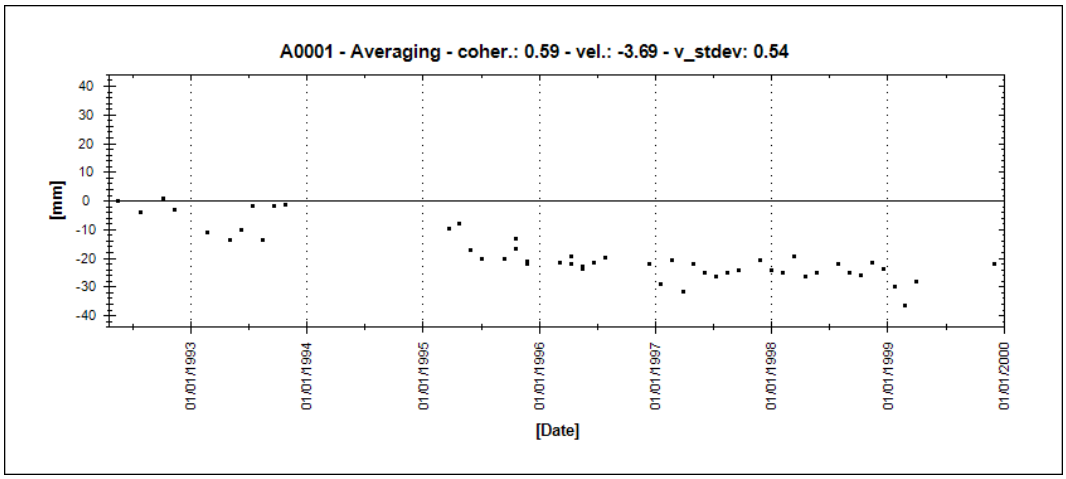

Figure 26: Average time series of measurement points identified within the area labeled Zone 1 in Figure 25.

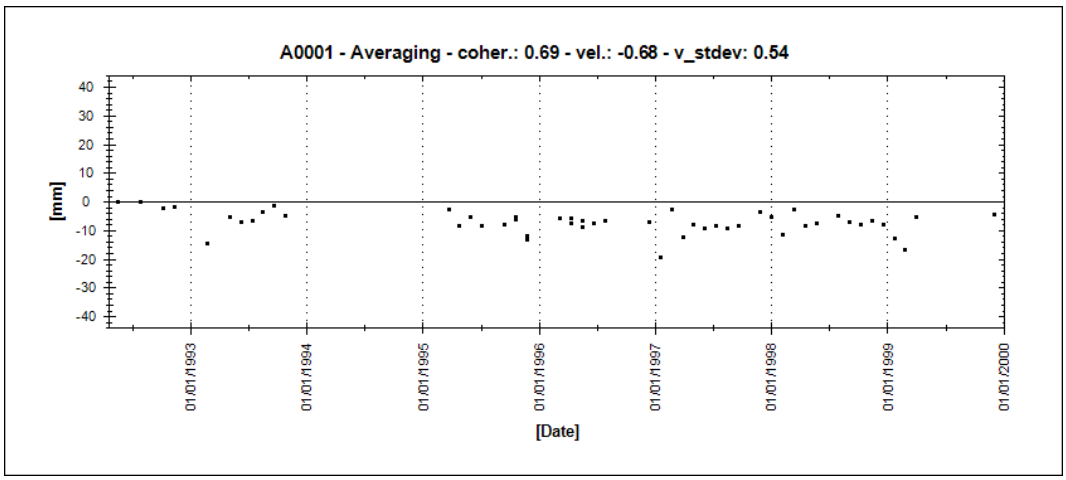

Figure 27: Average time series of measurement points identified within the area labeled Zone 2 in Figure 25.

6.3 Comparison to Gas Storage Operations Data over the Chester Field

Historical operations information provided by Battelle indicate that the Chester gas storage reef was operational beginning in 1980. Records indicate that up to 19.5 Bcf (billion cubic feet) of gas was stored in the summer months (April through October) and then extracted in the winter (November to April) to a minimum storage level of 6.1 Bcf. Therefore, it may be expected that displacement trends would demonstrate uplift in the summer and subsidence in the winter.

This pattern was not clearly identifiable in the measurement points identified over the Chester field. Several gaps in the archive image data set caused by missing acquisitions, combined with the challenging nature of the area for InSAR, meant time series can be challenging to interpret. As a result, it is difficult to isolate the precise timing of cyclical movement patterns. While direct correlations between historic gas storage activities and ground movement cannot be identified, the stronger degree of seasonal fluctuations within measurement points identified in the fields over the Chester reef can be highlighted in comparison to other areas within the Otsego AOI.

6.4 Measurement Point Density and Accuracy

A density of 33 measurement points per square mile was achieved from the InSAR analysis of the historic ERS data set. This is a lower density than typically achieved from InSAR analyses, and is likely due to the challenging ground conditions of this area, the gaps within the data set, and the lower resolution of the older satellite imagery used for this analysis.

Measurement precision is primarily assessed through the associated standard deviation of the displacement rates. The ERS results had an average precision of 0.5 mm/year. The precision of the results is due to the large number of images available and the length of time covered by the analysis.

6.5 Artificial Reflector Placement and Measurement Point Density

The analysis of historical data is also useful as input for the design of the AR network that will be used for monitoring surface deformation during CO_2 injection. The planned locations of all ARs being installed at the Dover site are shown in Figure 28, overlain with the distribution of measurement points identified in the present historical analysis. Figure 28 shows that in some areas, measurement points are located close to ARs; however, TRE does not recommend changing the locations of the reflectors as the processing of a different stack of radar imagery acquired over a more recent period of time will yield a different set of measurement points. Furthermore, 85% of the measurement points within the Dover field are of the Distributed Scatterer (DS) type, meaning they actually represent areas. The placement of the DS will likely shift in future analyses. The most useful application of the historical analysis is to use the results as a general guide for identifying the density and distribution of radar targets.

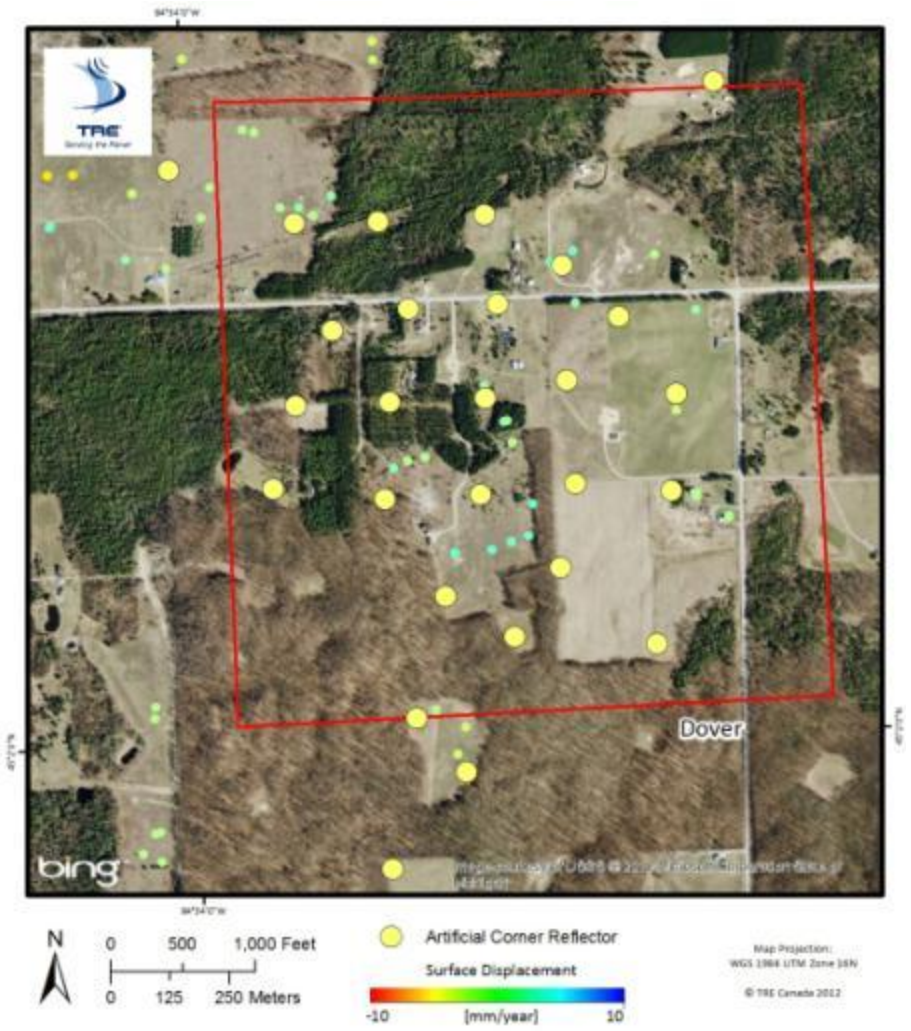

Figure 28: Planned locations of the ARs to be installed over the Dover field overlain with the results of the ERS historical analysis.

7 Summary

The results obtained from the historical analysis over Otsego County, Michigan demonstrated that several areas of slight subsidence or uplift were detected between 1992 and 1999, most notably over the Dover and Chester fields. Results were examined over multiple spatial scales, using average time series to capture general trends and examine seasonal trends, and individual time series to map local movement. Ongoing data is currently being acquired with the Cosmo-SkyMed (CSK) constellation of satellites.

8 Delivery of Data

The deliverables of the SqueeSAR analysis include the present report, the PS data files and a software tool for assisting with the loading, viewing and interrogation of the data in ESRI ArcGIS 10 software. Table 2 lists the files contained on the accompanying CD.

File name	Description
OTSEGO_ERS_D_T269-TSR.dbf	Table containing the height, velocity, velocity standard deviation, acceleration, coherence and time series of all the PS identified in the analysis.
OTSEGO_ERS_D_T269-TSR.SHP	ESRI Shapefile for displaying the database (dbf) file in a GIS environment.
OTSEGO_ERS_D_T269-REF.dbf	The reference point used for the ascending data processing.
OTSEGO_ERS_D_T269-REF.shp	ESRI Shapefile for displaying the reference point file in a GIS environment.
Otsego Historical Analysis Results.mxd	ESRI ArcGIS 10 project containing all PS data and the AOI shapefile.

Table 2: List of delivered files.

The ESRI ArcGIS 10 project file is included to make it easier to view the data. Once the data contained in the CD have been saved to the user's hard drive it will be sufficient to open the project file with ArcGIS and update the links to indicate the new locations of the data.

9 The Structure of the Database Files

Table 3 below, describes the attributes of each PS within the database.

Field	Description
CODE	Unique identification code.
SHAPE	Indicates type of geometry (point).
HEIGHT (m)	Elevation above sea level of the PS.
H_STDEV (m)	Standard deviation of PS elevation value.
VEL (mm/yr)	PS movement rate. Positive values correspond to movement toward the satellite (uplift); negative values correspond to motion away from the satellite (subsidence).
V_STDEV (mm/yr)	Standard deviation of PS deformation rate.
ACC (mm/yr^2)	PS acceleration rate.
A_STDEV (mm/yr2)	Standard deviation of PS acceleration value.
COHERENCE	Quality measure [between 0 and 1].
EFF_AREA (m^2)	Size of the area belonging to the PS. For PS EFF_AREA = 0, for DS EFF_AREA > 0.
D(year/month/day) (mm)	Following the EFF_AREA column are a series of fields that contain the displacement values of successive acquisitions relative to the Master, expressed in mm.

Table 3: Description of the fields contained in the Shapefile.

Appendix 1: Additional Properties of the SqueeSAR results over Otsego County

Radar Data Acquisition Geometry

InSAR-based approaches measure surface displacement on a one-dimensional plane, along the satellite line-of-sight (LOS). The LOS angle varies depending on the satellite and on the acquisition parameters while another important angle, that between the orbit direction and the geographic North, is nearly constant.

All images for the present analysis were acquired from an descending orbit (satellite travelling from south to north and imaging to the east). The symbol δ (delta) represents the angle the LOS forms with the vertical and Θ (theta) the angle formed with the geographic north (Figure 29). Table 4 lists the values of the angles for this study.

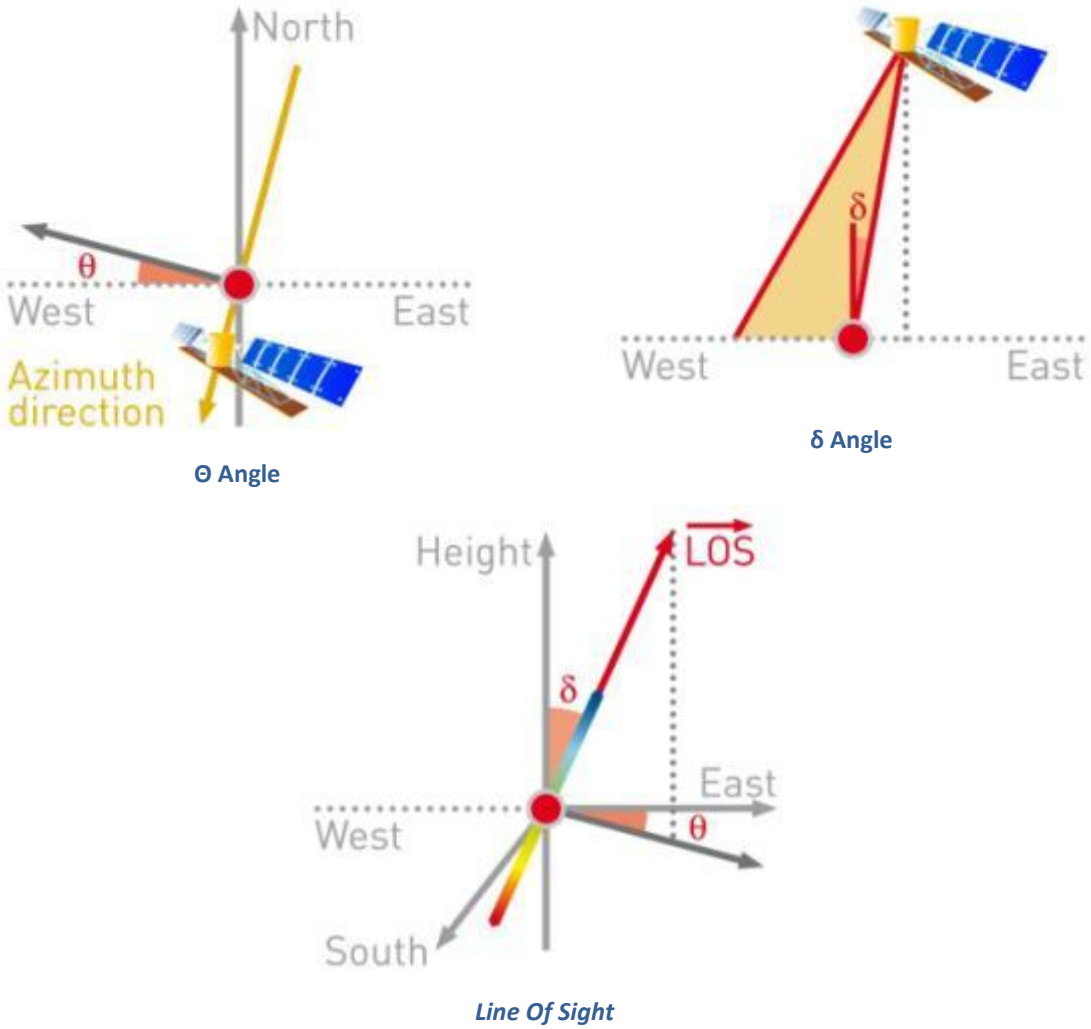

Figure 29: Geometry of the ERS descending image acquisitions over the present site.

Satellite	Symbol	Angle
ERS	δ	22.23°
	θ	10.79°

Table 4: Satellite viewing angles for the ERS historical imagery.

Data Processing

Both permanent scatterers (PS) and distributed scatterers (DS) were identified at this site. Buildings and other man-made structures provide the basis for many PS points in the present SqueeSAR analysis. Many natural features such as rocks or exposed ground were also likely sources of stable PS targets.

DS correspond to large areas (up to hundreds of square meters) and were identified from exposed areas such as abandoned or fallow fields. It is important to consider that while DS are represented as individual points for clarity of presentation and ease of interpretation, these measurements actually correspond to non-point features that are multiple pixels in size. The size of the DS within the AOI range from 1,210 to 16,733 m^2.

Table 5, shown below, provides a summary of the other properties relative to the data processing.

Satellite	ERS1/ERS2
Acquisition geometry	Descending
Analysis time interval	20 May 1992 – 04 December 1999
Number of scenes processed	51
Georeferencing	PS aligned on Bing Maps
Projection system used / datum	WGS 1984 UTM Zone 16 N
Reference Point location	NORTH: 4984272.1239 EAST: 689691.4742
Area of interest	31 $mile^2$ (80 km^2)
Number of Measurement Points Number of PS Number of DS	**1037** 155 882
Average PS density	34 PS and DS/ $mile^2$ (13 PS and DS/km^2)

Table 5: Statistics of the ERS processed data.

Standard Deviation and Precision

Standard deviation values of the displacement measurements are a function of the factors listed below and of local ground movement dynamics.

- Spatial density of the PS and DS (higher densities produce higher precisions)
- Quality of the radar targets (signal-to-noise ratio levels)
- Distance from the reference point
- Number of images processed
- Period of time covered by the imagery
- Climatic conditions at the time of the acquisitions
- Distance between the measurement point and the reference

In addition to each measurement point having an associated standard deviation value to represent the error of the displacement measured, results can also be characterized by the accuracy of the technique. Specifically, three parameters are used to characterize the overall accuracy of the results:

- Precision of the estimated deformation rates;
- Precision of the estimated elevations;
- Precision of the geocoding.

Table 6 summarizes the typical precision values applicable to PS located within 2 km from the reference point when **at least 45 radar images** have been processed.

DEFORMATION RATE	< 1 [mm/yr]
DISPLACEMENT ERROR (single displacement between contiguous satellite images)	< 5 [mm]
ELEVATION	± 1.5 [m]
POSITIONING ERROR ALONG EAST DIRECTION	± 3 [m]
POSITIONING ERROR ALONG NORTH DIRECTION	± 2 [m]

Table 6: Measurement accuracies for PS located within 2 km of the reference point, based on the processing of at least 45 SAR images.

Appendix 2: InSAR Processing

InSAR

Interferometric Synthetic Aperture Radar, also referred to as SAR interferometry or InSAR, is the measurement of signal phase change (interference) between radar images. When a point on the ground moves, the distance between the sensor and the point changes, thereby producing a corresponding shift in signal phase. This shift is used to quantify the ground movement.

An interferogram is a 2D representation of the difference in phase values. Variations of phase in an interferogram are identified by fringes, colored bands that indicate areas where and how much movement is occurring. The precision with which the movement can be measured is usually in the centimetre (cm) range as the phase shift is also impacted by topographic distortions, atmospheric effects, and other sources of noise.

DInSAR

When InSAR is used to identify and quantify ground movement the process is referred to as Differential InSAR (DInSAR). In DInSAR topographic effects are removed by using a DEM of the area of interest to create a differential interferogram.

Differential InSAR is still impacted by atmospheric effects, as there is no method for removing this signal phase contribution. It is a useful tool for identifying footprints of progressing movement and creating deformation maps. The limitations of DInSAR are its relatively low precision (cm scale) and that it cannot distinguish between linear and non-linear motion.

PSInSAR™

Permanent Scatterer SAR Interferometry is an advanced form of DInSAR. The fundamental difference is that it uses multiple interferograms created from a stack of at least 15 radar images.

Permanent Scatterer SAR Interferometry was developed to overcome the errors produced by atmospheric artifacts on signal phase. The PSInSAR algorithm automatically searches the interferograms for pixels that display stable radar reflectivity characteristics throughout every image of the data set. In PSInSAR these pixels are referred to as Permanent Scatterers (PS). The result is the identification of a sparse grid of point-like targets on which an atmospheric correction procedure can be performed. Once these errors are removed, a history of motion can be created for each target, allowing the detection of both linear and non-linear motion.

The result is a sparse grid of PS that are color-coded according to their deformation rate and direction of movement. The information available for each PS includes its deformation rate, acceleration, total deformation, elevation, coherence as well as a time series of movement. The PSInSAR algorithm measures ground movement with millimetre accuracy.

SqueeSAR™

Permanent Scatterers are objects, such as buildings, fences, lampposts, transmission towers, crash barriers, rocky outcrops, etc, that are excellent reflectors of radar microwaves. However, TRE has noticed that many other signals are present in the processed data. These do not produce the same high signal-to-noise ratios of PS but are nonetheless distinguishable from the background noise. Upon further investigation it was found that the signals are reflected from extensive homogeneous areas where the back-scattered energy is less strong, but statistically consistent. These areas have been called distributed scatterers (DS) and correspond to rangeland, pastures, bare earth, scree, debris fields, arid environments, etc (Figure 30).

The SqueeSAR algorithm was developed to process the signals reflected from these areas. As SqueeSAR incorporates PSInSAR no information is lost and movement measurement accuracy is unchanged.

The SqueeSAR algorithm also produces improvements in the quality of the displacement time series. The homogeneous areas that produce DS normally comprise several pixels. The single time series attributed to each DS is estimated by averaging the time series of all pixels within the DS, effectively reducing noise in the data.

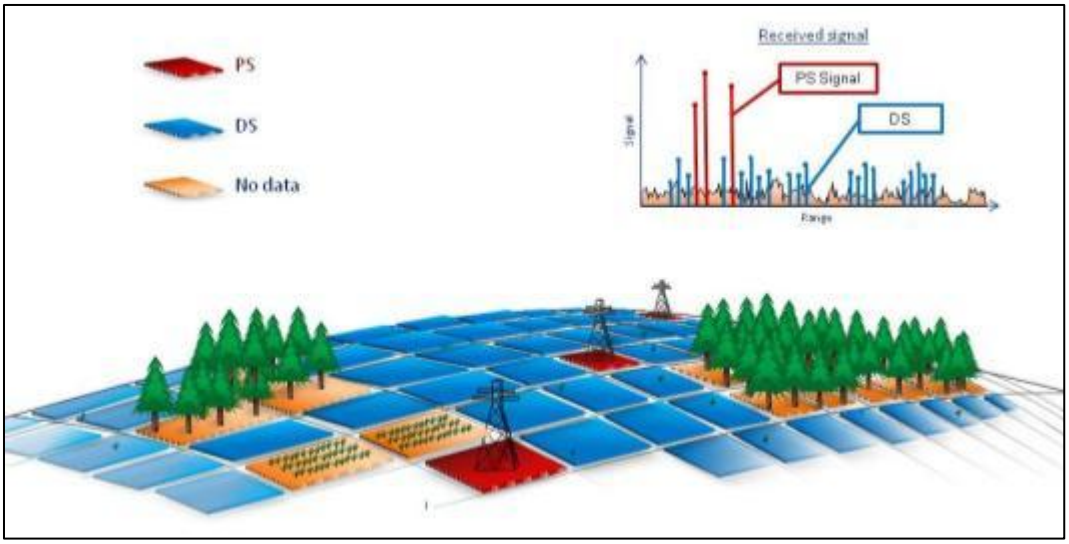

Figure 30: Illustration of the identification of permanent (PS) and distributed scatterers (DS) by the SqueeSAR algorithm.

Appendix 3: Data Processing

Methodology

The identification of PS and DS in a series of radar images comprises a sequence of steps.

First, all radar data archives are screened to determine the most suitable source of raw data for the particular area of interest and to select all the high quality images within the chosen data set.

As the signal echo from a single point target contains many returning radar pulses it appears defocused in a synthetic aperture radar (SAR) raw image. The first processing step is therefore to focus all the received energy from a target in one pixel. The images are then precisely aligned to each other, or co-registered, and analyzed for their suitability for interferometry. The parameters that are analyzed are the normal baseline and the temporal distribution of the images.

There then follows a number of statistical analyses on the phase and amplitude characteristics of the backscattered radar signal that return to the satellite. If a concentrated number of signals reflect off a particular feature within a pixel and backscatter to the satellite, the feature is referred to as a 'scatterer'. When the same scatterer appears in all, or most, of a data set of SAR images of a particular location, then the scatterer is deemed to be 'permanent'.

At this stage it is possible to identify a subset of pixels, referred to as Permanent Scatterer Candidates (PSC), that are used to estimate the impact on signal phase of ionospheric, tropospheric and atmospheric effects, as well as possible orbit errors.

Once the signal phase has been corrected for these effects, any remaining changes in signal phase directly reflect ground movement.

Master Image Selection

SqueeSAR requires that one image (or scene) in each data set has to become both a geometric and temporal reference to which all the other images are then related. This image is referred to as the master image and those that remain are slave images.

The master image should be chosen according to the following criteria:

- it minimizes the spread of normal baseline values for the slave images;
- similarly, it minimizes the temporal baseline values between the master and each slave image; and
- it minimizes the effects of signal noise arising from changes in vegetation cover and/or small changes in the look angle of the satellite from one scene to another.

Signal Phase and Amplitude Analysis

General

Each pixel of a SAR image contains information on the amplitude of signals that are backscattered toward the satellite, as well as on the signal phase. The amplitude is a measure of the amount of the radar pulse energy reflected, while the phase is related to the length of the path of the electromagnetic wave, from the platform to the ground and back again.

Analyses of both amplitude and phase of the SAR image provide an indication of the stability of each pixel, over time, whereby it is possible to identify those pixels that are most likely to behave as Permanent Scatterers. Statistical methods are used extensively in this process.

Among the different statistical parameters that can be computed two are of particular interest: the Phase Stability Index (PSI), obtained from the phases of the images within the data set, and the Multi Image Reflectivity (MIR) map, derived from the amplitude values of the available acquisitions.

Radar phase and coherence

In standard SqueeSAR analyses, the phase stability is strongly linked to the concept of coherence. Pixels that consistently display high phase stability are said to be coherent. Coherence is measured by an index that ranges from 0 to 1. When a pixel is completely coherent, it will have a coherence value of 1. Correspondingly, if a pixel has a low phase stability, its coherence index will be 0. In general, interferometry is successful when the coherence index lies between 0.5 and 1.0.

Radar amplitude and multi-image reflectivity

The amplitude of a pixel within a SAR image is the aggregate of the backscattered energy toward the satellite from within the pixel's equivalent land area. This equivalent land area is referred to as the radar resolution, and in the case of the ERS and RSAT satellites, it measures about 20 m by 4 m, and 7 m by 5 m, respectively. It is necessary to look into the amplitude values of all the images in the data set, in order to understand exactly what was seen by the satellite at the time of each acquisition.

If a target has experienced significant change in its surface characteristics it will exhibit variation in its reflectivity (electromagnetic response) between two acquisitions. In such circumstances, the possibility of detecting movement by means of SAR interferometry is seriously compromised. The signal phase difference between the two images now contains not only the contribution due to displacement, but also that due to the change in the reflectivity of the target. This prevents, in the worst case, the obtaining of any useful information on ground movement.

Accordingly, it is necessary to look into the amplitude values of all the images in the data set, in order to understand exactly what was seen by the satellite at the time of each acquisition.

Another artifact linked to amplitude is known as speckle. Speckle is random noise that appears as a grainy salt and pepper texture in an amplitude image. This is caused by random interference from the multiple scattering returns that occur within each resolution cell. Speckle has an adverse impact on the quality and usefulness of SAR images. However, the higher the number of images taken of the same area at different times or from slightly different 'look' angles, the easier it is to reduce speckle. This increases the quality and level of details of the amplitude image enabling it to be used as a background layer for observing the presence of PS results.

The Multi Image Reflectivity (MIR) map is the means by which speckle reduction is accomplished. Averaging a number of images tends to negate the random amplitude variability, leaving the uniform amplitude level unchanged.

It should be emphasised that the information in the MIR map is the reflectivity of each pixel, i.e. the ability to backscatter the incident wave toward the satellite. Flat surfaces (roads, highway, rivers, lakes) act like a mirror, meaning that if their orientation is not exactly perpendicular to the incident wave negligible energy is reflected back to the sensor; they appear dark in the image. On the other hand, because of their irregular physical shape, metal structures or buildings reflect a significant portion of the incident signal back to the radar, resulting in very bright pixels in the MIR map.

Interferograms

After the statistical analyses of the SAR images have been completed, a set of differential interferograms is generated. This entails subtracting the phase of each slave image from the phase of the master image. In doing so, the difference in signal path length between the two images is calculated. This difference is related to possible ground motion.

In any SAR image, there are embedded topographic distortions that arise during image acquisition. These are removed using a reference Digital Elevation Model (DEM), leaving ground movement and the signal phase distortions arising from atmospheric effects as the only embedded variables.

The differential interferograms represent the starting point for applying the PSInSAR approach.

Estimation of the Atmospheric Effects

When a radar signal enters and exits a moisture-bearing layer in the atmosphere, its wavelength can be affected, introducing potential errors into the signal path length. The removal of atmospheric impacts is fundamental for increasing the precision of ground movement measurement.

A sub-set of pixels, usually corresponding to buildings, lampposts, antennas, small structures and exposed rocks, is chosen from among those that have high PSI values. These are referred to as PS Candidates (PSC). PSC density is, of course, higher in towns and cities rather than in forests and vegetated areas. However, it is often possible to obtain good PSC density in rural areas.

For each image, the atmospheric impacts are estimated at each PSC location. The process is statistically based and benefits in accuracy by the greater the number of available images for the analysis. By comparing the atmospheric contribution on neighboring pixels that would be experiencing the same atmospheric conditions, the atmospheric contribution can be reconstructed over the whole image.

The processed data set allows identification of a PSC cluster dense enough to identify and extract the atmospheric contribution over the entire area of interest.

Post-processing

In this stage the processed data undergoes a thorough quality control following ISO 9001:2000 guidelines. The PS data is checked for anomalies, aligned on an optical image layer usually provided by the client and the final report is prepared.

Appendix 4: Abbreviations and Acronyms

AOI	Area Of Interest
DEM	Digital Elevation Model
DS	Distributed Scatterer(s)
DInSAR	Differential Interferometric SAR
GIS	Geographic Information System
InSAR	Interferometric SAR
LOS	Line Of Sight
PS	Permanent Scatterer(s)
PSInSAR	Permanent Scatterers SAR Interferometry is a world-wide POLIMI Trademark
SAR	Synthetic Aperture Radar
SqueeSAR	The most recent InSAR algorithm patented by TRE
TRE	Comprehensive term for Tele-Rilevamento Europa and TRE Canada
TS	(Permanent Scatterer Displacement) Time Series

TRE Canada Inc.
475 West Georgia Street, Suite 410
Vancouver, B.C., V6B 4M9
Canada

Tel. 604 331-2512
www.trecanada.com

Appendix B.

Baseline Analysis

TRE®
Sensing the Planet

InSAR Baseline Analysis

For the Monitoring of Ground Movement over Otsego County, Michigan

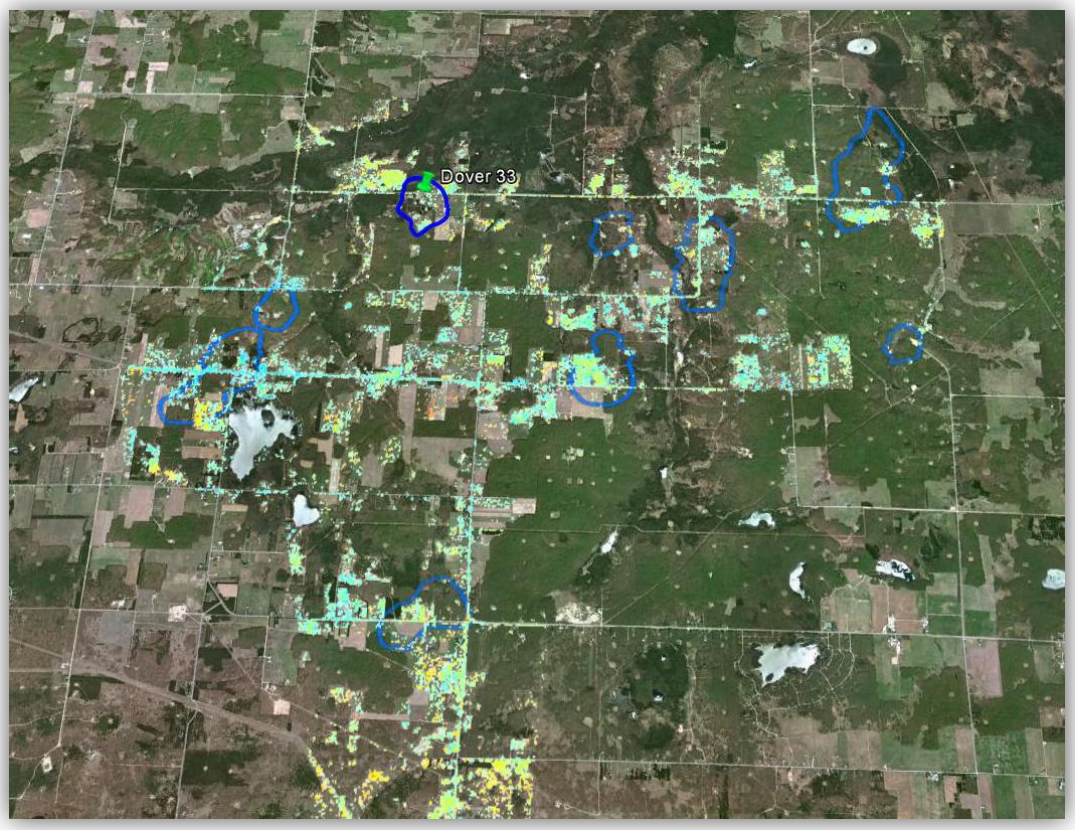

Submitted to:
Lydia Cumming
Battelle
505 King Avenue
Columbus, Ohio 43201

Prepared by:
TRE Canada Inc.
Doc. Ref.: JO12-3008-REP2.0

21 December 2012

Prepared by: Jessica Morgan
GIS Analyst
TRE Canada Inc.

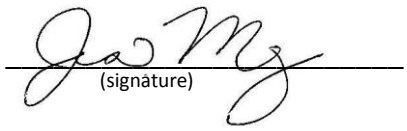
(signature)

Vicky Hsiao
GIS Analyst
TRE Canada Inc.

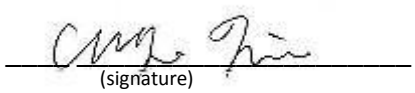
(signature)

Approved by: Giacomo Falorni
Operations Manager
TRE Canada Inc.

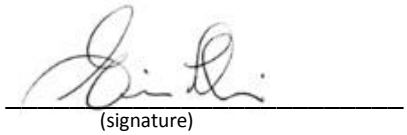
(signature)

Executive Summary

This report describes the approach and results of the baseline analysis carried out on the first six months of Cosmo-SkyMed radar imagery acquired over Otsego County, Michigan. The results provide an overview of ground movement during the time period prior to the start of injection, as well as the density of points that can be identified from InSAR using natural features on the ground for ongoing monitoring.

The following points summarize the key findings of this analysis:

- Most of the area was observed to be stable, with minimal deformation (less than 15 mm of movement) measured during the six-month time period of the baseline analysis.
- Surface displacement results were examined within the boundaries of operational reefs, including the Dover 33 field and the South Chester 15 Gas Storage field (section 6.2). Results were also examined according to well location and type (section 6.3). No large movement trends were identified.
- The short time span (six months) covered by the radar data resulted in an average measurement standard deviation of 3.7 mm/year. The precision will increase with the continued acquisition of imagery over a longer time period. Ground movement will also become better characterized during the Phase 3 period.
- A density of 545 PS and DS per square mile (211 PS and DS per square kilometer) was achieved from the analysis of the CSK baseline data set, in comparison to a density of 33 PS and DS per square mile identified from the historical ERS analysis.

The deliverables for this stage of the project include the present report, which describes the results of the data processing, and a CD containing the displacement data. Imagery is currently being acquired on a 16-day repeat interval using the Cosmo-SkyMed constellation of satellites.

Table Of Contents

1 Background

The Battelle Memorial Institute (Battelle) is an independent, not-for-profit research and development organization that is currently heading the Mid-West Regional Carbon Sequestration Partnership (MRCSP). The MRCSP is focused on the investigation of the geological suitability of the north-west United States for carbon capture utilization and storage (CCUS), as part of a larger Department of Energy strategy for developing CO_2 emission reduction strategies. Now entering the development phase of this research project, the Dover 33 reef (a late stage enhanced oil recovery reservoir) in Otsego County in the northern Michigan Basin has been selected as a research and demonstration site for the investigation of CCUS strategies over the next several years.

As part of a comprehensive monitoring program being implemented during the injection process, InSAR is being used to map surface response to CO_2 injection and migration throughout the reservoir. TRE Canada Inc. (TRE) has been contracted by Battelle to provide ongoing InSAR monitoring of ground movement at this site and the surrounding area. This report details the results of the initial data processing with an objective to identify baseline movement trends in the area prior to the start of injection, and to assess the density and distribution of measurement points. TRE's proprietary SqueeSAR™ algorithm was used to perform the analysis of ground movement at this site using the 22 images collected at the time of data processing.

2 Overview of the Area of Interest

The area of interest (AOI) as indicated by Battelle has a surface area of 31 square miles (80 square kilometers) and is located east of Gaylord, Michigan in between Lake Michigan and Lake Huron (Figure 1). The majority of the AOI consists of cleared areas, active agriculture and forested regions. While the area is located in a predominantly non-urban environment, there are several man-made objects in the area related to oil and gas operations, houses, roads and other buildings. Measurement points can often be identified from these man-made features, as well as from cleared or sparsely vegetated areas. Forested regions and agricultural areas are more challenging for InSAR as their associated reflectivity changes over time.

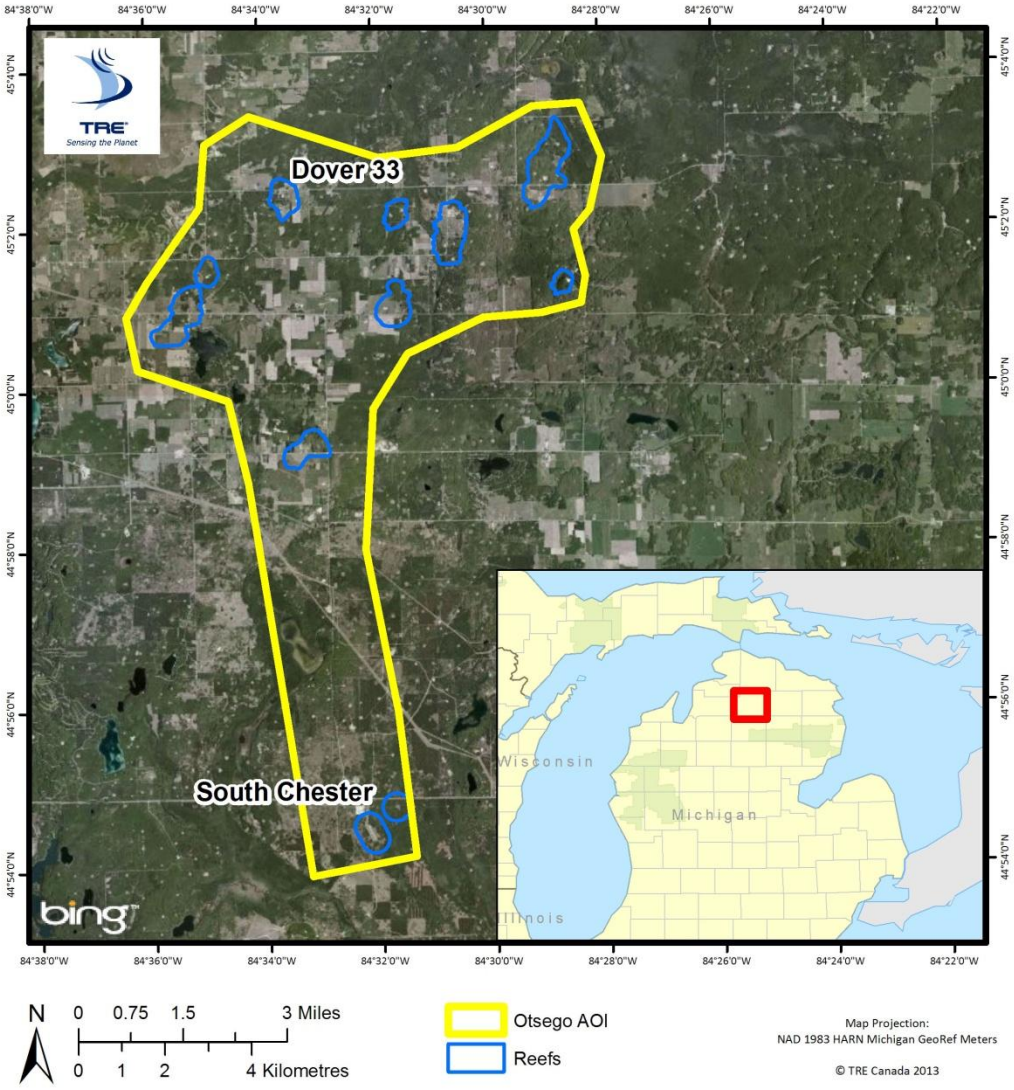

Figure 1: The Area of Interest (AOI) for Otsego County, Michigan as indicated by Battelle.

3 Radar Data

The radar imagery utilized for this baseline analysis consists of 22 images acquired between 22 April 2012 - 23 October 2012 (Table 1). All images in this stack were acquired from Track 191 of the Cosmo-SkyMed constellation of satellites, along a descending orbit (meaning the satellite is travelling from north to south and imaging to the east).

The first four images of the baseline monitoring period were acquired using all four satellites within the CSK constellation. After this point, only two satellites (CSK 1 and CSK 2) were tasked to acquire imagery with a decreased repeat frequency of eight days until the end of September. Currently, images are being acquired with one satellite (CSK 1) on a sixteen day frequency, which will be maintained throughout the remainder of the monitoring period.

The use of a constellation of synchronized satellites allows for data redundancy, meaning missed acquisitions can often be accounted and made up for by activating another satellite within the CSK constellation. Missed acquisitions are most often the result of scheduling conflicts, programmed satellite maintenance or unforeseen outages. Therefore, while a few images were missed over the course of baseline data collection, additional images were acquired using a different satellite within the CSK constellation to avoid gaps in the baseline data set (red and green images highlighted in Table 1).

Further information on InSAR is described in Appendix 2 and 3.

CSK Data			
1	22 April 2012	**12**	19 July 2012
2	23 April 2012	**13**	27 July 2012
3	26 April 2012	**14**	04 August 2012
4	30 April 2012	**15**	12 August 2012
	08 May 2012	**16**	20 August 2012
5	16 May 2012	**17**	28 August 2012
	24 May 2012		05 September 2012
6	01 June 2012	**18**	13 September 2012
7	09 June 2012		21 September 2012
8	17 June 2012	**19**	03 October 2012
9	25 June 2012	**20**	07 October 2012
10	03 July 2012	**21**	16 October 2012
11	11 July 2012	**22**	23 October 2012

Table 1: Dates of the CSK imagery used in the baseline analysis. Images highlighted in red correspond to missed images, while those in green indicate additional images acquired to make up for lost acquisitions.

4 Reference Point

SqueeSAR™ is a differential technique, meaning displacement is measured compared to a reference point that is assumed to be stable. The reference point used for the baseline analysis is shown in Figure 2. This point was selected using an optimization procedure which maximizes the quality of the results based on a suite of radar parameters including high coherence, low standard deviation values and low variability of movement over time. Reference point coordinates for the current analysis are listed in Appendix 1. As the selection of the reference point is based on the overall statistics of the data set, the optimal reference point is the one that shows the most stability over time.

At this early stage of the analysis, the use of one reference point allows for the results to be easily compared throughout the entire AOI, and avoids introducing additional variability into the results. Furthermore, several reference point locations were tested, all of which resulted in an overall decrease in the quality of the results.

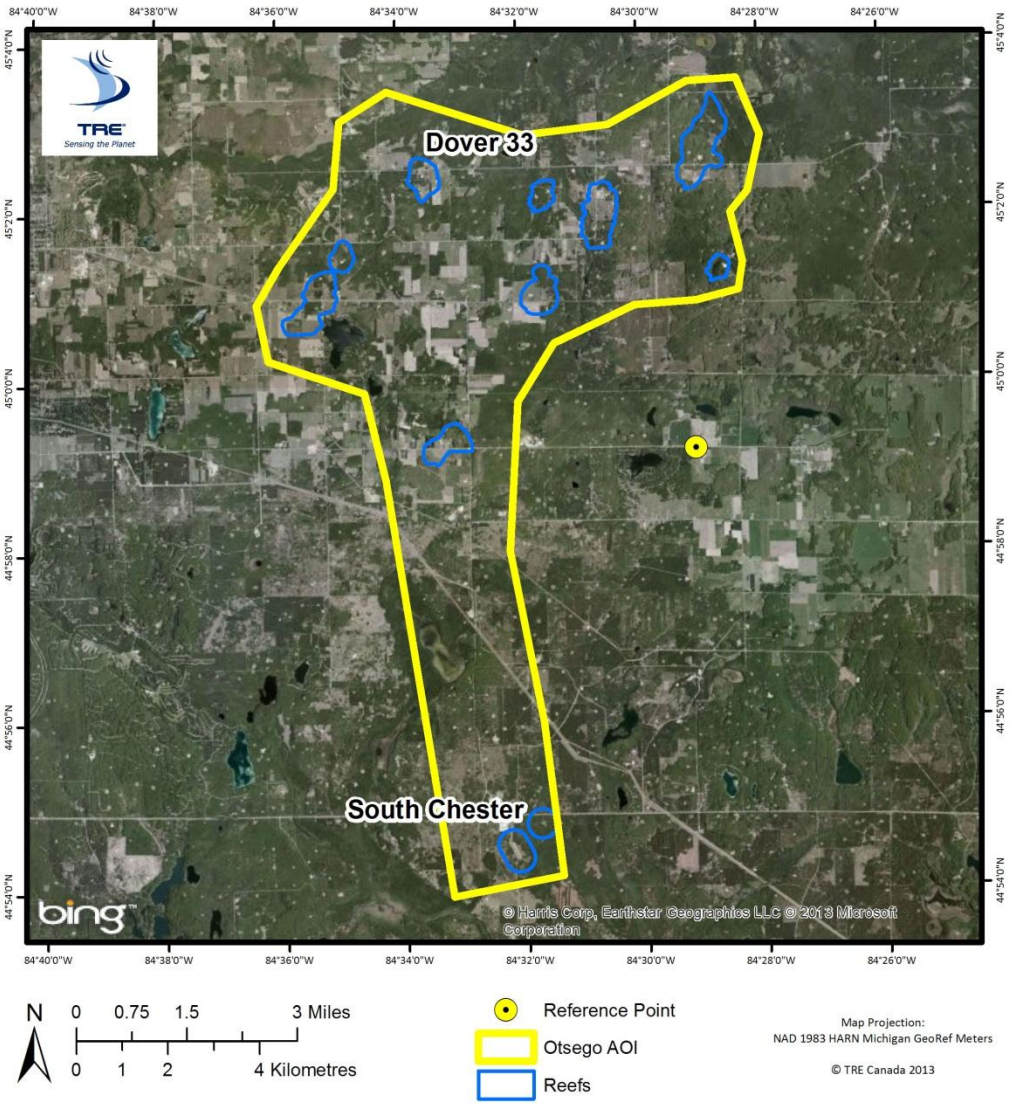

Figure 2: The location of the reference point used for the CSK baseline data set.

5 Results of the SqueeSAR™ Analysis

5.1 Cumulative Displacement

The total amount of displacement measured during the six month time span covered by the radar imagery is shown below, expressed in millimeters (Figure 3). Each point corresponds to a Permanent Scatterer (PS) or Distributed Scatterer (DS), and is color-coded according to the magnitude of total movement. Movement is measured along the satellite line-of-sight (LOS) relative to the first image of the data stack. See Appendix 2 for more information on the SqueeSAR technique and the identification of PS and DS measurement points.

Results indicate that most of the area is stable, with minimal deformation measured during the course of the baseline analysis (less than 15 mm). The only area of movement was over a field located immediately north of South Chester 15 gas storage field, where up -14.4 millimeters (mm) of subsidence was observed.

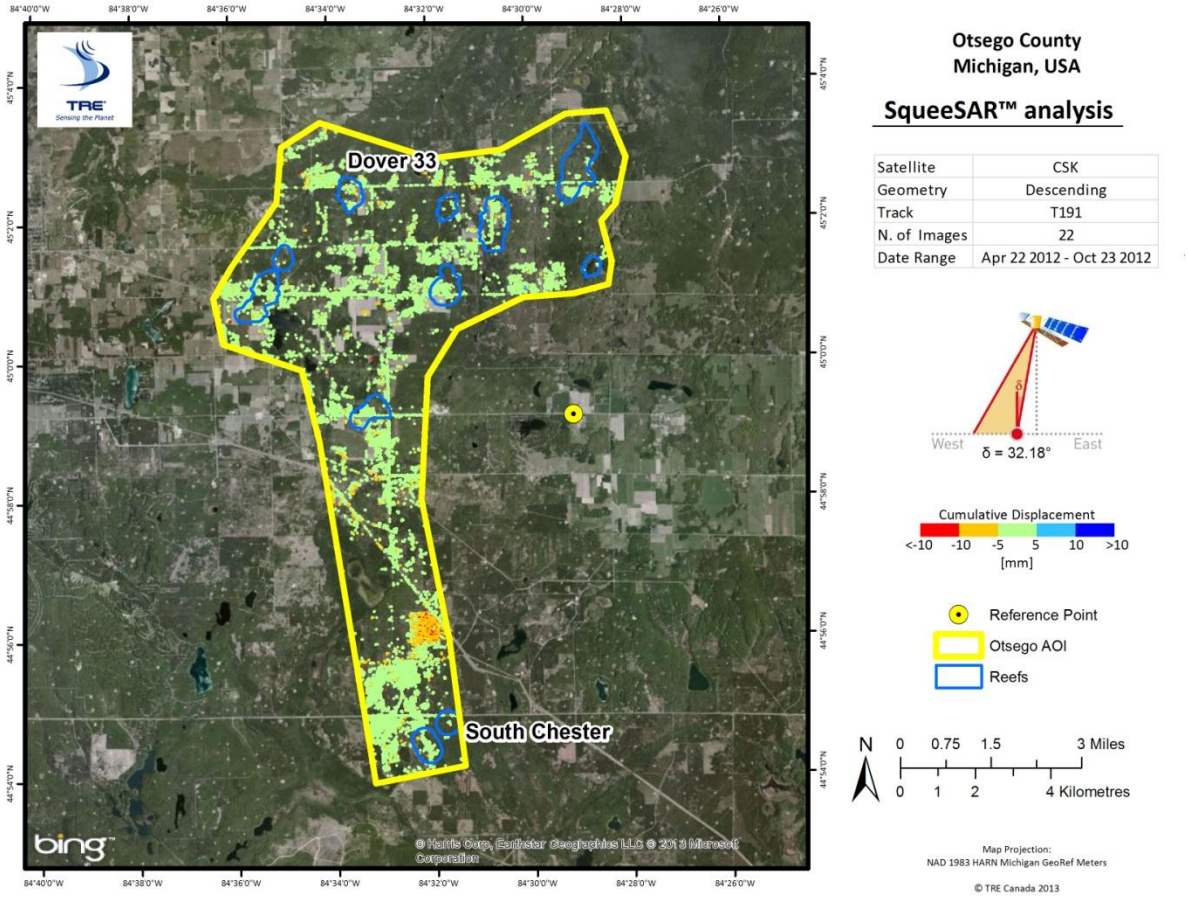

Figure 3: PS and DS cumulative deformation over the baseline period of data collection, expressed in millimeters.

5.2 Displacement Rate

The line-of-sight (LOS) displacement rates, expressed in millimeters per year (mm/yr), as detected from the processing of the dataset is presented in Figure 4. Each point corresponds to a Permanent Scatterer (PS) or a Distributed Scatterer (DS), and is color-coded according to its annual rate of movement. Average displacement values are calculated from a linear regression of the ground movement measured over the entire period covered by the satellite images. Results should be interpreted taking into account their associated standard deviations (see Section 5.3 and 5.4). Detailed information on ground motion is also provided by means of displacement time series, which are provided for each PS and DS (refer to Section 6.2).

In general, the AOI was stable during the baseline time period, with an average surface deformation rate of -1 mm/year identified from all measurement points. Similar to the cumulative displacement results, a zone of subsidence was observed over the field immediately north of the South Chester 15 gas storage field.

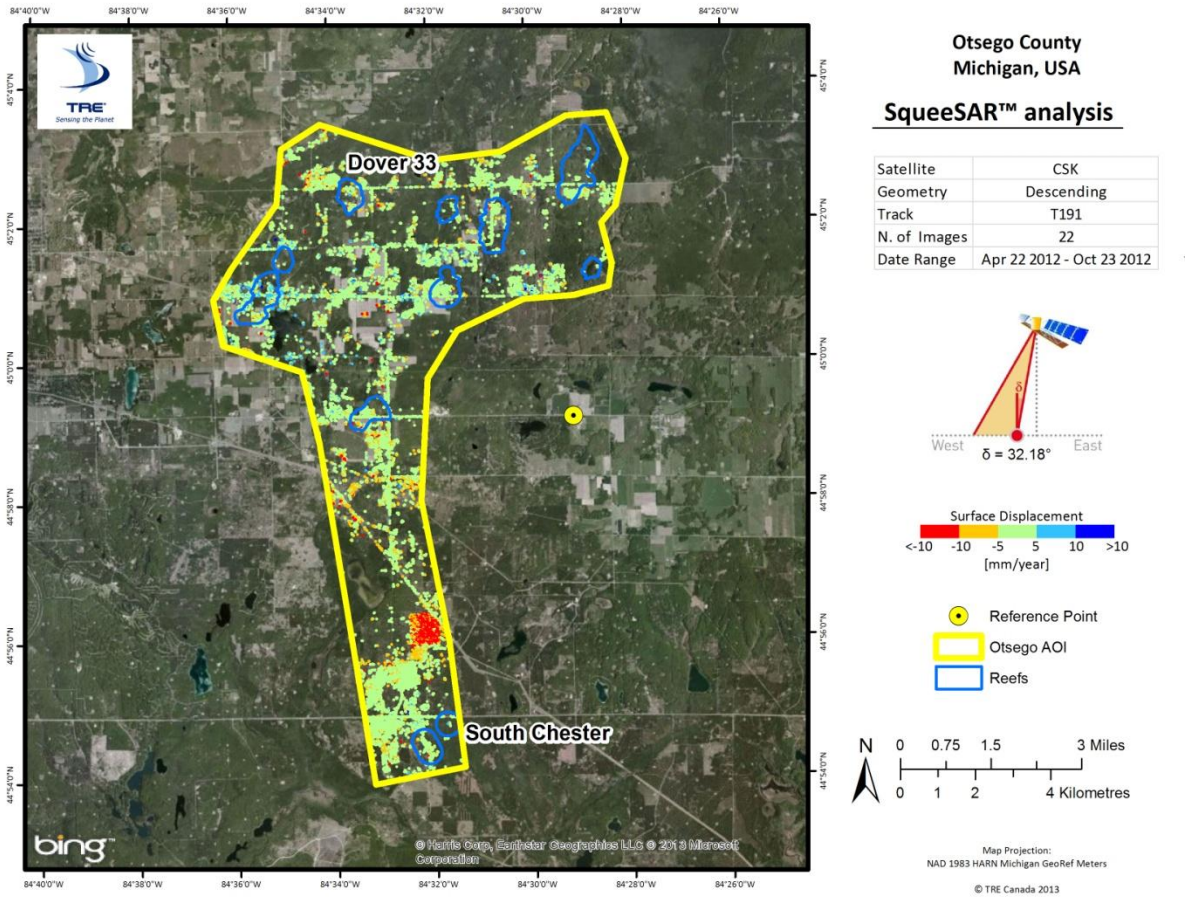

Figure 4: PS and DS deformation rates, expressed in millimeters per year.

5.3 Displacement Rate Standard Deviation

The standard deviation of the surface displacement data characterizes the error of the measurements (Figure 5). The displacement rate for a given point should be read in the form of *Displacement Rate ± Standard Deviation*. Areas impacted by higher standard deviations indicate a greater variability in measured displacement. Additional information on standard deviation can be found in Appendix 1.

The average confidence interval associated with the measured displacement rates is 3.7 mm/year. This rate is slightly higher than the millimeter precision typically associated with InSAR, due to the smaller number of images (22) and the shorter time span covered by the data stack (six months). The precision of the estimated displacement values will increase as more images are acquired over a longer time period.

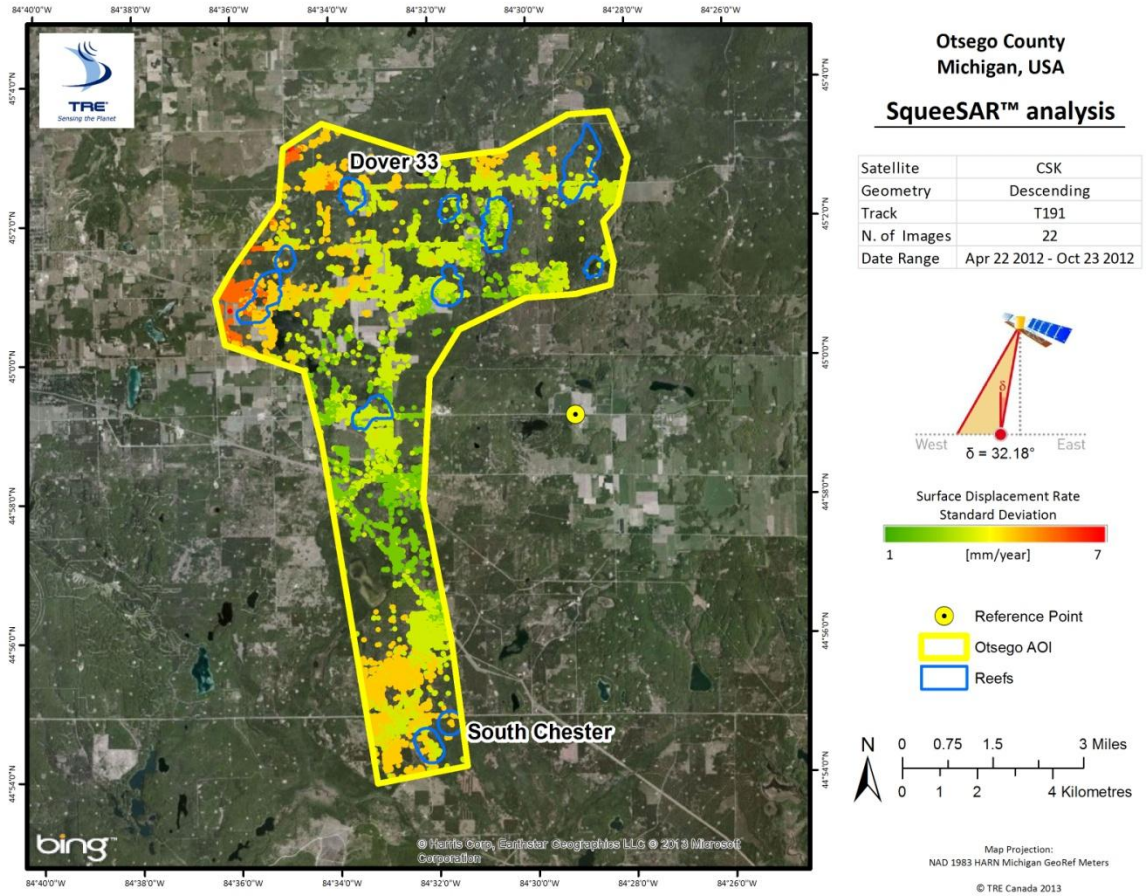

Figure 5: Standard deviation of the displacement rates, expressed in millimeters per year.

5.4 Normalized Displacement Rates

Due to the limited number of images and time span covered by this data set, it is important to interpret the displacement results taking into account their standard deviation. One way in which this can be done is by normalizing the annual displacement rates (Figure 6). The result is a dimensionless index, (obtained by dividing measured ground movement by their associated standard deviation), which can be used to highlight areas where large identified ground movement patterns can be interpreted with a higher degree of confidence.

Normalized results confirm the presence of subsidence within the field located northeast of the South Chester 15 gas storage field, as well as other areas indicating mild uplift or subsidence throughout the remainder of the AOI.

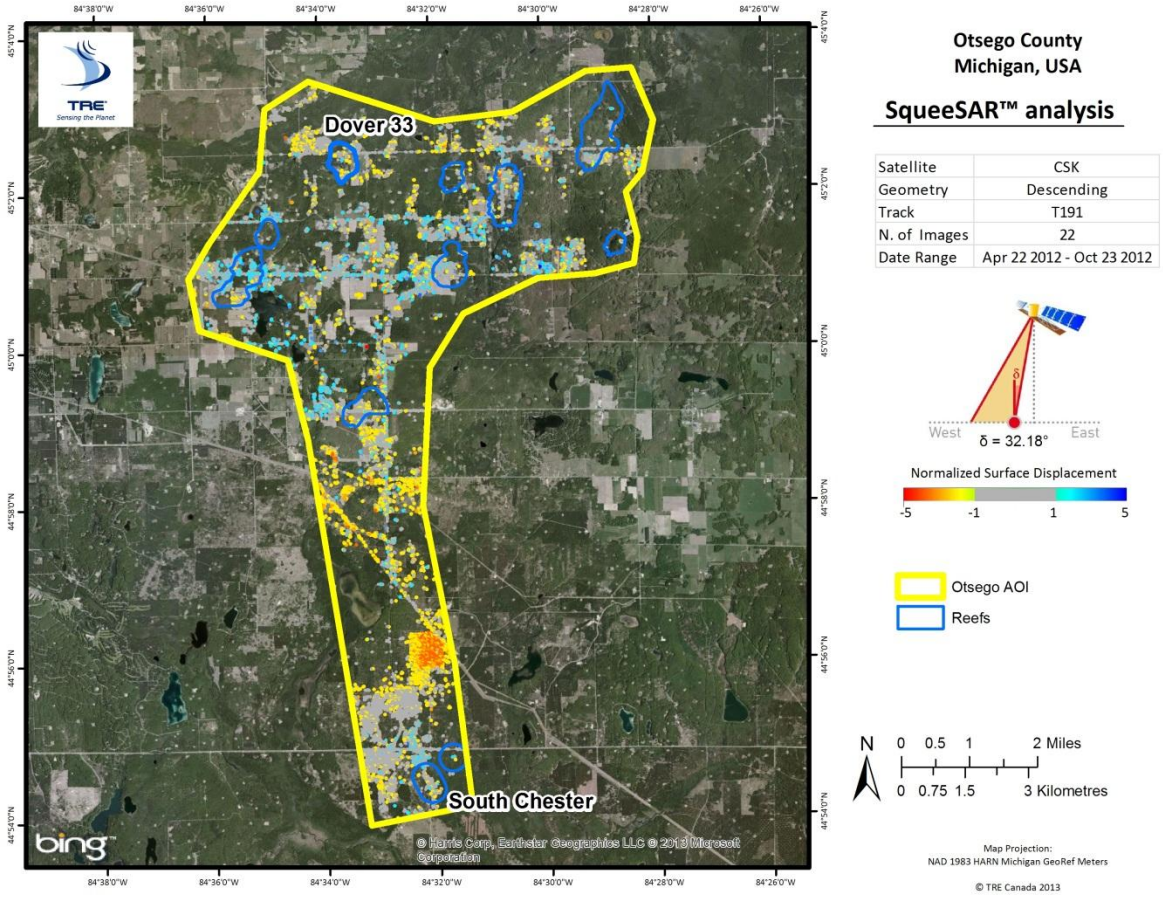

Figure 6: Normalized displacement values.

6 Observations

6.1 Overview of Ground Deformation

The current baseline analysis, conducted using imagery acquired between 22 April 2012 and 23 October 2012, indicates that most of the area is stable. Average displacement rates measured across this region were approximately -1 ± 3.7 mm/year, with most estimated movement rates within the range of their confidence intervals. The maximum amount of total displacement observed within the AOI was less than 15 mm over the six-month time period analyzed.

The slightly larger standard deviation values associated with these results are caused by the small number of images used in the data processing and the short time span of the data. In particular, the accuracy of the annual displacement results will be limited as these values are extrapolated from a data set that span less than one year. Therefore, while the estimated annual surface displacement rates ranged between -26.5 to 15 mm/year, it is important to interpret results taking into consideration their associated standard deviation values (between 1.7 and 6.5 mm/year).

Interpretation should also involve the analysis of groups of measurement points rather than individual points, allowing for a more robust interpretation of cumulative movement in an areas. Group time series were created to show a generalized overview of any movement trends identified within the AOI, particularly for results identified within the spatial boundaries of individual reefs (section 6.2). A brief analysis of baseline ground movement trends identified within close proximity to wells was also undertaken and is described in section 6.3.

6.2 Features of Interest

Movement identified over the nine reefs located across the northern portion of the AOI were examined to highlight any trends occurring during the baseline period of analysis (Figure 7). Average time series, generated by averaging the ground movement measured from all points contained within a specified area, were generated for each reef using the boundaries shown below (Figure 9 to Figure 15, inclusive). In all cases, the average displacement rates identified within each of the reefs indicate stability, and are within the range of their associated confidence interval. Similar patterns of surface displacement were observed for locations both on- and off-reef within the AOI.

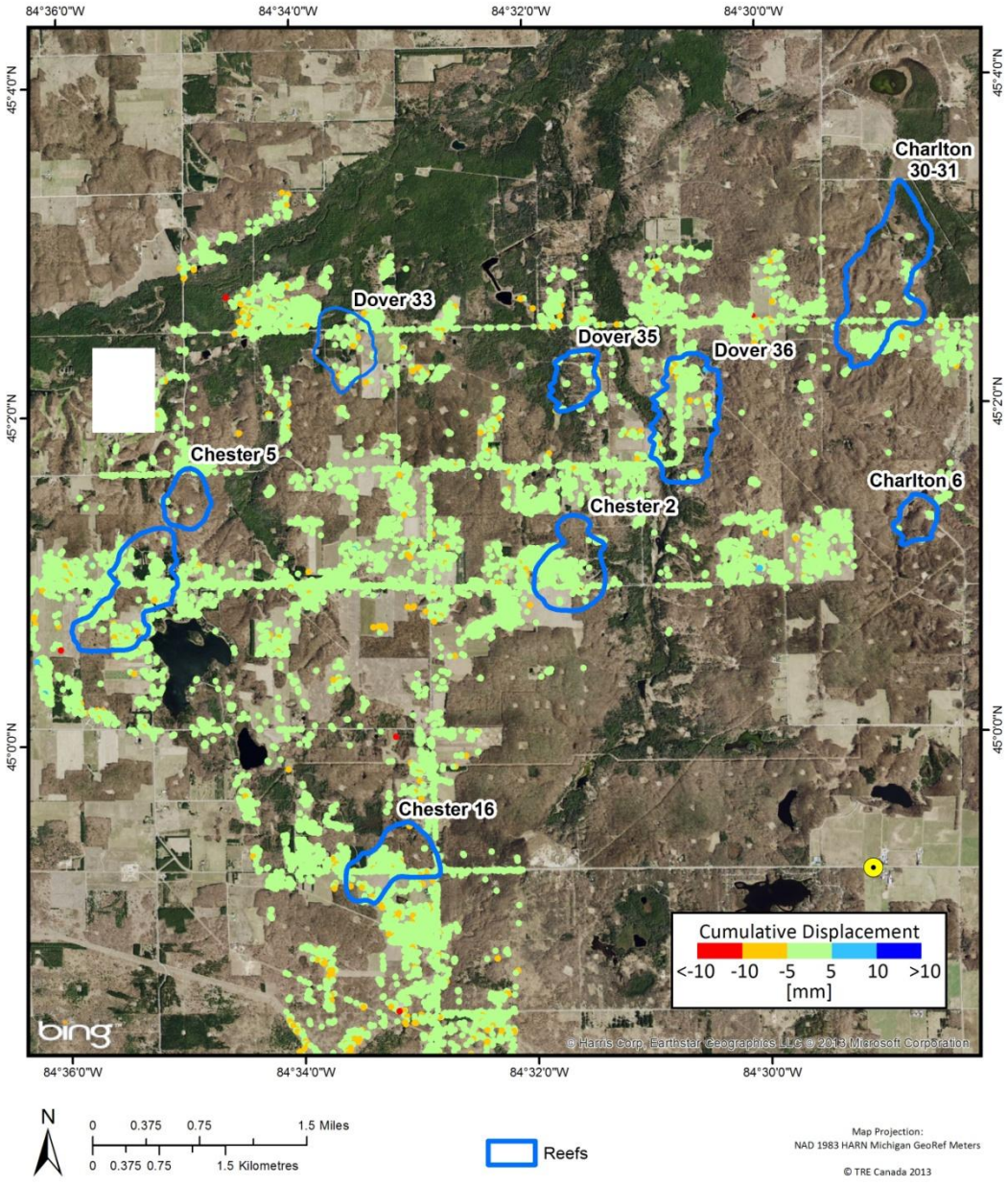

Figure 7: Baseline surface displacement results over eight reefs located in the northern portion of the AOI.

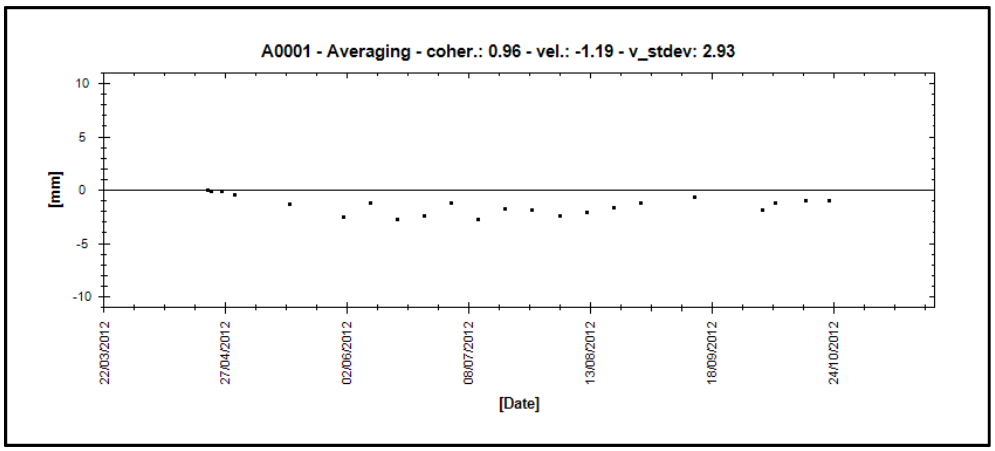

Figure 8: Average time series of all measurement points identified over the Charlton 6 reef.

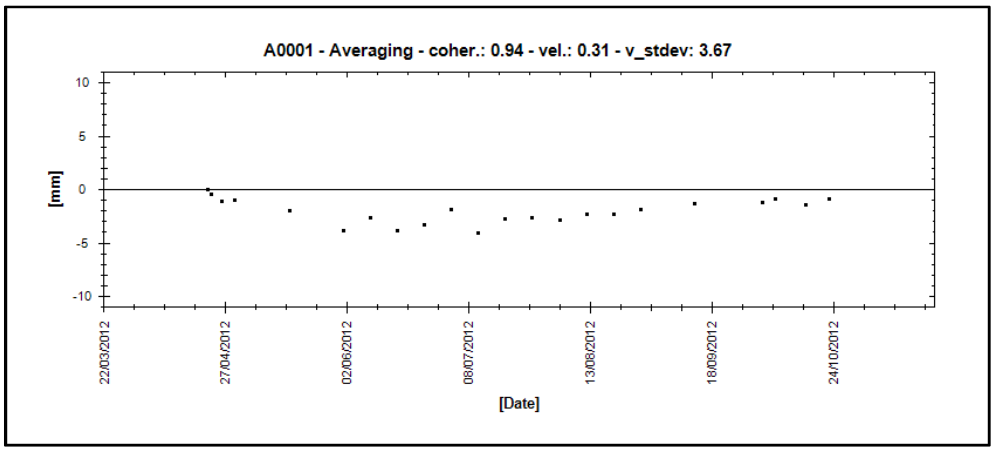

Figure 9: Average time series of all measurement points identified over the Charlton 30-31 reef.

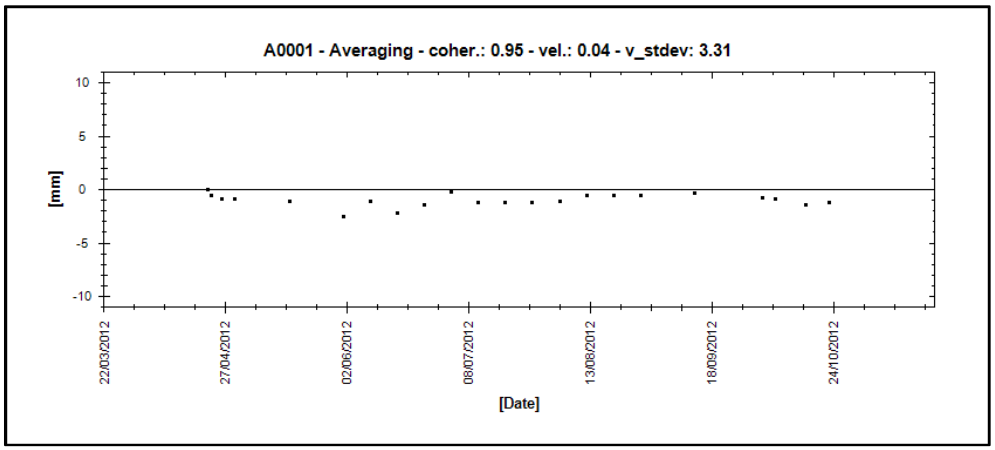

Figure 10: Average time series of all measurement points identified over the Chester 2 reef.

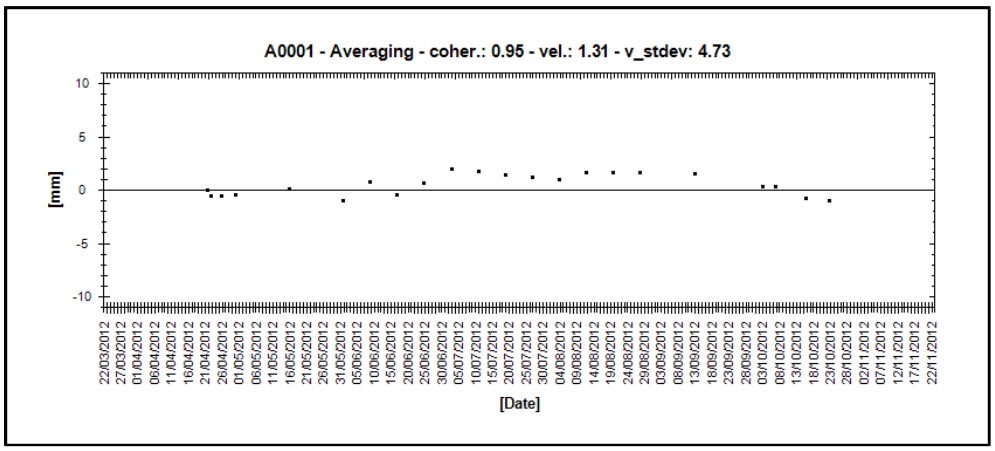

Figure 11: Average time series of all measurement points identified over the Chester 5 reef.

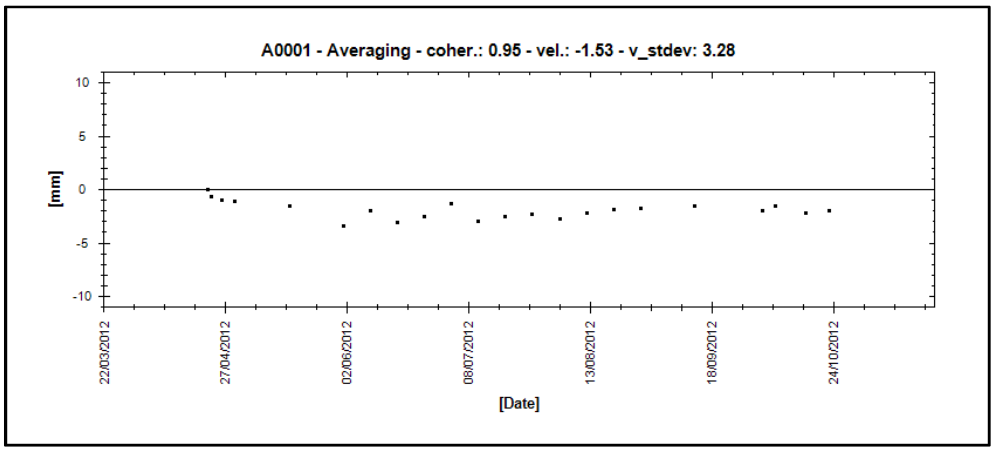

Figure 12: Average time series of all measurement points identified over the Chester 16 reef.

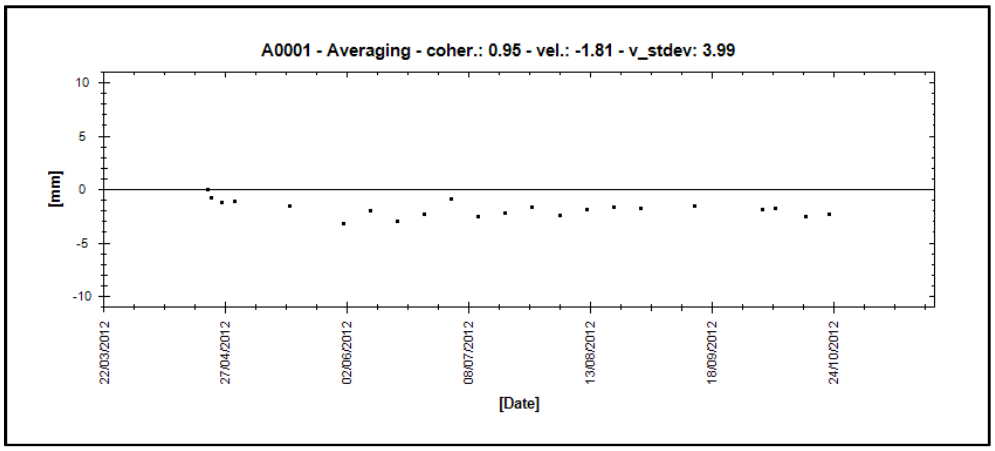

Figure 13: Average time series of all measurement points identified over the Dover 33 reef.

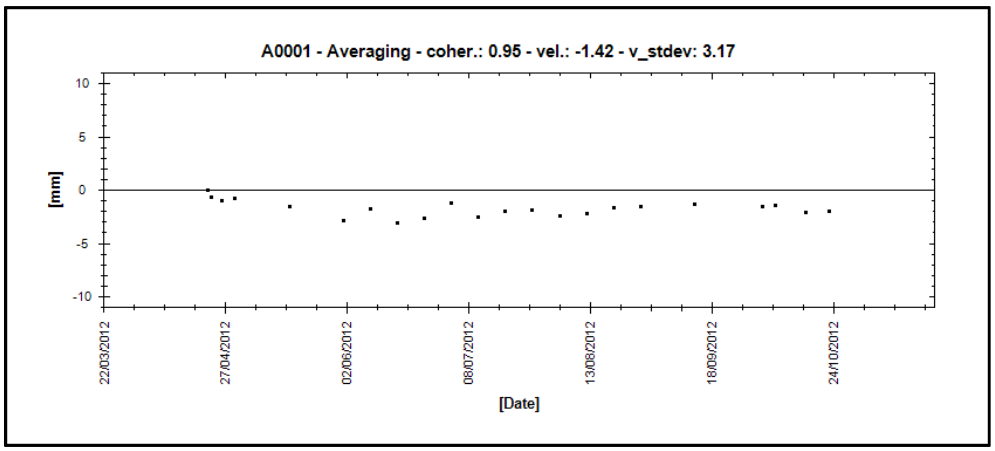

Figure 14: Average time series of all measurement points identified over the Dover 35 reef.

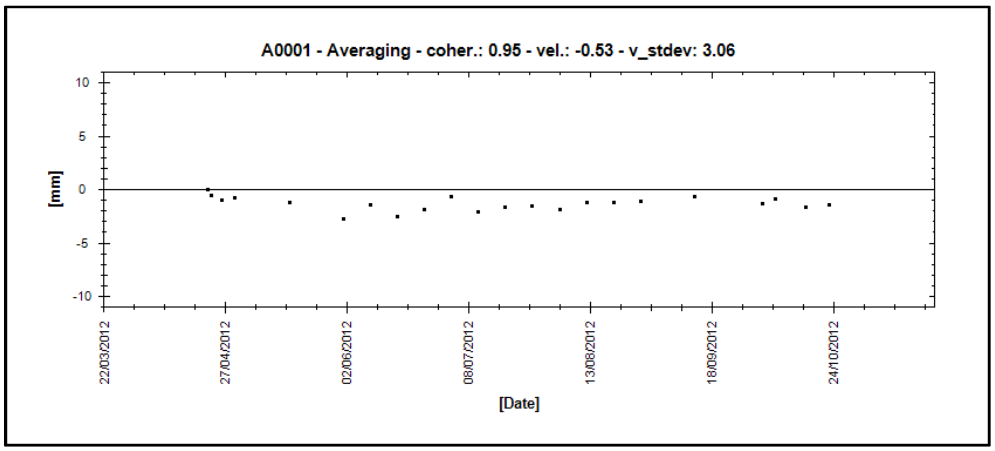

Figure 15: Average time series of all measurement points identified over the Dover 36 reef.

6.2.1 Dover 33 Field

Baseline displacement results obtained over the Dover 33 field and surrounding area are shown in Figure 16. These results will be used as a baseline for long-term monitoring of this injection program.

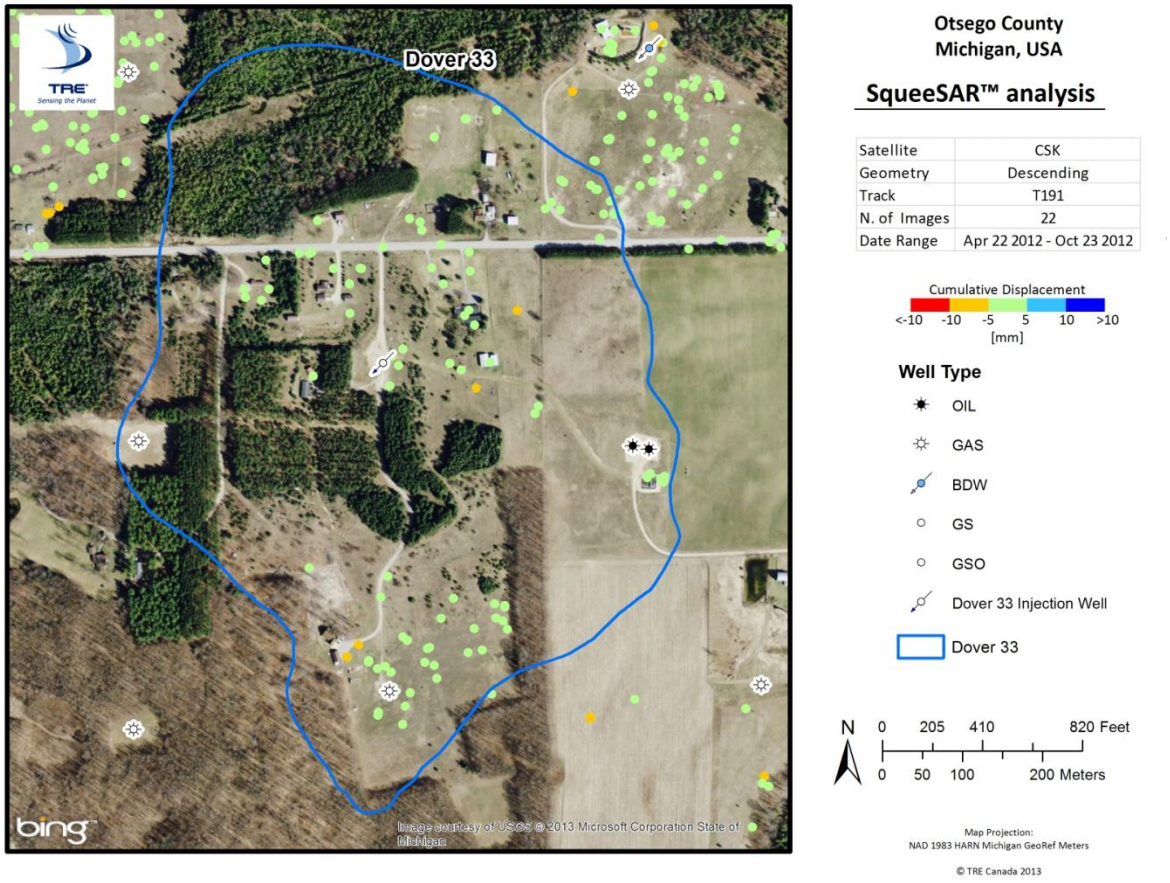

Figure 16: Displacement results obtained over the Dover 33 field.

6.2.2 South Chester 15 Gas Storage Field

Displacement results over the South Chester 15 gas storage field are shown in Figure 17, below. Measurement points identified from structures in this area are stable, with measured displacement rates within the range of their associated confidence interval.

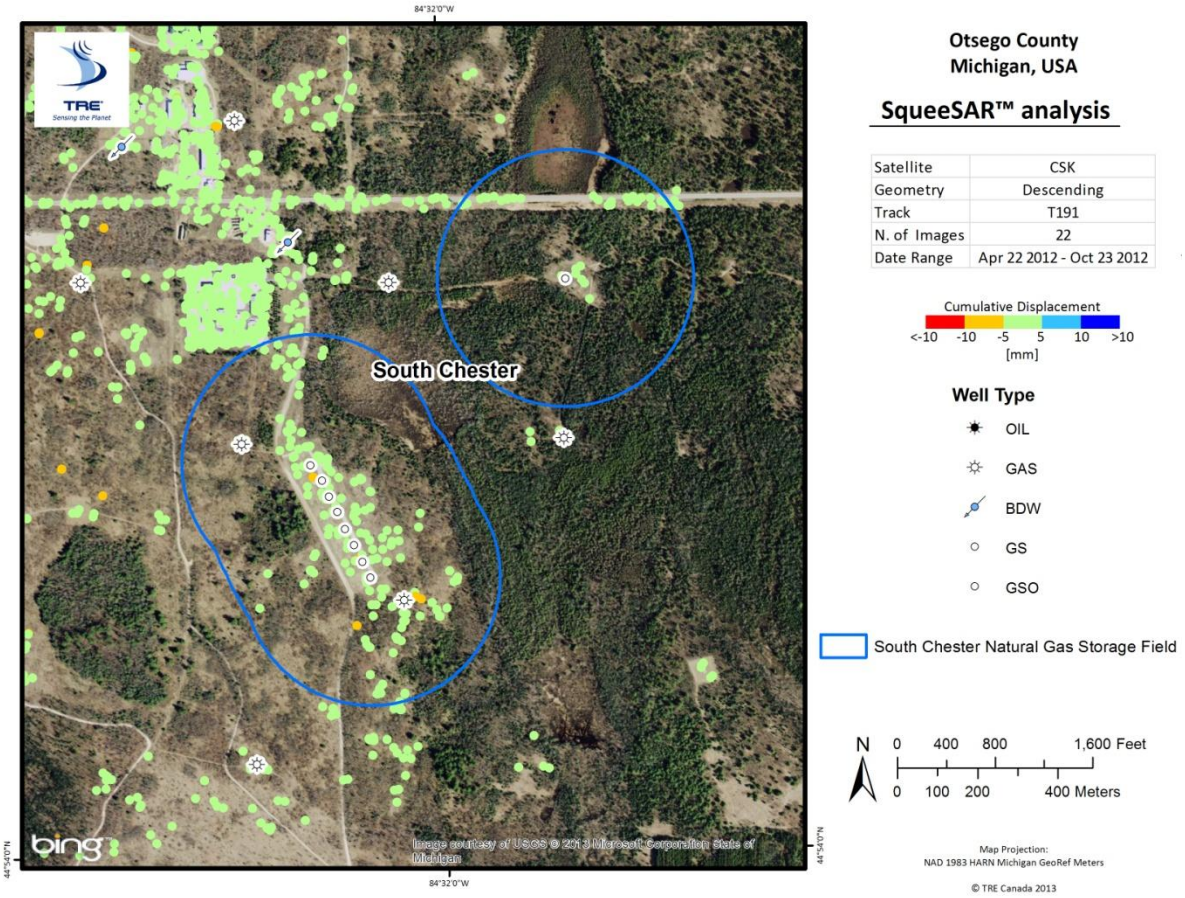

Figure 17: Displacement results obtained over the South Chester 15 gas storage field.

6.3 Comparison to Well Data

Well type and locations provided by Battelle were used to guide a brief analysis focused on movement trends identified in close proximity to oil and gas operations. All measurement points identified within a 500 foot (150 meter) buffer of every well was used to calculate an average displacement rate, which was then assigned to that well (Figure 18). A summary of the displacement rates calculated according to well type are shown in Table 2. Results were compared to a random sample of measurements taken from areas where no wells were present, as well as the average displacement value of the entire data set.

No obvious correlations were identified in this preliminary analysis as results were highly similar when compared between different well types, areas with no wells and over the entire AOI. Once surface displacement rates (including any seasonal influences) have been better characterized, it will be easier to determine whether any patterns between ground movement and operations exist.

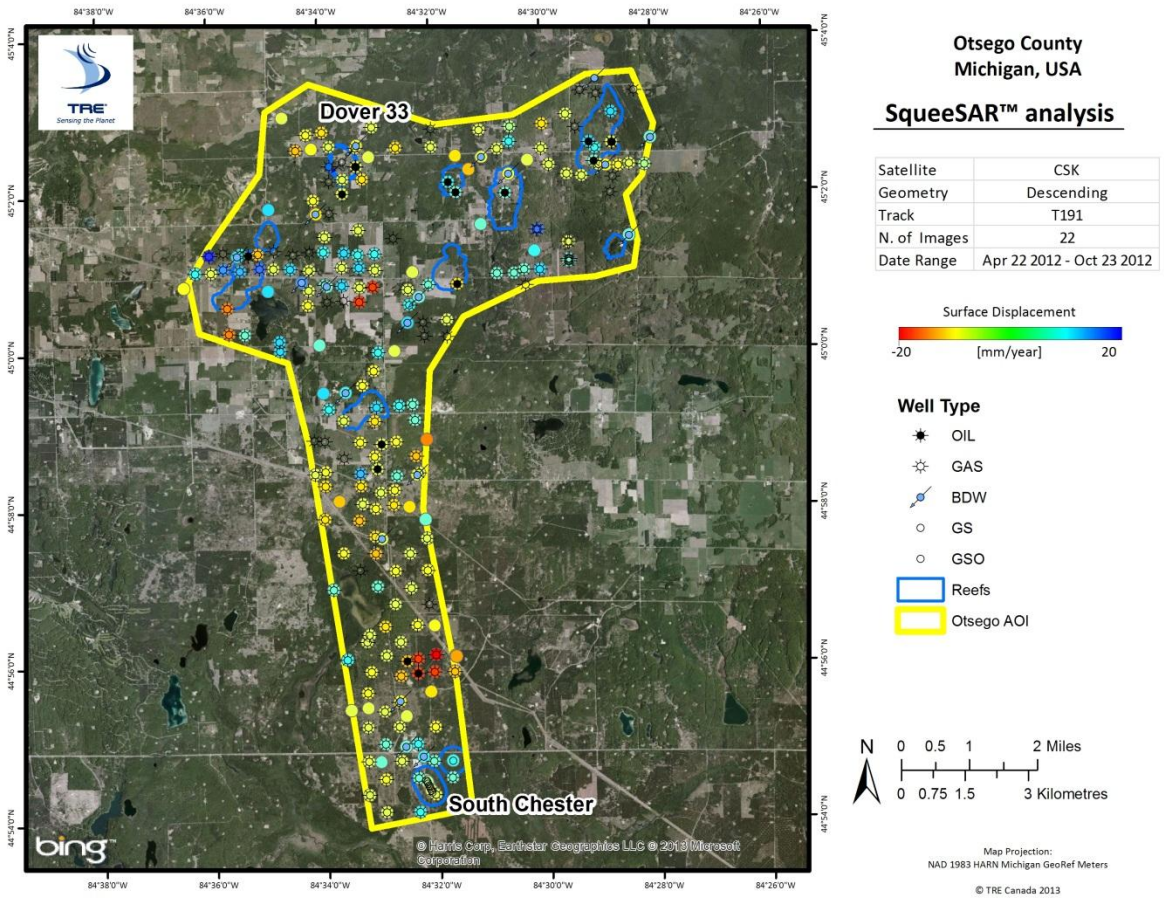

Figure 18: Surface displacement results identified within a 500 foot (150 meter) buffer around all wells included in the files provided by Battelle.

Well Type	Average Displacement Rate (mm/year)	Standard Deviation (mm/year)	Number of Samples
GS/GSO	-0.01	4.03	10
Oil	-1.32	3.44	15
Gas	-1.06	3.60	151
BDW	-0.26	3.57	19
Random Sample (No Wells within 150 m)	-0.88	3.61	20
All Measurement Points (PS and DS)	-1.19	3.69	16,914

Table 2: Summary of the average displacement rates identified within a 500 foot (150 meter) buffer of all wells within the AOI, a random sample of areas with no wells within 500 feet (150 m), and the entire AOI.

6.4 Measurement Point Density and Accuracy

The analysis of X-band imagery has resulted in a density of 545 PS and DS per square mile (211 PS and DS per square kilometer). In comparison, a density of 33 PS and DS per square mile was identified from the historical ERS analysis. While the distribution of points is still uneven across the AOI due to the challenging ground conditions of this area, the greater density of the results allowed for an improved spatial coverage over several areas, including over the Dover 33 field and the South Chester 15 gas storage field. The most noticeable gains were over non-urban areas, including exposed ground and sparsely vegetated fields.

Measurement precision is primarily assessed through the associated standard deviation of the displacement rates. As discussed in section 5.3 and highlighted throughout the report, the measurement precision is limited due to the short time span and smaller number of images used in the analysis. The average standard deviation of 3.7 mm/year is expected to improve over time as more data is collected, allowing for an increase in the statistical robustness of the data processing.

6.5 Artificial Reflector Placement and PS Measurement Point Density

The planned locations of all artificial reflectors (AR) at the Dover 33 site are shown in Figure 19, overlain with all of the PS-type points (corresponding to measurements obtained from specific structures) identified in the present baseline analysis. It is important to note that many additional points of the DS-type were identified at the Dover 33 field, which correspond to movement across areas up to hundreds of square meters in size. The baseline results indicate that the proposed distribution of ARs will be a good supplement to the current distribution of PS-type radar targets identified in the area.

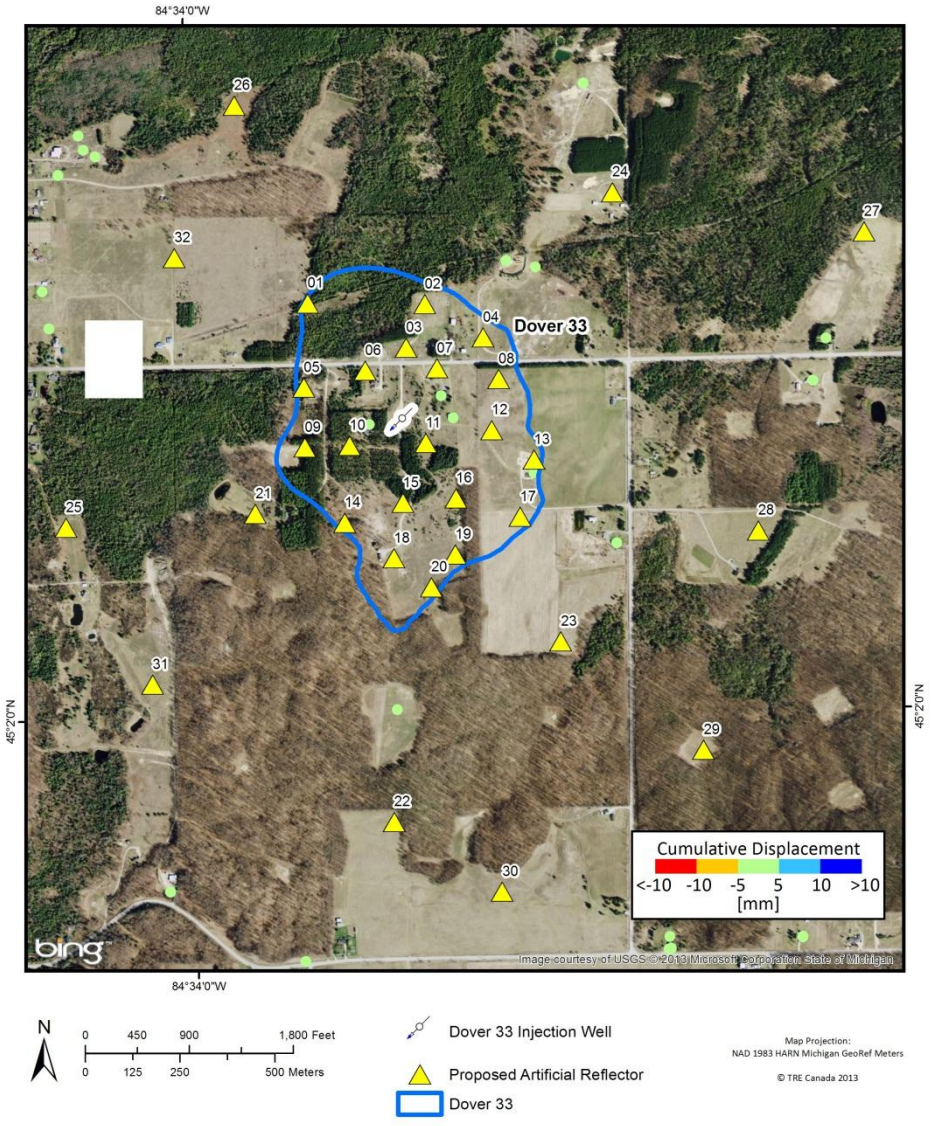

Figure 19: Planned locations of the ARs to be installed over the Dover field shown with all PS-type measurement points identified from the baseline analysis.

7 Summary

The results obtained from the baseline analysis of the CSK imagery collected over Otsego County, Michigan demonstrated that most of the area is stable. With the exception of one field located to the northeast of the South Chester 15 gas storage field, no large movement trends were observed, with over 90% of the measurement points identified indicating displacement less than 5 mm. Due to the short time span of the data, only movement rates larger than their associated confidence interval (standard deviation) should be considered reliable. No large displacement trends within operational areas were identified, particularly considering the constrained precision of the measurements. Radar imagery is continuing to be acquired with the Cosmo-SkyMed (CSK) constellation of satellites.

A historical analysis conducted over this site indicated that there was a mild seasonal component present over part of this area (typified by the appearance of a cyclical pattern). Therefore, it may be expected that a similar trend would be present for ongoing monitoring. Once at least one full year of data has been collected, any seasonal trends that may be influencing the displacement results this area will start to become better characterized.

8 Delivery of Data

The deliverables of the SqueeSAR™ analysis include the present report, the PS data files and a software tool for assisting with the loading, viewing and interrogation of the data in ESRI ArcGIS 10 software. Table 3 lists the files contained on the accompanying CD.

File name	Description
OTSEGO_CSK_H4_04_D_T191-TSR.dbf	Table containing the height, velocity, velocity standard deviation, acceleration, coherence and time series of all the PS identified in the analysis.
OTSEGO_CSK_H4_04_D_T191-TSR.shp	ESRI Shapefile for displaying the database (dbf) file in a GIS environment.
OTSEGO_CSK_H4_04_D_T191-REF.dbf	The reference point used for the ascending data processing.
OTSEGO_CSK_H4_04_D_T191-REF.shp	ESRI Shapefile for displaying the reference point file in a GIS environment.
Otsego Baseline Analysis Results.mxd	ESRI ArcGIS 10 project containing all PS data and the AOI shapefile.

Table 3: List of delivered files.

The ESRI ArcGIS 10 project file is included to make it easier to view the data. Once the data contained in the CD have been saved to the user's hard drive it will be sufficient to open the project file with ArcGIS and update the links to indicate the new locations of the data.

9 The Structure of the Database Files

Table 4 below, describes the attributes of each PS within the database.

Field	Description
CODE	Unique identification code.
SHAPE	Indicates type of geometry (point).
HEIGHT (m)	Elevation above sea level of the PS.
H_STDEV (m)	Standard deviation of PS elevation value.
VEL (mm/yr)	PS movement rate. Positive values correspond to movement toward the satellite (uplift); negative values correspond to motion away from the satellite (subsidence).
V_STDEV (mm/yr)	Standard deviation of PS deformation rate.
ACC (mm/yr^2)	PS acceleration rate.
A_STDEV (mm/yr2)	Standard deviation of PS acceleration value.
COHERENCE	Quality measure [between 0 and 1].
EFF_AREA (m^2)	Size of the area belonging to the PS. For PS EFF_AREA = 0, for DS EFF_AREA > 0.
D(year/month/day) (mm)	Following the EFF_AREA column are a series of fields that contain the displacement values of successive acquisitions relative to the Master, expressed in mm.

Table 4: Description of the fields contained in the Shapefile.

Appendix 1: Additional Properties of the SqueeSAR™ results over Otsego County

Radar Data Acquisition Geometry

InSAR-based approaches measure surface displacement on a one-dimensional plane, along the satellite line-of-sight (LOS). The LOS angle varies depending on the satellite and on the acquisition parameters while another important angle, that between the orbit direction and the geographic North, is nearly constant.

All images for the present analysis were acquired from a descending orbit (satellite travelling from south to north and imaging to the east). The symbol δ (delta) represents the angle the LOS forms with the vertical and Θ (theta) the angle formed with the geographic north (Figure 20). Table 5 lists the values of the angles for this study.

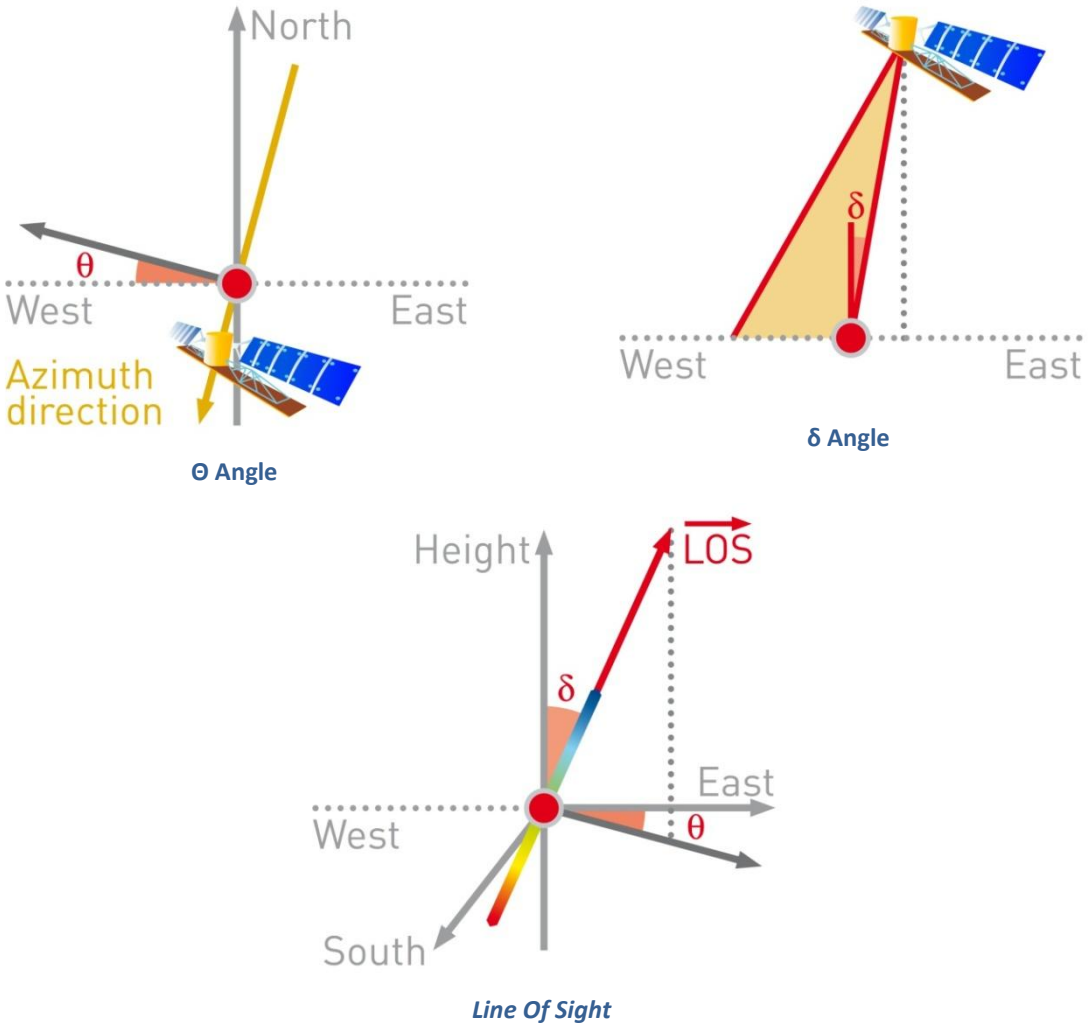

Figure 20: Geometry of the CSK descending image acquisitions over the present site.

Satellite	Symbol	Angle
ERS	**δ**	32.18°
	θ	9.04°

Table 5: Satellite viewing angles for the CSK imagery.

Data Processing

Both permanent scatterers (PS) and distributed scatterers (DS) were identified at this site. Buildings and other man-made structures provide the basis for many PS points in the present SqueeSAR™ analysis. Many natural features such as rocks or exposed ground were also likely sources of stable PS targets.

DS correspond to large areas (up to hundreds of square meters) and were identified from exposed areas such as abandoned or fallow fields. It is important to consider that while DS are represented as individual points for clarity of presentation and ease of interpretation, these measurements actually correspond to non-point features that are multiple pixels in size. The size of the DS within the AOI range from 86 to 888 m^2.

Table 6, shown below, provides a summary of the other properties relative to the data processing.

Satellite	Cosmo-SkyMed
Acquisition geometry	Descending
Analysis time interval	22 April 2012 – 23 October 2012
Number of scenes processed	22
Georeferencing	PS aligned on Bing Maps
Projection system used / datum	WGS 1984 UTM Zone 16 N
Reference Point location	NORTH: 4984503.4461 EAST: 698262.4947
Area of interest	31 $mile^2$ (80 km^2)
Number of Measurement Points Number of PS Number of DS	**16,914** 779 16,135
Average PS density	545 PS and DS/ $mile^2$ (211 PS and DS/km^2)

Table 6: Statistics of the CSK processed data.

Standard Deviation and Precision

Standard deviation values of the displacement measurements are a function of the factors listed below and of local ground movement dynamics.

- Spatial density of the PS and DS (higher densities produce higher precisions)
- Quality of the radar targets (signal-to-noise ratio levels)
- Distance from the reference point
- Number of images processed
- Period of time covered by the imagery
- Climatic conditions at the time of the acquisitions
- Distance between the measurement point and the reference

In addition to each measurement point having an associated standard deviation value to represent the error of the displacement measured, results can also be characterized by the accuracy of the technique. Specifically, three parameters are used to characterize the overall accuracy of the results:

- Precision of the estimated deformation rates;
- Precision of the estimated elevations;
- Precision of the geocoding.

Table 7 summarizes the typical precision values applicable to PS located within 2 km from the reference point when **at least 45 radar images** have been processed.

DEFORMATION RATE	< 1 [mm/yr]
DISPLACEMENT ERROR (single displacement between contiguous satellite images)	< 5 [mm]
ELEVATION	± 1.5 [m]
POSITIONING ERROR ALONG EAST DIRECTION	± 3 [m]
POSITIONING ERROR ALONG NORTH DIRECTION	± 2 [m]

Table 7: Measurement accuracies for PS located within 2 km of the reference point, based on the processing of at least 45 SAR images.

Appendix 2: InSAR Processing

InSAR

Interferometric Synthetic Aperture Radar, also referred to as SAR interferometry or InSAR, is the measurement of signal phase change (interference) between radar images. When a point on the ground moves, the distance between the sensor and the point changes, thereby producing a corresponding shift in signal phase. This shift is used to quantify the ground movement.

An interferogram is a 2D representation of the difference in phase values. Variations of phase in an interferogram are identified by fringes, colored bands that indicate areas where and how much movement is occurring. The precision with which the movement can be measured is usually in the centimeter (cm) range as the phase shift is also impacted by topographic distortions, atmospheric effects, and other sources of noise.

DInSAR

When InSAR is used to identify and quantify ground movement the process is referred to as Differential InSAR (DInSAR). In DInSAR topographic effects are removed by using a DEM of the area of interest to create a differential interferogram.

Differential InSAR is still impacted by atmospheric effects, as there is no method for removing this signal phase contribution. It is a useful tool for identifying footprints of progressing movement and creating deformation maps. The limitations of DInSAR are its relatively low precision (cm scale) and that it cannot distinguish between linear and non-linear motion.

PSInSAR™

Permanent Scatterer SAR Interferometry is an advanced form of DInSAR. The fundamental difference is that it uses multiple interferograms created from a stack of at least 15 radar images.

Permanent Scatterer SAR Interferometry was developed to overcome the errors produced by atmospheric artifacts on signal phase. The PSInSAR algorithm automatically searches the interferograms for pixels that display stable radar reflectivity characteristics throughout every image of the data set. In PSInSAR these pixels are referred to as Permanent Scatterers (PS). The result is the identification of a sparse grid of point-like targets on which an atmospheric correction procedure can be performed. Once these errors are removed, a history of motion can be created for each target, allowing the detection of both linear and non-linear motion.

The result is a sparse grid of PS that are color-coded according to their deformation rate and direction of movement. The information available for each PS includes its deformation rate, acceleration, total deformation, elevation, coherence as well as a time series of movement. The PSInSAR algorithm measures ground movement with millimeter accuracy.

SqueeSAR™

Permanent Scatterers (PS) are objects, such as buildings, fences, lampposts, transmission towers, crash barriers, rocky outcrops, etc, that are excellent reflectors of radar microwaves. However, TRE has noticed that many other signals are present in the processed data. These do not produce the same high signal-to-noise ratios of PS but are nonetheless distinguishable from the background noise. Upon further investigation it was found that the signals are reflected from extensive homogeneous areas where the back-scattered energy is less strong, but statistically consistent. These areas have been called distributed scatterers (DS) and correspond to rangeland, pastures, bare earth, scree, debris fields, arid environments, etc (Figure 21).

The SqueeSAR™ algorithm was developed to process the signals reflected from these areas. As SqueeSAR™ incorporates PSInSAR no information is lost and movement measurement accuracy is unchanged.

The SqueeSAR™ algorithm also produces improvements in the quality of the displacement time series. The homogeneous areas that produce DS normally comprise several pixels. The single time series attributed to each DS is estimated by averaging the time series of all pixels within the DS, effectively reducing noise in the data.

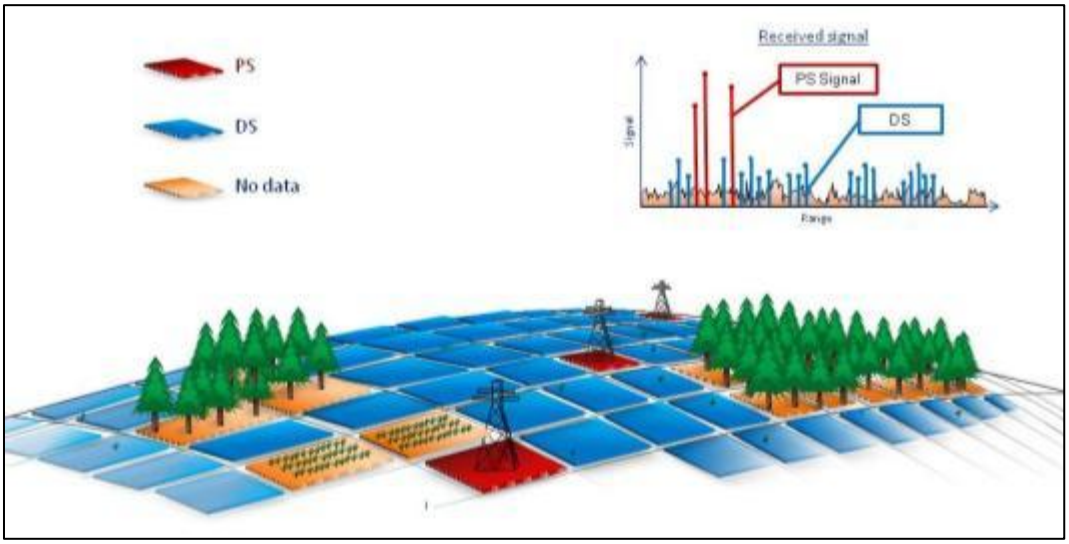

Figure 21: Illustration of the identification of permanent (PS) and distributed scatterers (DS) by the SqueeSAR™ algorithm.

Appendix 3: Data Processing

Methodology

The identification of PS and DS in a series of radar images comprises a sequence of steps.

First, all radar data archives are screened to determine the most suitable source of raw data for the particular area of interest and to select all the high quality images within the chosen data set.

As the signal echo from a single point target contains many returning radar pulses it appears defocused in a synthetic aperture radar (SAR) raw image. The first processing step is therefore to focus all the received energy from a target in one pixel. The images are then precisely aligned to each other, or co-registered, and analyzed for their suitability for interferometry. The parameters that are analyzed are the normal baseline and the temporal distribution of the images.

There then follows a number of statistical analyses on the phase and amplitude characteristics of the backscattered radar signal that return to the satellite. If a concentrated number of signals reflect off a particular feature within a pixel and backscatter to the satellite, the feature is referred to as a 'scatterer'. When the same scatterer appears in all, or most, of a data set of SAR images of a particular location, then the scatterer is deemed to be 'permanent'.

At this stage it is possible to identify a subset of pixels, referred to as Permanent Scatterer Candidates (PSC), that are used to estimate the impact on signal phase of ionospheric, tropospheric and atmospheric effects, as well as possible orbit errors.

Once the signal phase has been corrected for these effects, any remaining changes in signal phase directly reflect ground movement.

Master Image Selection

SqueeSAR™ requires that one image (or scene) in each data set has to become both a geometric and temporal reference to which all the other images are then related. This image is referred to as the master image and those that remain are slave images.

The master image should be chosen according to the following criteria:

- it minimizes the spread of normal baseline values for the slave images;
- similarly, it minimizes the temporal baseline values between the master and each slave image; and
- it minimizes the effects of signal noise arising from changes in vegetation cover and/or small changes in the look angle of the satellite from one scene to another.

Signal Phase and Amplitude Analysis

General

Each pixel of a SAR image contains information on the amplitude of signals that are backscattered toward the satellite, as well as on the signal phase. The amplitude is a measure of the amount of the radar pulse energy reflected, while the phase is related to the length of the path of the electromagnetic wave, from the platform to the ground and back again.

Analyses of both amplitude and phase of the SAR image provide an indication of the stability of each pixel, over time, whereby it is possible to identify those pixels that are most likely to behave as Permanent Scatterers. Statistical methods are used extensively in this process.

Among the different statistical parameters that can be computed two are of particular interest: the Phase Stability Index (PSI), obtained from the phases of the images within the data set, and the Multi Image Reflectivity (MIR) map, derived from the amplitude values of the available acquisitions.

Radar phase and coherence

In standard SqueeSAR™ analyses, the phase stability is strongly linked to the concept of coherence. Pixels that consistently display high phase stability are said to be coherent. Coherence is measured by an index that ranges from 0 to 1. When a pixel is completely coherent, it will have a coherence value of 1. Correspondingly, if a pixel has a low phase stability, its coherence index will be 0. In general, interferometry is successful when the coherence index lies between 0.5 and 1.0.

Radar amplitude and multi-image reflectivity

The amplitude of a pixel within a SAR image is the aggregate of the backscattered energy toward the satellite from within the pixel's equivalent land area. This equivalent land area is referred to as the radar resolution, and in the case of the ERS and RSAT satellites, it measures about 20 m by 4 m, and 7 m by 5 m, respectively. It is necessary to look into the amplitude values of all the images in the data set, in order to understand exactly what was seen by the satellite at the time of each acquisition.

If a target has experienced significant change in its surface characteristics it will exhibit variation in its reflectivity (electromagnetic response) between two acquisitions. In such circumstances, the possibility of detecting movement by means of SAR interferometry is seriously compromised. The signal phase difference between the two images now contains not only the contribution due to displacement, but also that due to the change in the reflectivity of the target. This prevents, in the worst case, the obtaining of any useful information on ground movement.

Accordingly, it is necessary to look into the amplitude values of all the images in the data set, in order to understand exactly what was seen by the satellite at the time of each acquisition.

Another artifact linked to amplitude is known as speckle. Speckle is random noise that appears as a grainy salt and pepper texture in an amplitude image. This is caused by random interference from the multiple scattering returns that occur within each resolution cell. Speckle has an adverse impact on the quality and usefulness of SAR images. However, the higher the number of images taken of the same area at different times or from slightly different 'look' angles, the easier it is to reduce speckle. This increases the quality and level of details of the amplitude image enabling it to be used as a background layer for observing the presence of PS results.

The Multi Image Reflectivity (MIR) map is the means by which speckle reduction is accomplished. Averaging a number of images tends to negate the random amplitude variability, leaving the uniform amplitude level unchanged.

It should be emphasised that the information in the MIR map is the reflectivity of each pixel, i.e. the ability to backscatter the incident wave toward the satellite. Flat surfaces (roads, highway, rivers, lakes) act like a mirror, meaning that if their orientation is not exactly perpendicular to the incident wave negligible energy is reflected back to the sensor; they appear dark in the image. On the other hand, because of their irregular physical shape, metal structures or buildings reflect a significant portion of the incident signal back to the radar, resulting in very bright pixels in the MIR map.

Interferograms

After the statistical analyses of the SAR images have been completed, a set of differential interferograms is generated. This entails subtracting the phase of each slave image from the phase of the master image. In doing so, the difference in signal path length between the two images is calculated. This difference is related to possible ground motion.

In any SAR image, there are embedded topographic distortions that arise during image acquisition. These are removed using a reference Digital Elevation Model (DEM), leaving ground movement and the signal phase distortions arising from atmospheric effects as the only embedded variables.

The differential interferograms represent the starting point for applying the PSInSAR approach.

Estimation of the Atmospheric Effects

When a radar signal enters and exits a moisture-bearing layer in the atmosphere, its wavelength can be affected, introducing potential errors into the signal path length. The removal of atmospheric impacts is fundamental for increasing the precision of ground movement measurement.

A sub-set of pixels, usually corresponding to buildings, lampposts, antennas, small structures and exposed rocks, is chosen from among those that have high PSI values. These are referred to as PS Candidates (PSC). PSC density is, of course, higher in towns and cities rather than in forests and vegetated areas. However, it is often possible to obtain good PSC density in rural areas.

For each image, the atmospheric impacts are estimated at each PSC location. The process is statistically based and benefits in accuracy by the greater the number of available images for the analysis. By comparing the atmospheric contribution on neighboring pixels that would be experiencing the same atmospheric conditions, the atmospheric contribution can be reconstructed over the whole image.

The processed data set allows identification of a PSC cluster dense enough to identify and extract the atmospheric contribution over the entire area of interest.

Post-processing

In this stage the processed data undergoes a thorough quality control following ISO 9001:2000 guidelines. The PS data is checked for anomalies, aligned on an optical image layer usually provided by the client and the final report is prepared.

Appendix 4: Abbreviations and Acronyms

AOI	Area Of Interest
DEM	Digital Elevation Model
DS	Distributed Scatterer(s)
DInSAR	Differential Interferometric SAR
GIS	Geographic Information System
InSAR	Interferometric SAR
LOS	Line Of Sight
PS	Permanent Scatterer(s)
PSInSAR	Permanent Scatterers SAR Interferometry is a world-wide POLIMI Trademark
SAR	Synthetic Aperture Radar
SqueeSAR™	The most recent InSAR algorithm patented by TRE
TRE	Comprehensive term for Tele-Rilevamento Europa and TRE Canada
TS	(Permanent Scatterer Displacement) Time Series

TRE Canada Inc.
475 West Georgia Street, Suite 410
Vancouver, B.C., V6B 4M9
Canada

Tel. 604 331-2512
www.trecanada.com

Appendix C.

CCS Monitoring Analysis

InSAR Analysis

Of Ground Deformation at Dover 33 during CCS operations

Fourth Monitoring Report

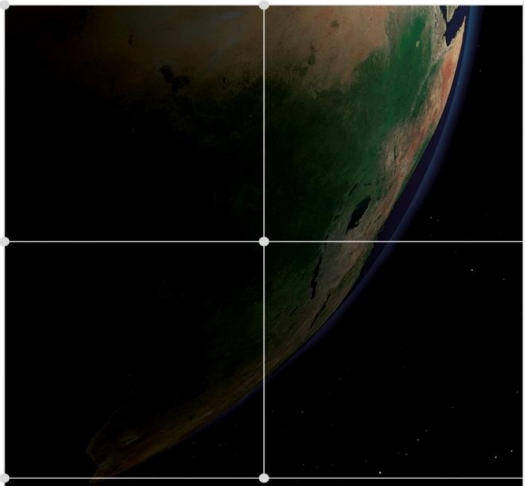

TRE®
Sensing the Planet

Submitted to:
Lydia Cumming
Battelle
505 King Avenue
Columbus, Ohio 43201
USA

Prepared by:
TRE Canada Inc.
Suite 410, 475 West Georgia Street
Vancouver, B.C., V6B 4M9
Canada

Prepared by: Vicky Hsiao
GIS Analyst
TRE Canada Inc.

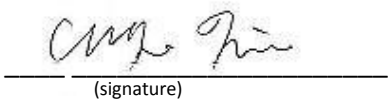
(signature)

Approved by: Giacomo Falorni
Operations Manager
TRE Canada Inc.

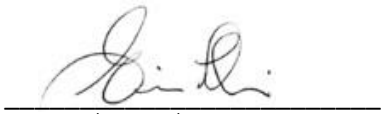
(signature)

Doc. Ref.: JO12-3008-REP6.0
June 10 2015

Executive Summary

This report describes the approach and results of the surface deformation monitoring analysis carried out over the Dover 33 reef in Otsego County, Michigan during CO_2 injection. The results provide an overview of ground movement following 12 months of baseline monitoring and 23 months of CO_2 injection. The following points summarize the key findings of this analysis:

- Satellite imagery was processed in two steps for the current analysis. One processing comprised the full stack of images (full data set) from the start of satellite image acquisitions to the end of March 2015 while the second processing was performed on all images acquired after the start of CO_2 injection (co-injection data set).
    - A total of 111 measurement points were identified within Dover 33 (292 pts/km^2 or 740 pts/sq. mi), compared to a density of 269 pts/km^2 (697 pts/sq. mi) over the entire AOI for the full data set. In the co-injection data set 42 pts were identified within Dover 33 (111 pts/km^2 or 280 pts/sq. mi) compared to 83 pts/km^2 (213 pts/sq. mi) within the AOI for the co-injection data).
    - 26 Artificial Reflectors are also installed within Dover 33 and its immediate surroundings.
    - The displacement rate measurements for both the full data and co-injection data have reached millimeter precision, with an average of (±0.4 mm/yr (±0.02 in/yr) and ±0.9 mm/yr (±0.04 in/yr), respectively.
- No observable ground deformation was detected in response to CO_2 injection. Ground deformation rates from natural radar targets in the full data set and co-injection data showed little movement, with average rates of -0.3 mm/yr (-0.01 in/yr) and +0.7 mm/yr (+0.03 in/yr), respectively, over Dover 33.
- The 26 Artificial Reflectors (AR) confirm the lack of injection-related deformation, as rates ranged from -1.5 mm/yr to +3.9 mm/yr (-0.06 in/yr to +0.14 in/yr). Minimal differences were observed within the reef and the surrounding area.
- No discernable correlation between ground deformation and bottomhole pressure or injected CO_2 volume was identified.
- A comparison of deformation patterns between a CCS site in which ground response to CO_2 injection was identified highlights the different behaviour at Dover 33, where a lack of surface deformation at Dover 33 was observed.

- In displacement time series of some natural radar targets it is possible to observe noise during the winter months. This is likely caused by the presence of snow on the ground surface, which can mitigate the radar signal.

The deliverables for this stage of the project include the present report and a CD containing the displacement data.

Table of Contents

1 Introduction

The Battelle Memorial Institute (Battelle) is an independent, not-for-profit research and development organization that heads the Midwest Regional Carbon Sequestration Partnership (MRCSP). The MRCSP is focused on the investigation of the geological suitability of the midwestern United States for carbon capture utilization and storage (CCUS), as part of a larger Department of Energy strategy for developing CO_2 emission reduction strategies. The Dover 33 reef (a late stage enhanced oil recovery reservoir) in Otsego County of the northern Michigan Basin has been selected as a research and demonstration site for the investigation of CCUS strategies over the next several years. While the focus of this study is Dover 33, the AOI covers a broader area in order to compare Dover 33 with regional trends and other reefs.

As part of a comprehensive monitoring program being implemented during the injection process, InSAR is being used to map surface response to CO_2 injection and migration throughout the reservoir. TRE Canada Inc. (TRE) has been contracted by Battelle to provide ongoing InSAR monitoring of ground movement at this site and the surrounding area. TRE has extensive experience with CCUS projects, including, for example, the In Salah project in Algeria and the Illinois Basin Decatur Project in Illinois.

The area of interest (AOI) in the current project is located east of Gaylord, Michigan between Lake Michigan and Lake Huron (Figure 1). The AOI covers 32 square miles (83 square kilometers) with the majority of the area consisting of active agricultural areas and forests. While the environment is predominantly non-urban, there are structures in the area related to oil and gas infrastructure, housing, roads and other buildings. Measurement points are often identified from these man-made features, as well as from cleared or sparsely vegetated areas. Forest regions and agricultural areas are more challenging for InSAR, as their reflectivity changes over time.

This fourth monitoring report details the results of the SqueeSAR™ analysis of ground deformation from April 2012 to March 2015 over the Dover 33 reef and surrounding area. Ground movement trends in the AOI are measured both before and during CO_2 injection, using natural radar targets and 26 Artificial Reflectors (ARs). Seventy-six images were acquired and processed over the course of the 3-year project.

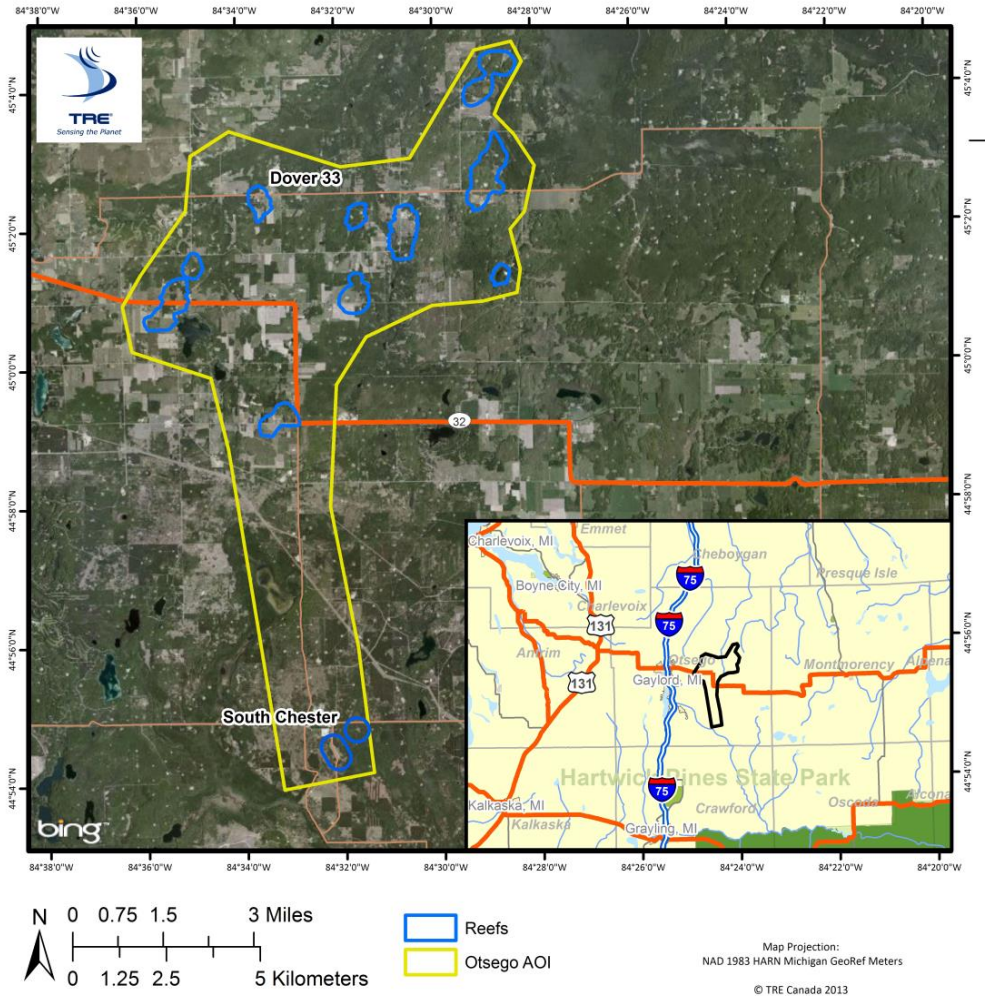

Figure 1: The area of interest in Otsego County, Michigan.

2 Radar Data

The radar imagery utilized for this monitoring analysis consists of 76 images acquired between April 22, 2012 and March 22, 2015. All images were acquired by Cosmo-SkyMed (CSK) from a descending orbit. Imagery is currently being acquired with a 16-day frequency. All eleven of the images scheduled for this monitoring period were successfully acquired and processed. Table 1 provides more information regarding the radar imagery while Table 2 contains the dates of the acquired images.

Radar Data Information	
Constellation	Cosmo-SkyMed (CSK)
Resolution	3x3m
LOS Off-Nadir Angle	32.48°
Orbit Direction	Descending
Track	191
Revisit Interval	16-Day
Period Covered by Imagery	April 22, 2012 – March 22, 2015
Number of Processed Images	76

Table 1: Information regarding the radar imagery used in the analysis.

TRE separately processed two sub-sets of the radar imagery, as requested by Battelle:

1. Full data processing.

   This processing was performed using the full set of images (April 22, 2012 to March 22, 2015). The results lead to a higher density of points, a full temporal period including before and during injection, as well as more robust and precise measurements.

2. Co-injection data processing.

   This processing was performed using only images acquired after the start of injection (May 06, 2013 to Mar 22, 2015). This setup focuses on analyzing potential deformation occurring after the start of injection. It also coincides with the installation of the artificial reflectors and thereby used a reflector as the reference point.

CSK Data							
No.	Date	Interval	CSK	No.	Date	Interval	CSK
1	Apr-22-2012		2	38	Jul-22-2013	16	1
2	Apr-23-2012	1	3	39	Aug-07-2013	16	1
3	Apr-26-2012	3	4	40	Aug-23-2013	16	1
4	Apr-30-2012	4	1	41	Sep-08-2013	16	1
	May-08-2012		2	42	Sep-24-2013	16	1
5	May-16-2012	16	1	43	Oct-10-2013	16	1
	May-24-2012		2	44	Oct-26-2013	16	1
6	Jun-01-2012	16	1	45	Nov-11-2013	16	1
7	Jun-09-2012	8	2	46	Nov-27-2013	16	1
8	Jun-17-2012	8	1	47	Dec-13-2013	16	1
9	Jun-25-2012	8	2	48	Dec-29-2013	16	1
10	Jul-03-2012	8	1	49	Jan-14-2014	16	1
11	Jul-11-2012	8	2	50	Jan-30-2014	16	1
12	Jul-19-2012	8	1		Feb-15-2014		1
13	Jul-27-2012	8	2	51	Feb-23-2014	24	2
14	Aug-04-2012	8	1		Mar-03-2014		1
15	Aug-12-2012	8	2	52	Mar-11-2014	16	2
16	Aug-20-2012	8	1	53	Mar-19-2014	8	1
17	Aug-28-2012	8	2	54	Apr-04-2014	16	1
	Sep-05-2012		1	55	Apr-20-2014	16	1
18	Sep-13-2012	16	2	56	May-06-2014	16	1
	Sep-21-2012		1	57	May-22-2014	16	1
19	Oct-03-2012	20	3	58	Jun-07-2014	16	1
20	Oct-07-2012	4	1	59	Jun-23-2014	16	1
21	Oct-23-2012	16	1	60	Jul-09-2014	16	1
22	Nov-08-2012	16	1	61	Jul-25-2014	16	1
23	Nov-24-2012	16	1	62	Aug-10-2014	16	1
24	Dec-10-2012	16	1	63	Aug-26-2014	16	1
25	Dec-26-2012	16	1	64	Sep-11-2014	16	1
26	Jan-11-2013	16	1	65	Sep-27-2014	16	1
27	Jan-27-2013	16	1	66	Oct-13-2014	16	1
28	Feb-12-2013	16	1	67	Oct-29-2014	16	1
29	Feb-28-2013	16	1		Nov-14-2014		1
	Mar-16-2013		1	68	Nov-22-2014	24	2
30	Mar-28-2013	28	4	69	Nov-30-2014	8	1
31	Apr-01-2013	4	1	70	Dec-16-2014	16	1
32	Apr-17-2013	16	1	71	Jan-01-2015	16	1
33	May-03-2013	16	1	72	Jan-17-2015	16	1
34	May-19-2013	16	1	73	Feb-02-2015	16	1
35	Jun-04-2013	16	1	74	Feb-18-2015	16	1
36	Jun-20-2013	16	1	75	Mar-06-2015	16	1
37	Jul-06-2013	16	1	76	Mar-22-2015	16	1

Table 2: Dates of the CSK imagery. Images highlighted in red correspond to missed images, while those in green indicate additional images acquired. Boxes shaded in light gray indicate new images acquired in the data processing.

3 Reference Point

SqueeSAR™ is a differential technique, meaning displacement is measured compared to a reference point that is assumed to be stable. The reference point is selected using an optimization procedure that maximizes the quality of the results based on a suite of radar parameters including high coherence, low standard deviation values and low variability of movement over time.

A centrally located measurement point (Distributed Scatterer) not falling within any reefs was utilized as reference point for the full data set. It is sited 3,017 metres (9,898 feet) south of the CO_2 injection well.

Reflector #28 was selected as the reference for the co-injection data. It falls outside of Dover 33 and is 1,081 metres (3,547 feet) north of the injection well (Figure 2 and Figure 3).

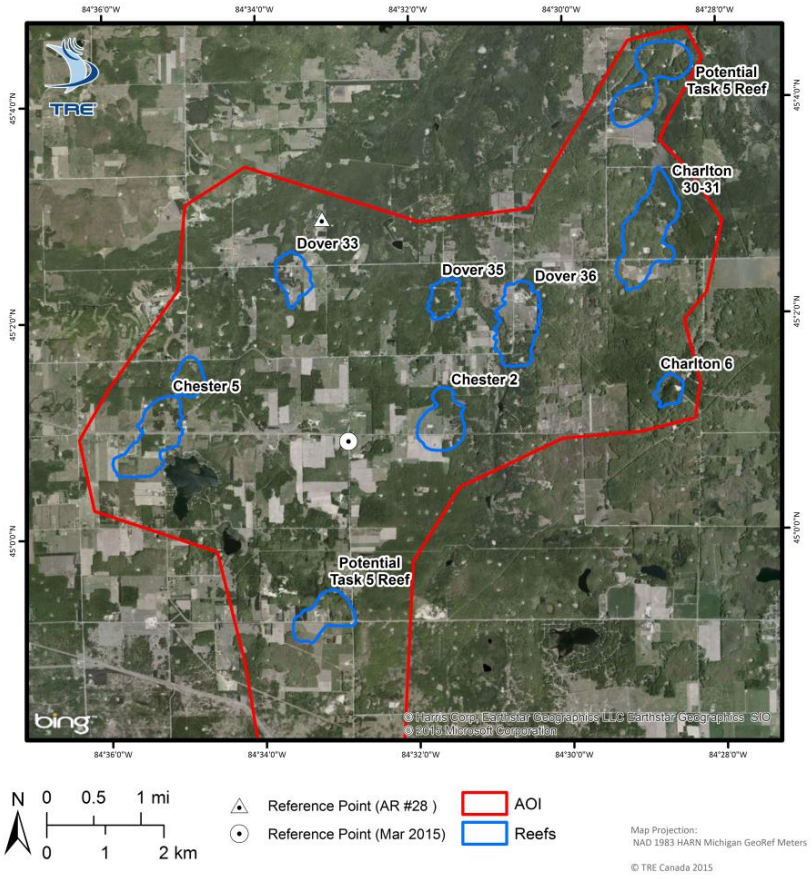

Figure 2: The location of the reference points used for the initial and current data processing.

Figure 3: Close-up indicating the location of the reference points.

4 Results of the SqueeSAR™ Analysis

4.1 Cumulative Displacement

The total amount of displacement measured during the 35 month time span of the analysis is shown in Figure 4, while cumulative displacement measured during the co-injection period is shown in Figure 5. Each point corresponds to a PS or DS, and is color-coded according to the magnitude and direction of total movement. Movement is measured along the satellite line-of-sight (LOS) relative to the first image (April 22, 2012) of the data stack. Cumulative displacement represents the net displacement, which is the sum of displacement from the first image to the last acquired image (March 22, 2015).

Cumulative displacement from April 2012 to March 2015 ranges from -60.5 to +49.1 mm (-2.4 to +1.9 inches) within the nine reefs, as compared to -60.5 to +50.7 mm (-2.4 to +2.0 inches) over the entire AOI (Figure 4). Mild uplift was observed throughout the AOI, with an average of +1.2 mm (+0.05 inches) in the full data. A few localized areas of subsidence are found mostly outside of the reefs.

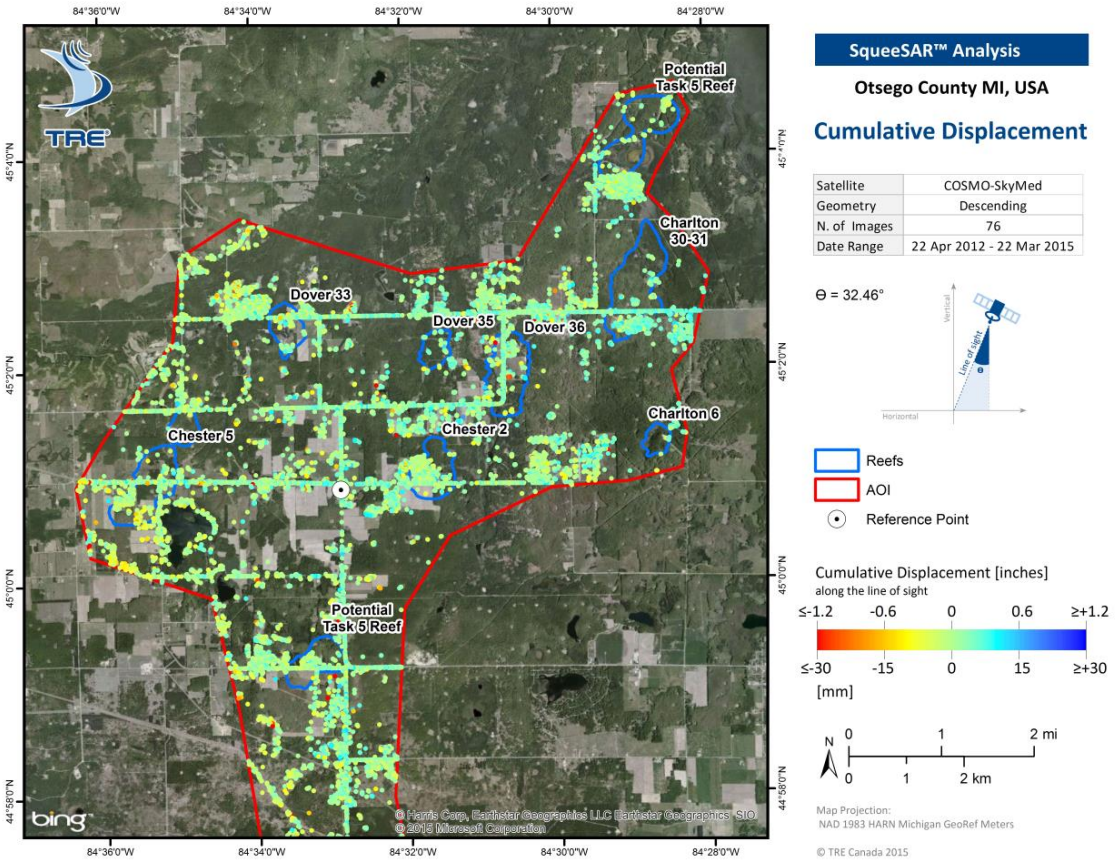

Figure 4: Cumulative deformation, expressed in millimeters, from April 22, 2012 to March 22, 2015.

Total displacement during the co-injection period also showed no observable difference between reefs (-31.6 to +11.4 mm or -1.2 to +0.5 inches) and the rest of the AOI (-34.1 to +30.3 mm, or -1.3 to +1.2 inches, Figure 5).

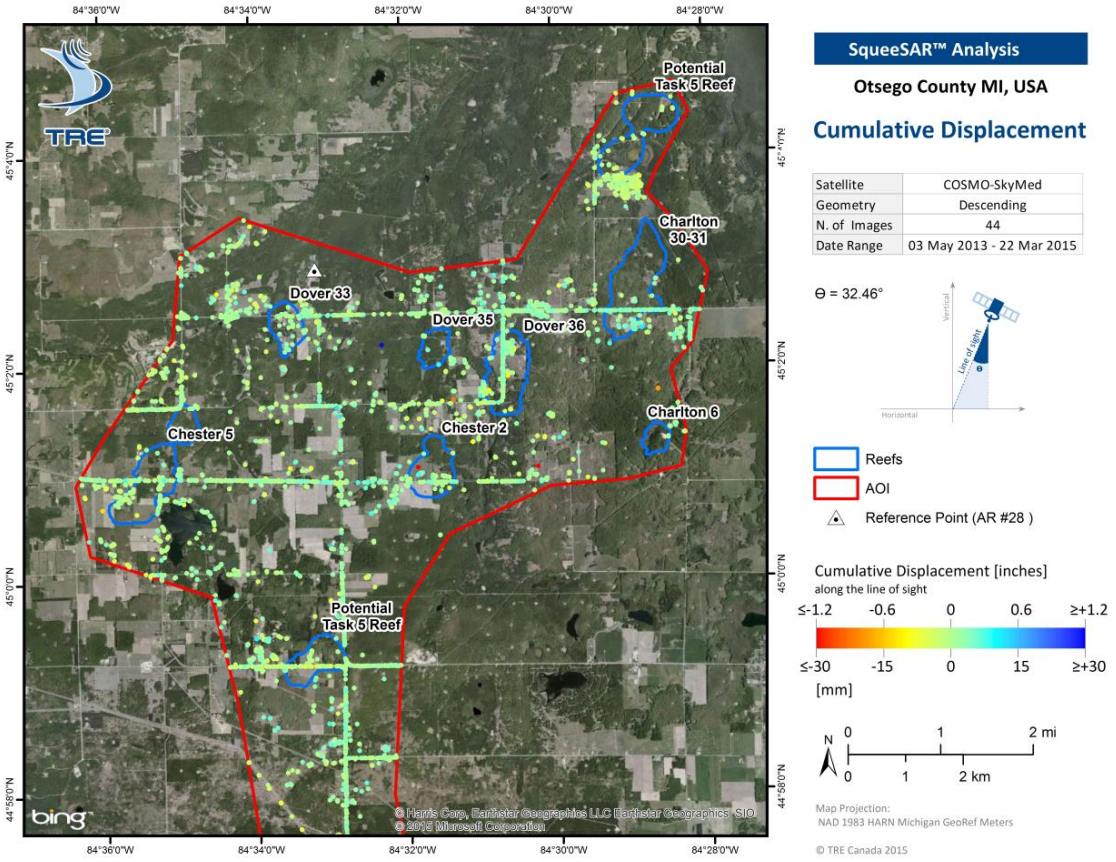

Figure 5: Cumulative deformation since the start of injection, expressed in millimeters, from May 3, 2013 to March 22, 2015.

4.2 Displacement Rate

The line-of-sight (LOS) displacement rates, expressed in millimeters per year (mm/yr), are presented in Figure 6 and Figure 7 for the full data and co-injection data, respectively. Each point corresponds to a Permanent Scatterer (PS) or a Distributed Scatterer (DS), and is color-coded according to its annual rate of movement. Average displacement values are calculated from a linear regression of the ground movement measured relative to the reference point over the entire period covered by the satellite images. Measurements should be interpreted taking into account the associated standard deviations. Detailed information on ground motion is also provided by means of displacement time series, which are provided for each PS and DS (refer to Section 5).

An average surface deformation rate of 0.04 ±0.4 mm/yr (-0.002 ±0.02 inches/yr) was identified within the nine reefs, compared to -0.2 ±0.4 mm/yr (-0.01 ±0.02 inches/yr) for the entire AOI (Figure 6). Maximum values ranged from -20.0 to +16.7 mm/yr (-0.8 to +0.7 inches/yr) in the reefs and from -21.4 to +16.7 mm/yr (-0.8 to +0.7 inches/yr) over the entire AOI.

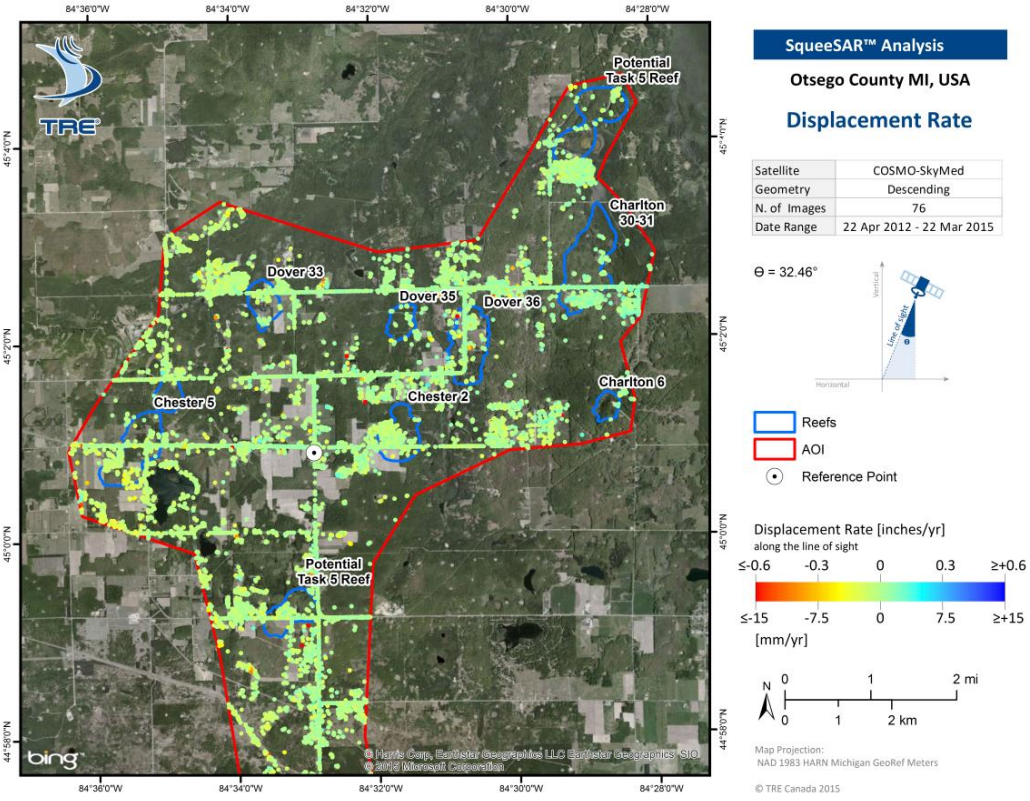

Figure 6: PS and DS deformation rates, expressed in millimeters per year.

For the co-injection data, an average surface deformation rate of 1.0 ±0.9 mm/yr (-0.04 ±0.04 inches/yr) was identified within the nine reefs with a range of -16.6 mm/yr to +5.0 mm/yr (-0.7 to +0.2 inches/yr). In the remainder of the AOI, an average surface deformation rate of 0.3 ±0.9 mm/yr (-0.01 ±0.04 inches/yr) was obtained, with rates ranging from -16.6 mm/yr to +15.8 mm/yr (-0.7 to +0.6 inches/yr).

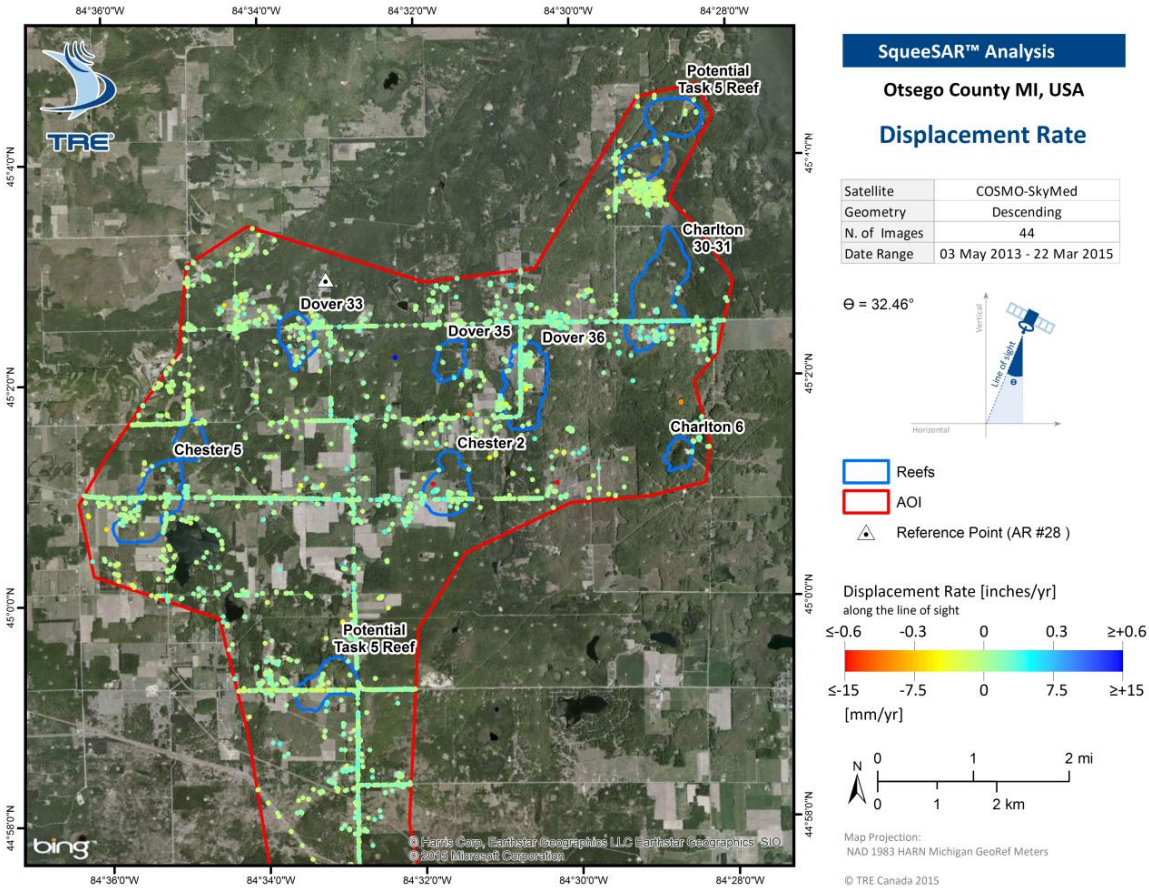

Figure 7: PS and DS deformation rates, expressed in millimeters per year.

4.3 Displacement Rate Standard Deviation

The standard deviation of the surface displacement data characterizes the error of the measurements (Figure 8 and Figure 9). For this reason, any measurement should be interpreted in the form of Displacement Rate ± Standard Deviation. Standard deviation values tend to increase with distance from the reference point. Higher values indicate a greater variability in displacement rates and are often associated with areas of rapid and/or irregular ground movement.

The precision of the displacement rates for the full and co-injection data are both at millimeter level, with an average standard deviation value of ±0.4 mm/yr (±0.02 inches/yr) and ±0.9 mm/yr (±0.04 inches/yr), respectively.

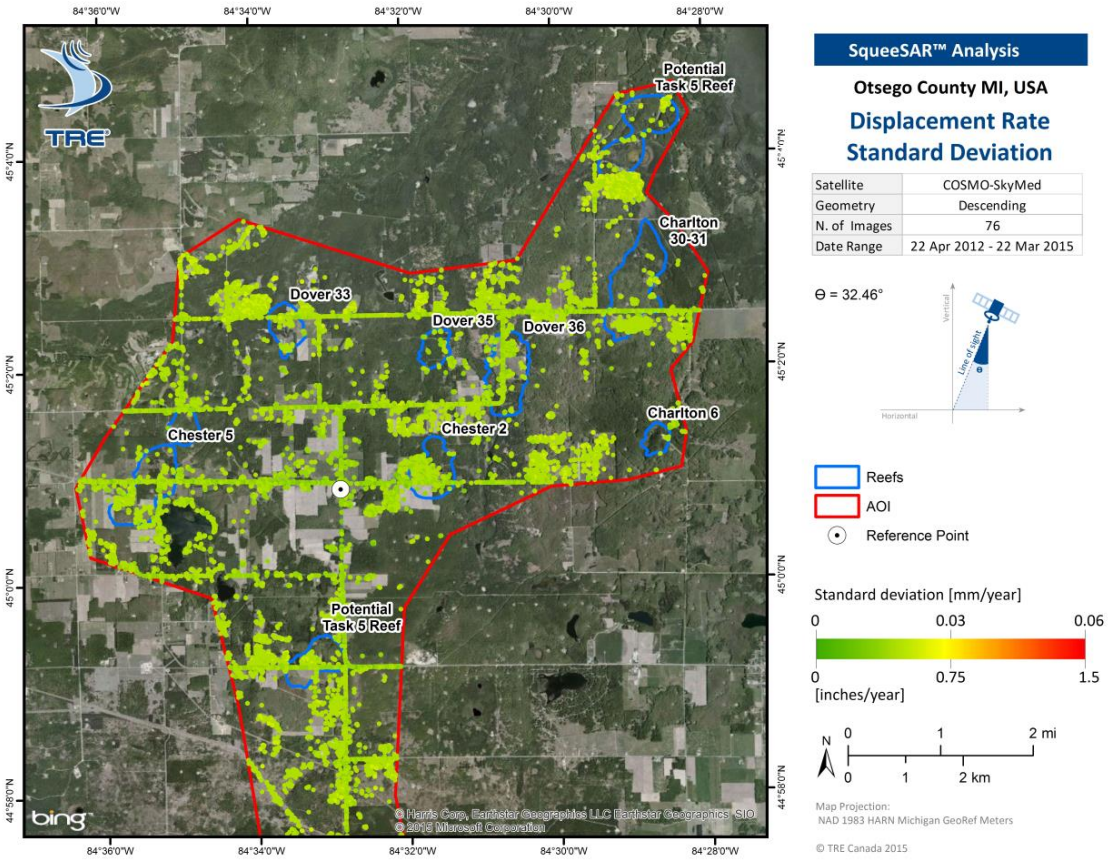

Figure 8: Standard deviation values of the displacement rates for the full data.

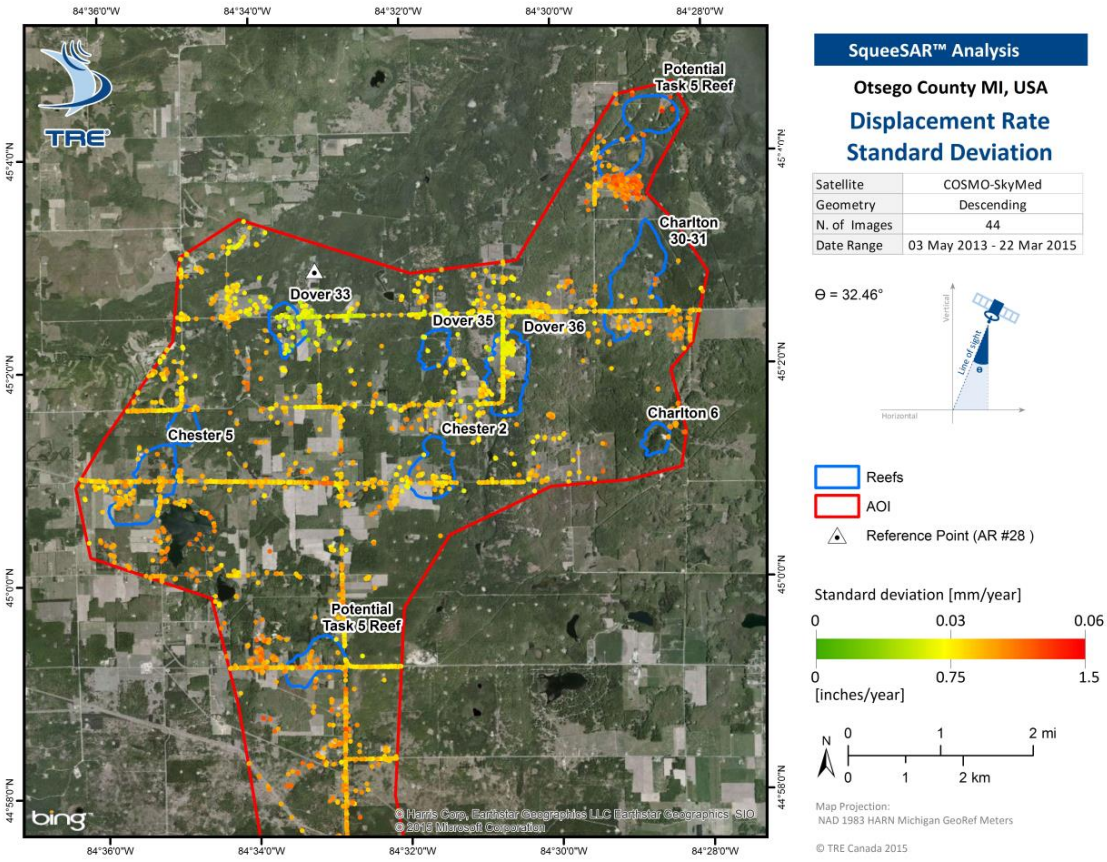

Figure 9: Standard deviation values of the displacement rates for the co-injection data.

5 Observations

The satellite imagery was processed in two groups: one comprising the full image stack (full data, April 2012 to March 2015) and one containing only images acquired since the start of injection (co-injection data, May 2013 to March 2015). The addition of 11 images since the last processing has led to an improvement in the data sets statistics and the results of the full and co-injection data are now comparable in terms of precision. Table 3 contains relevant data processing statistics.

Ground movement patterns were similar within Dover 33 and the rest of the AOI in both the full and co-injection data. The reflectors showed between -1.5 mm/yr to +3.9 mm/yr of deformation, indicating that surface displacement is minimal both within and outside Dover 33. The InSAR results from natural targets and artificial reflectors are similar, with both indicating that there is no clear ground response to carbon dioxide injection operations.

Bottomhole pressure data was compared against artificial reflector and natural radar target displacements to identify any potential correlations. The results indicate that no discernable correlation was identified.

Attribute	Historic analysis	Baseline analysis	Monitoring analysis (Full data)	Monitoring analysis (Co-injection data)
Number of images processed	51	22	76	44
Dates	May/20/1992 – Dec/4/1999	Apr/22/2012 – Oct/23/2012	Apr/22/2012 – Mar/22/2015	May/03/2013 – Mar/22/2015
Number of PS	155 (15%)	779 (5%)	9,157 (41%)	2,032 (30%)
Number of DS	881 (85%)	16,135 (95%)	13,152 (59%)	4,777 (70%)
Total N. of measurement points	1,036	16,914	22,309	6,809
Measurement point density	13 pts/km^2 (33 pts/ sq. mi)	211 pts/km^2 (546 pts/ sq. mi)	269 pts/km^2 (697 pts/sq. mi)	83 pts/km^2 (213 pts/sq. mi)
Average Displacement Rate (mm/yr)	-1.2	-1.1	-0.2	0.3
Average Displacement Rate Standard Deviation (mm/yr)	0.5	3.7	0.4	0.9

Table 3: Statistics of the SqueeSAR analysis conducted over the AOI.

A few observations help interpret the results:

1. Effects of snowfall
   The significant snowfalls that occur in the area in winter (6 to 59 inches of snow from November 2014 to February 2015 - National Oceanic and Atmospheric Administration (NOAA)) can lead to periods of noise in time series. Time series tend to fluctuate more during the winter months before subsequently returning to more stable trends in the spring.

2. Large scale variation in deformation patterns
   Deformation trends affecting a large number of measurements points throughout the AOI can be observed in many time series. For instance, the following time series (Figure 10, Figure 11) highlight a 3 mm displacement from late November 2014 to February 2015. This same bump can be observed in many time series throughout the northern portion of the AOI. It is not known whether this is the result of an environmental factor. However, this fact should be borne in mind while interpreting all time series.

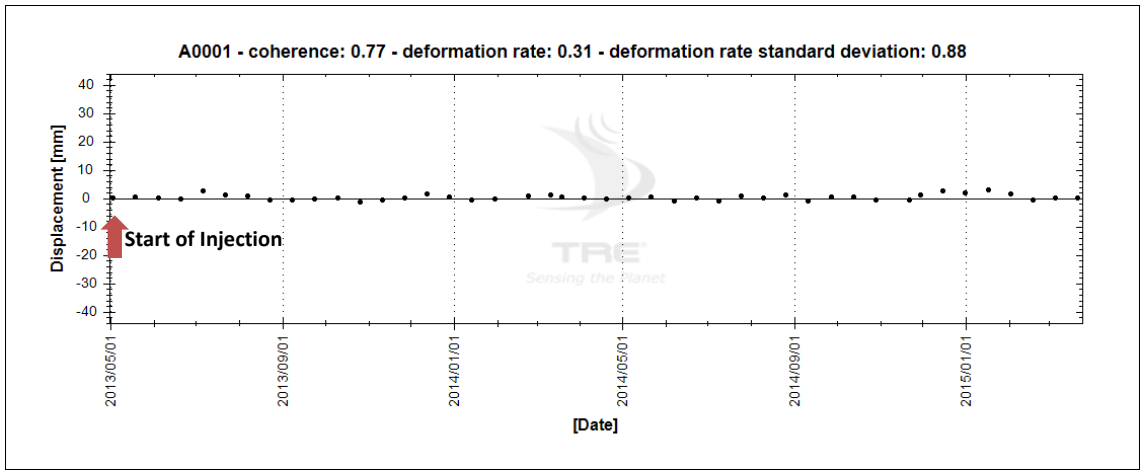

Figure 10: Average time series of all measurement points within the co-injection data.

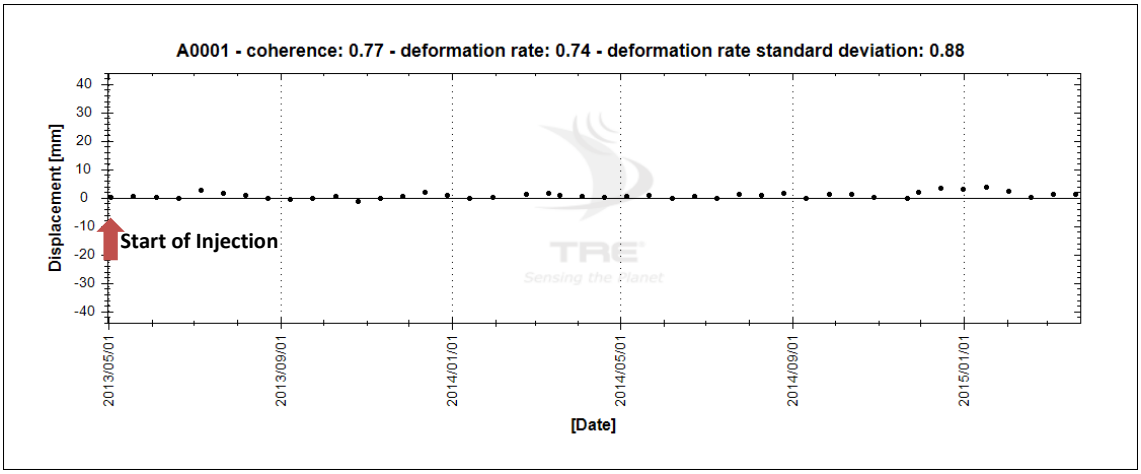

Figure 11: Average time series of all measurement points within the co-injection data over the north portion of the AOI.

The results obtained over Dover 33 are explored further in Section 5.1, which also includes a closer look into the SqueeSAR results, the artificial reflector analysis, and a comparison to the well data provided by Battelle. Section 0 describes the results for a larger set of reefs located within the AOI, while Section 5.3 includes a comparison between different well types.

5.1 Ground Deformation over Dover 33

5.1.1 SqueeSAR Analysis (Natural Radar Targets)

Displacement results over Dover 33 and the surrounding area are shown in Figure 12 for the full data and Figure 13 for the co-injection data, with Table 4 summarizing the results.

Average displacement rates in Dover 33 and in the AOI from all periods of analysis are within ±2 mm/yr. The results are consistent between the full and co-injection processings, as well as compared to the historical and baseline analyses. An average time series calculated from all measurement points within the Dover 33 reef is shown in Figure 14 for the full results and in Figure 15 for the co-injection results. Both displacement rates are within ±1 mm/yr and the time series indicate no discernible change in ground movement following the start of CO_2 injection.

Attribute	Historical analysis	Baseline analysis	Monitoring analysis (full data)	Monitoring analysis (Co-injection data)
Dates	May/20/1992 – Dec/4/1999	Apr/22/2012 – Oct/23/2012	Apr/22/2012 – Mar/22/2015	May/03/2013 – Mar/22/2015
Total N. of measurement points in Dover 33	16	80	111	42
Average Displacement Rate in Dover 33 (mm/yr)	0.3	-2	-0.3	0.7
Average Displacement Rate in AOI (mm/yr)	-1.2	-1.2	-0.2	0.3
Cumulative Displacement in Dover 33 (mm)	-1.0	-2.4	0.7	1.2
Cumulative Displacement in AOI (mm)	-10.7	-1.9	1.3	0.4

Table 4: Summary of average displacement rates and cumulative displacements identified from the InSAR monitoring over the Dover 33 reef and study area.

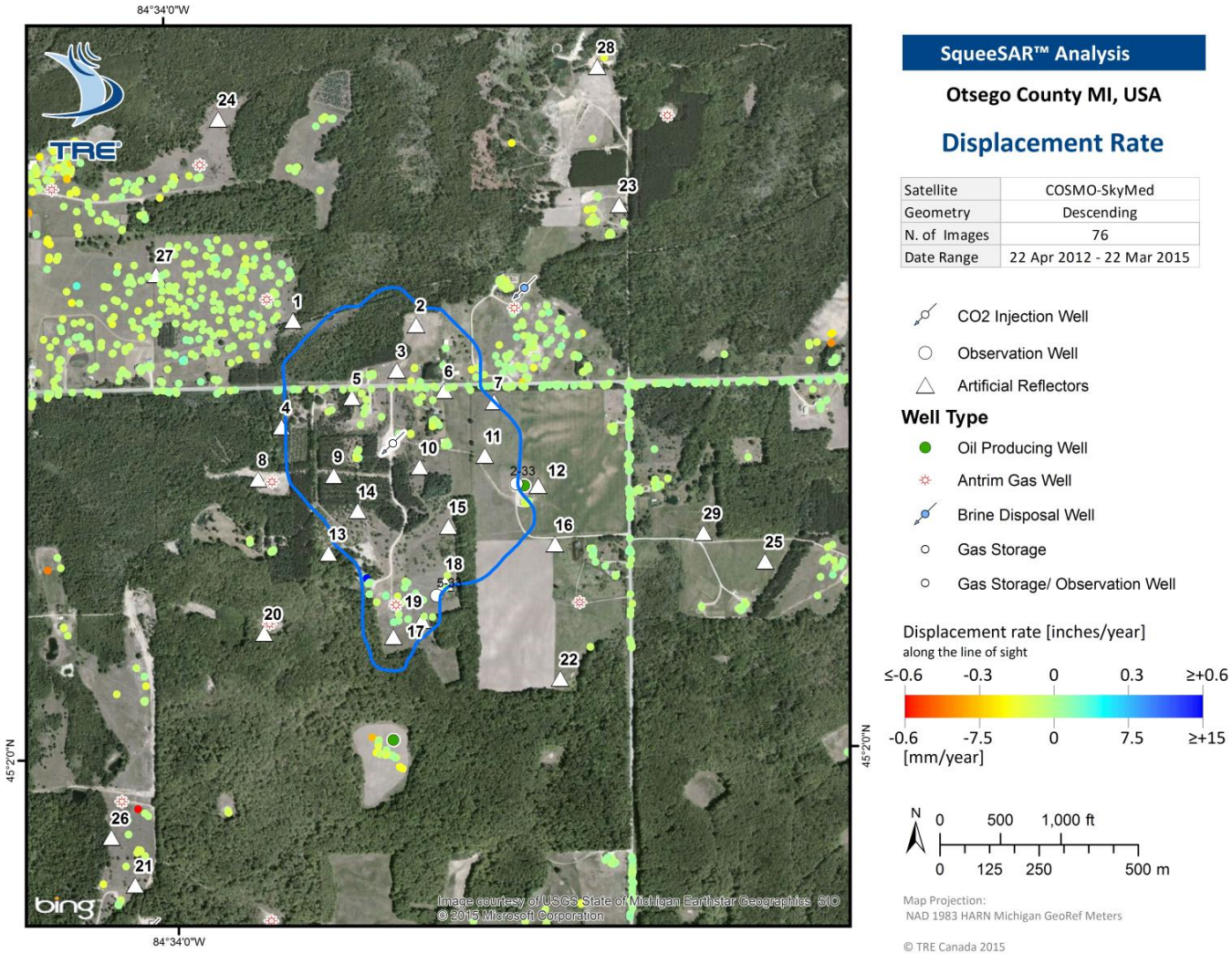

Figure 12: Displacement results from the full data over the Dover 33 field.

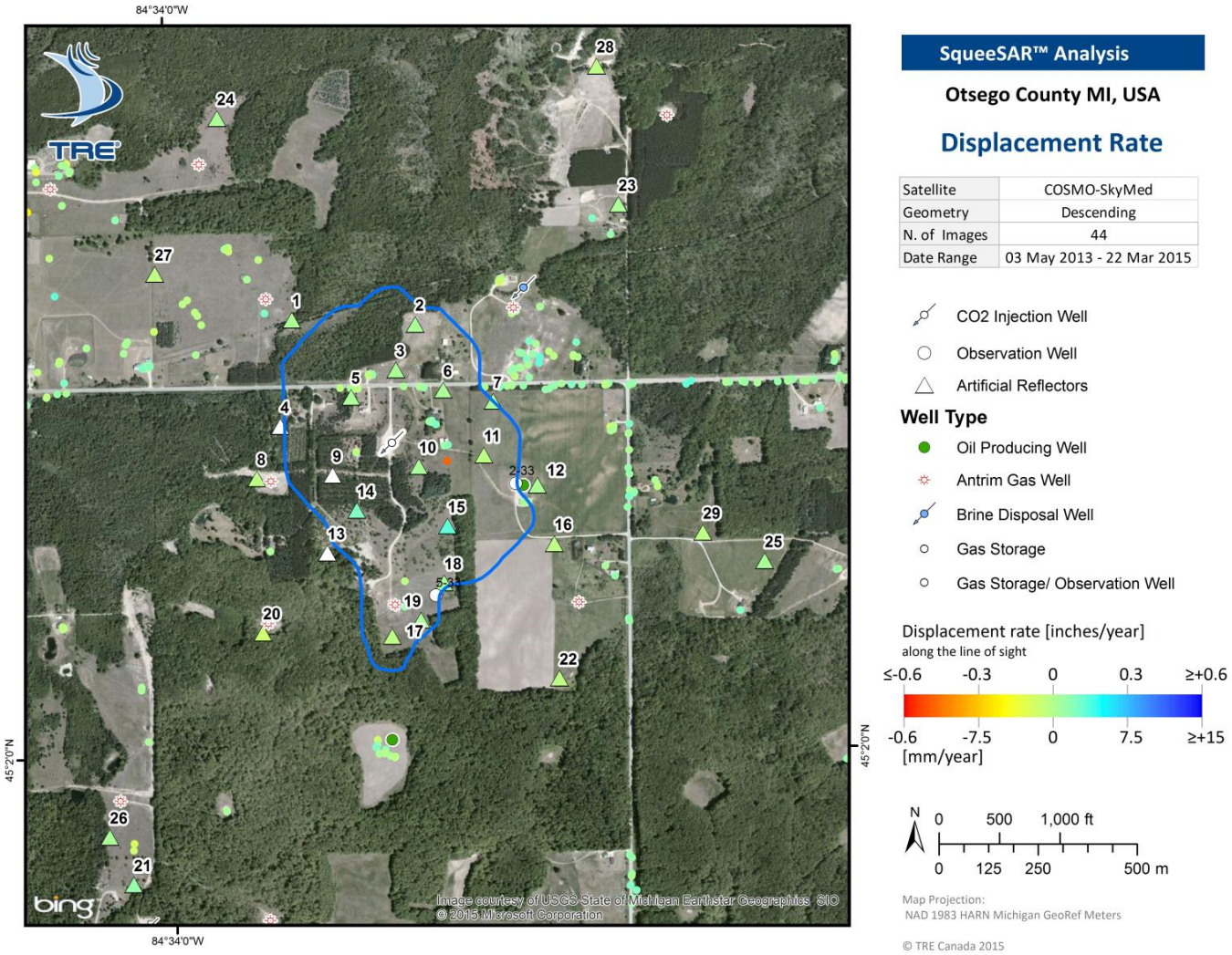

Figure 13: Displacement results from the co-injection data over the Dover 33 field.

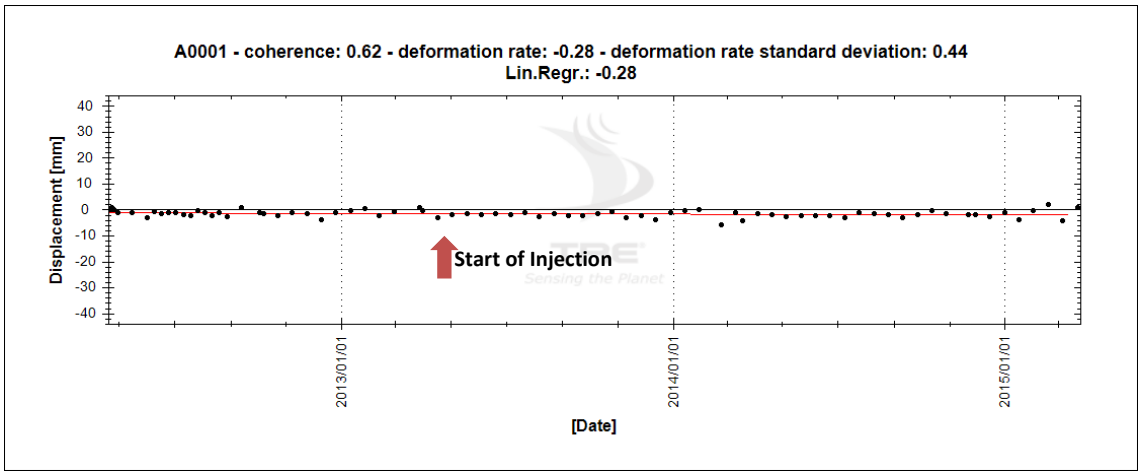

Figure 14: Average time series of all measurement points in the full data identified over the Dover 33 reef. The x axis represents the image acquisition date and the y axis denotes the measured ground deformation in millimeters. The red line indicates the linear regression.

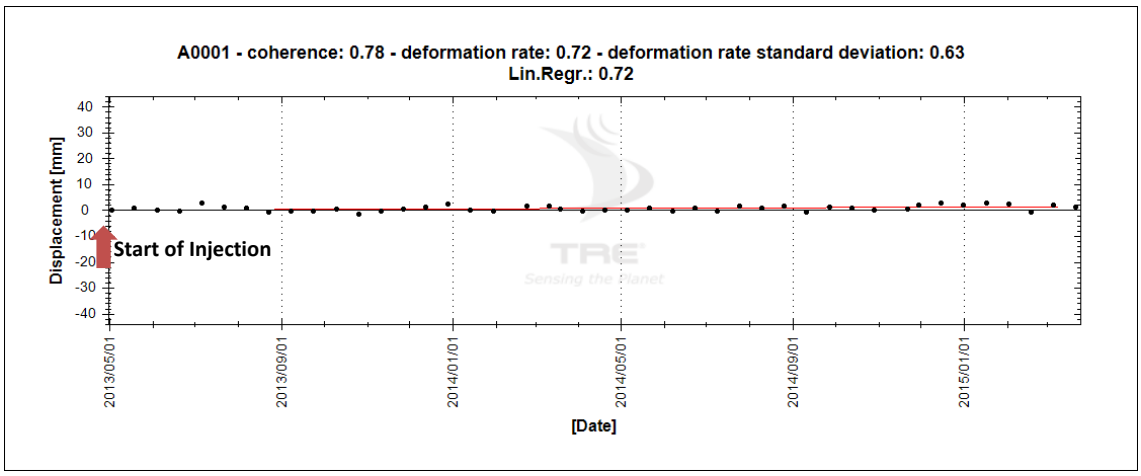

Figure 15: Average time series of all measurement points in the co-injection data identified over the Dover 33 reef.

Three average time series derived from measurement points in the full data in the vicinity of the injection well are shown in Figure 16 to Figure 19, inclusive. ATS1, located 90 metres (295 feet) west of the injection well exhibits minimal ground deformation rates of -0.4 mm/yr. Mild uplift with a ground deformation rate of +1.3 mm/yr was found within a 40 metre (131 feet) buffer of the injection well (ATS2). Slight subsidence (-1.8 mm) was observed 54 meters (177 feet) east of the injection well (ATS3 in Figure 16). The ground deformation results from the natural targets in the full data indicate no clear surface response to CO_2 injection. Ground deformation trends inside and outside of Dover 33 are consistently similar as well, when comparing the baseline and monitoring periods. No distinct change of ground deformation was detected temporally (pre- and co-injection) or spatially (inside/outside of Dover 33).

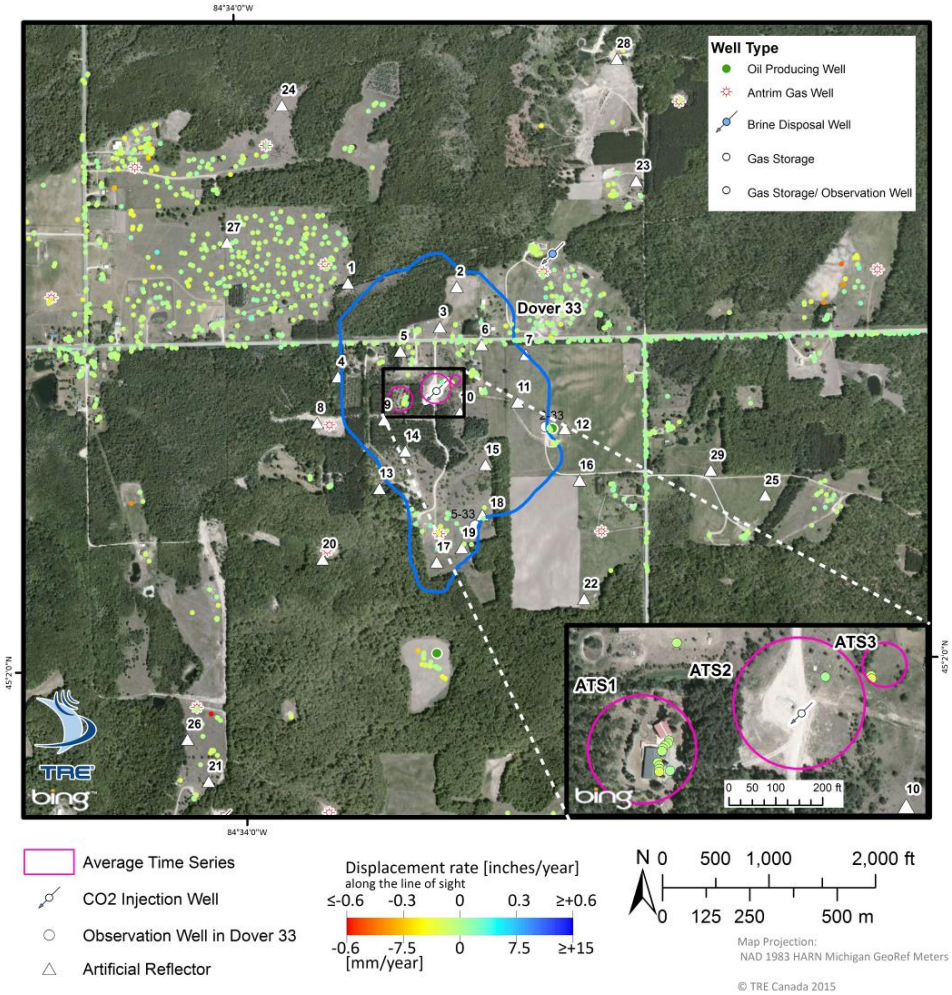

Figure 16: Overview of displacement results obtained within close proximity of the injection site. The top right window is a close up in the area of the injection well.

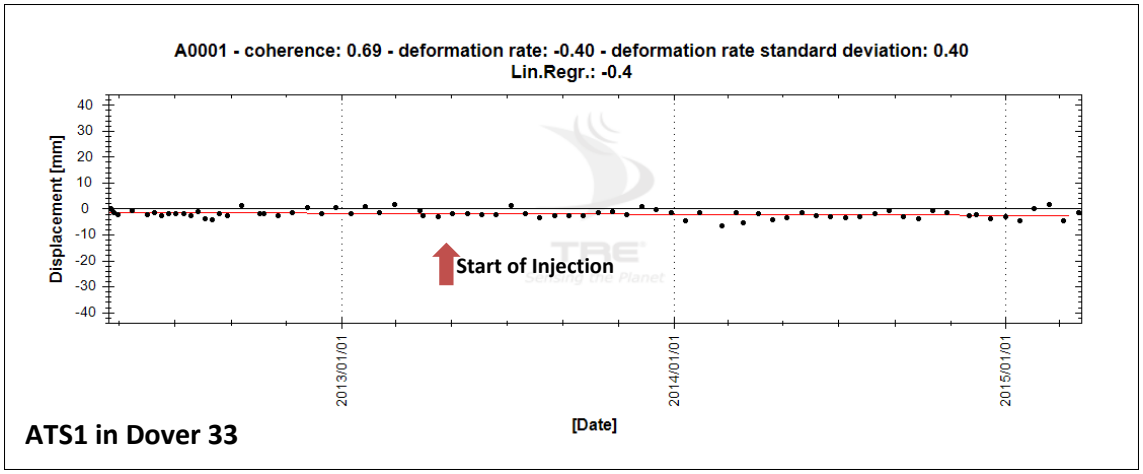

Figure 17: Average time series of measurement points identified within the area labeled ATS1 in Figure 16.

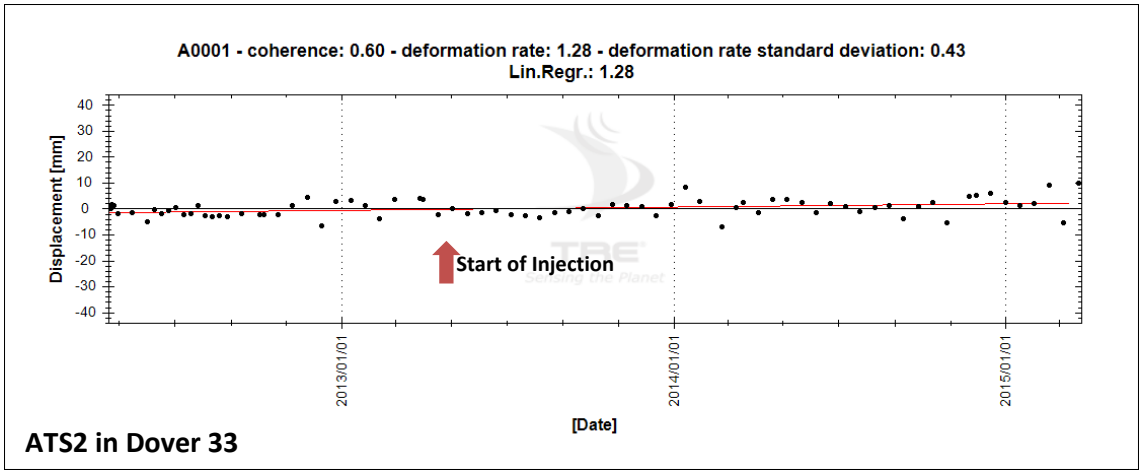

Figure 18: Average time series of measurement points identified within the area labeled ATS2 in Figure 16.

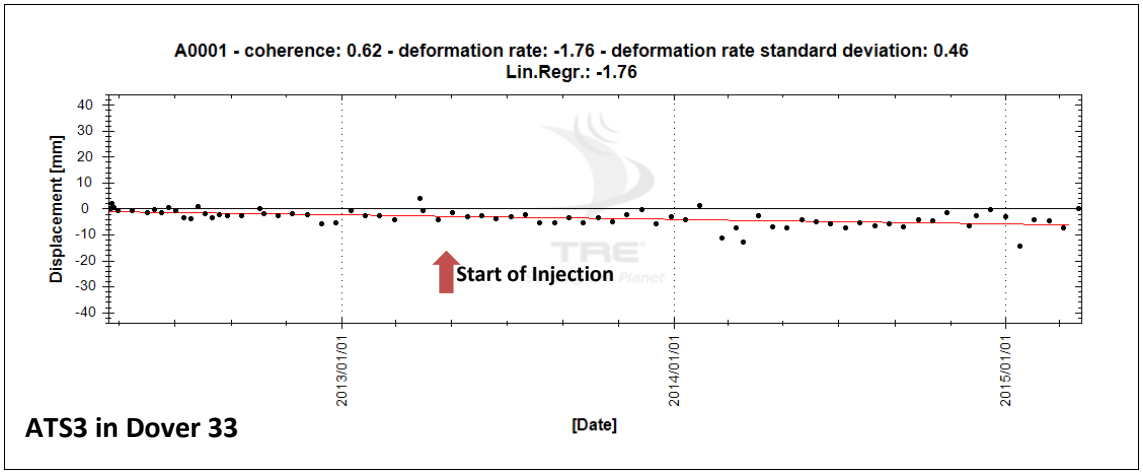

Figure 19: Average time series of measurement points identified within the area labeled ATS3 in Figure 16.

5.1.2 Artificial Reflector Analysis

A total of 29 Artificial Reflectors (AR) have been installed to supplement the distribution of natural measurement points over the Dover 33 reef. All ARs were installed in March 2013, prior to the start of CO_2 injection. Thirteen were installed within the Dover 33 reef boundary while the remaining 16 were positioned in the surrounding area to extend the AR network and provide reference point candidates. Displacement results for all reflectors are shown in Figure 20. Reflector #28 was selected to be the reference point and is located 1,081 metres (2,547 feet) from the injection well in Dover 33.

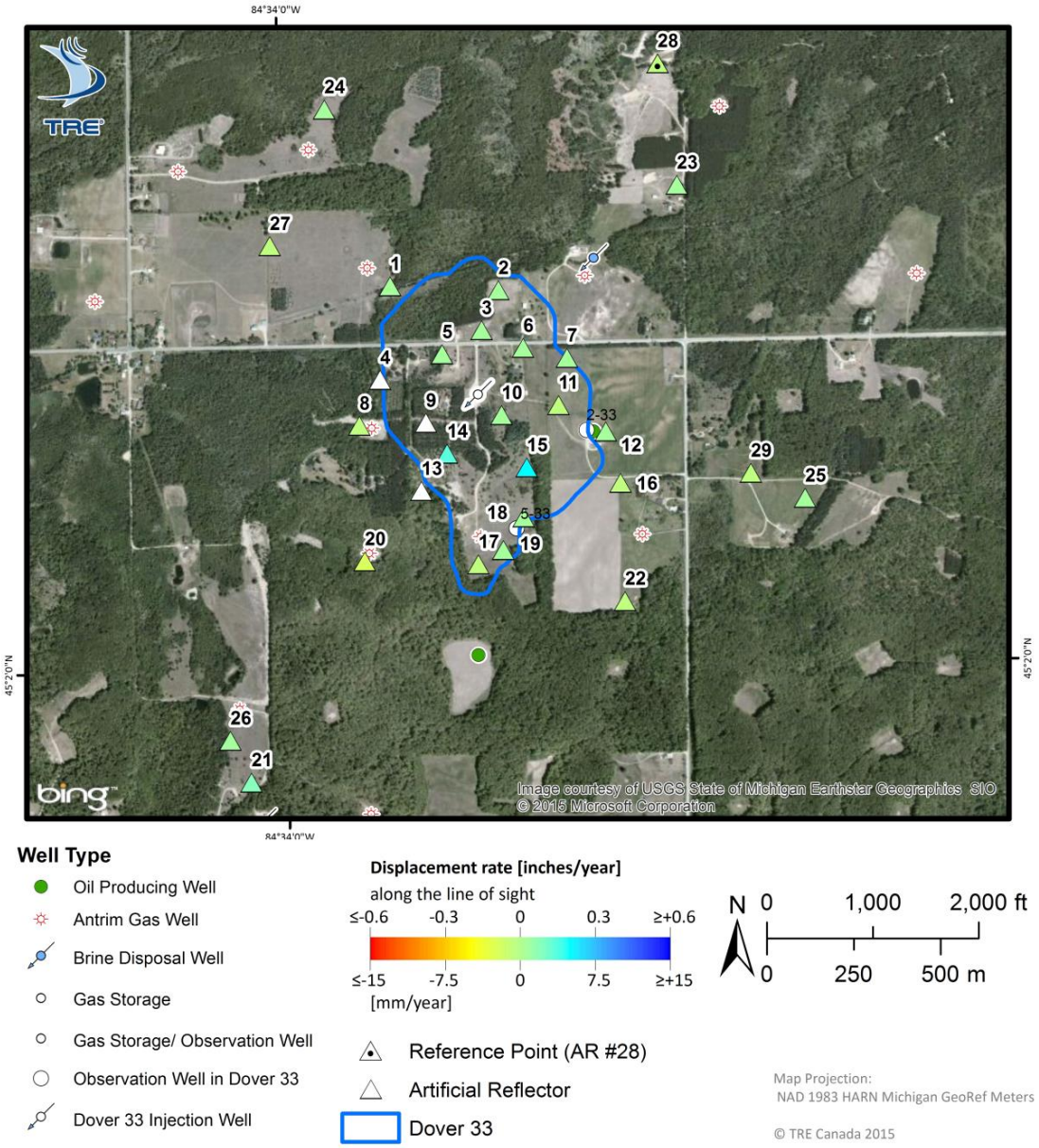

Figure 20: Displacement results obtained for all ARs installed at the Dover 33 site. Three ARs (shown in white) are not included in the present analysis, as they were not visible to the satellite.

The AR visibility check showed that 26 of 29 reflectors are visible to the satellite, with visibility of reflectors #4, #9 and #13 likely being obstructed by trees. Among the 26 visible reflectors, reflector #14, #20, and #26 (Figure 21, Figure 23, and Figure 24, respectively) exhibited a drop in reflectivity between January and February, 2015, possibly caused by heavy snow in winter months. AR #15 (Figure 22) had an abrupt drop in August 2014. The reflector may have been removed, rotated or damaged.

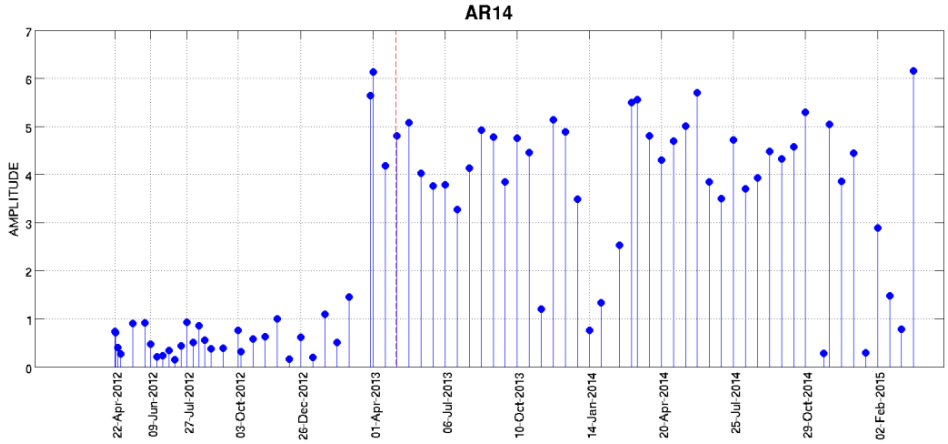

Figure 21: Reflectivity of AR #14. The x axis indicates the date of the radar image and the y axis denotes the strength of the reflectivity to radar signals. The vertical red line shows the time when the reflector was installed.

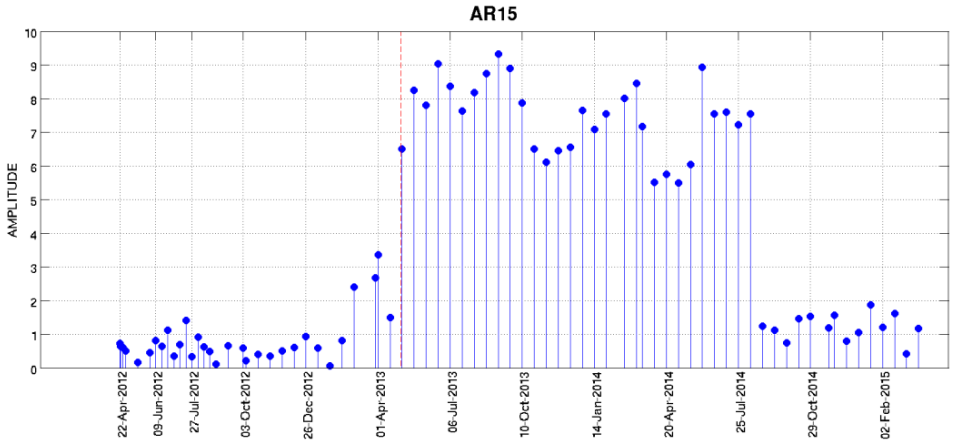

Figure 22: Reflectivity of AR #15.

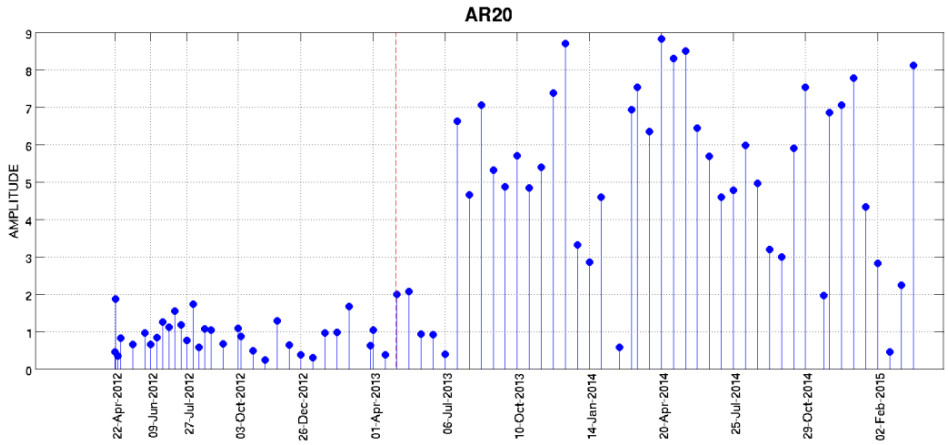

Figure 23: Reflectivity of AR #20.

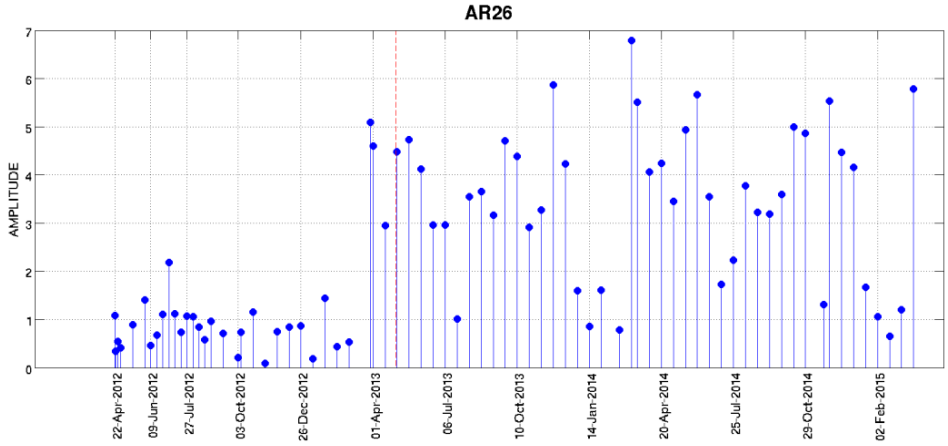

Figure 24: Reflectivity of AR #26.

A total of 44 images collected between May 03, 2013 and March 22, 2015 were processed for the AR analysis. Displacement rates over Dover 33 were between -0.1 mm/yr and +3.9 mm/yr. An average deformation rate of 1.1 mm/yr was obtained from the ARs over Dover 33, while the average for all ARs outside the reef was 0.01 mm/yr (Figure 25 and Figure 26). The results indicate that the reflectors within and outside of Dover 33 are mainly stable.

Displacement rates of all ARs are minimal, ranging from -1.5 mm/yr to +3.9 mm/yr, with an average of +0.4 mm/yr. Time series for individual ARs are shown in Figure 27 to Figure 52, inclusive. The five ARs closest to the injection well are AR #3, #5, #6, #10, #14, and have displacement rates ranging from +0.2 to +2.4 mm/yr. Some fluctuations due to snowfall in winter are visible in the time series (AR #14, #15, #20, #26), but no ground deformation trend related to CO_2 injection operations is observed in the AR results. The +3 mm uplift between November 2014 to February 2015 appears to be similar to the regional trend discussed in Page 17 and is likely unrelated to injection activities. The reflectivity analysis conducted in April 2015 is shown in the Technical Appendix.

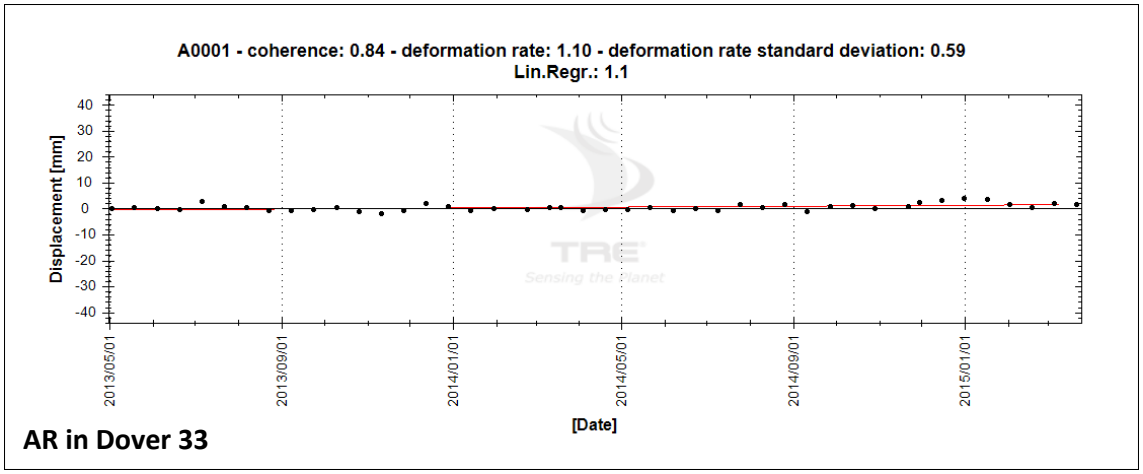

Figure 25: Average time series of the 12 reflectors located over the Dover 33 reef.

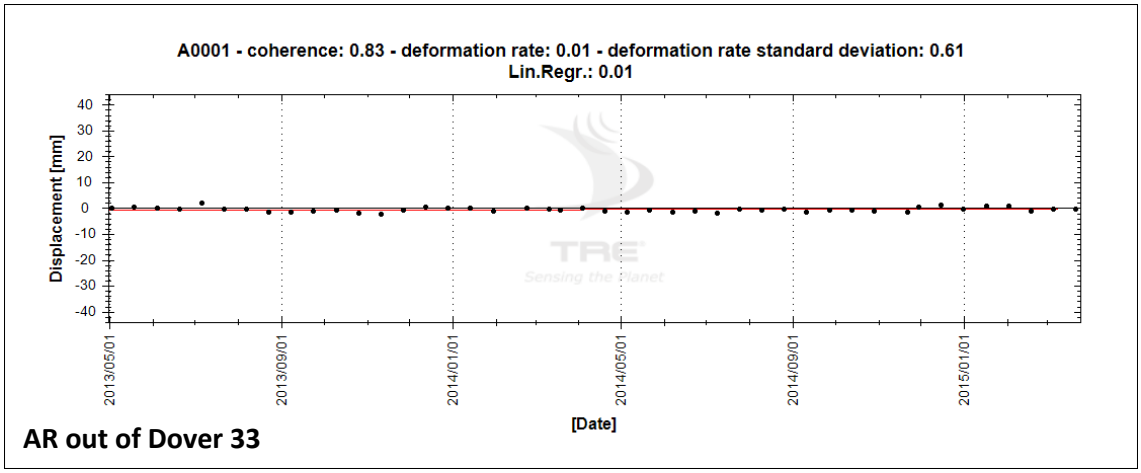

Figure 26: Average time series of the 14 reflectors located outside of the Dover 33 reef.

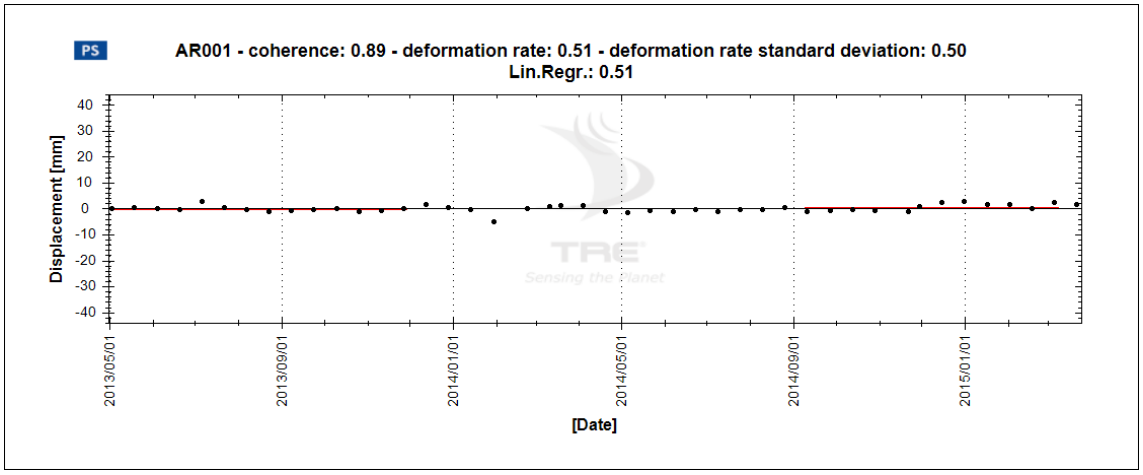

Figure 27: Time series of AR 1.

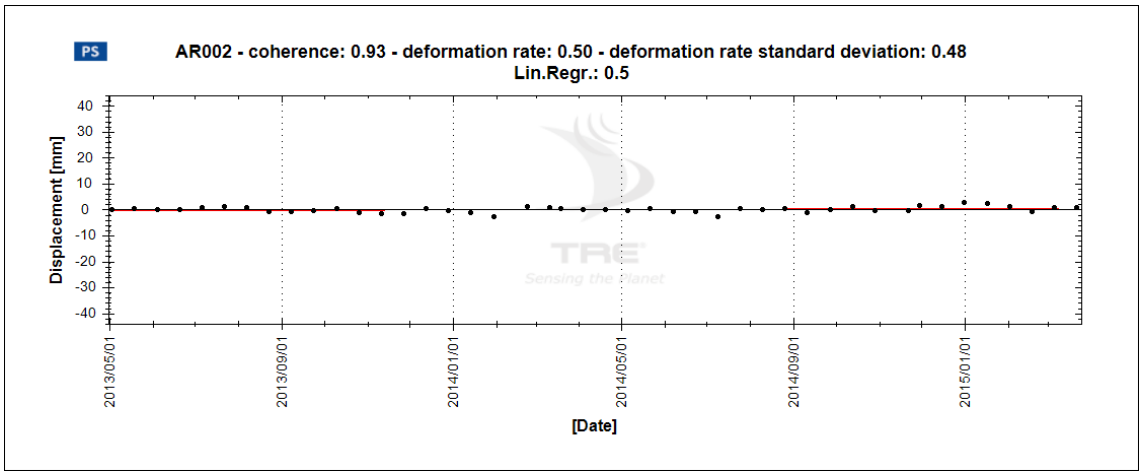

Figure 28: Time series of AR 2.

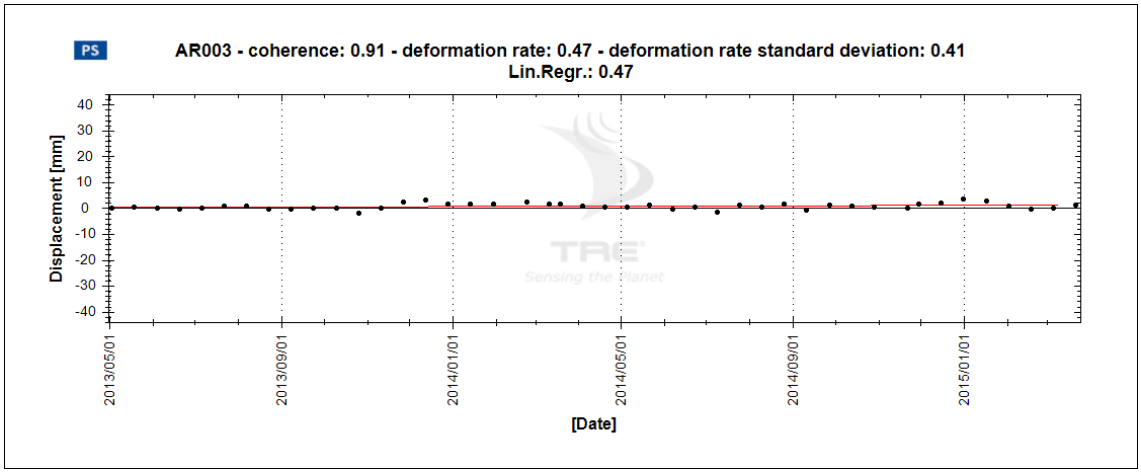

Figure 29: Time series of AR 3.

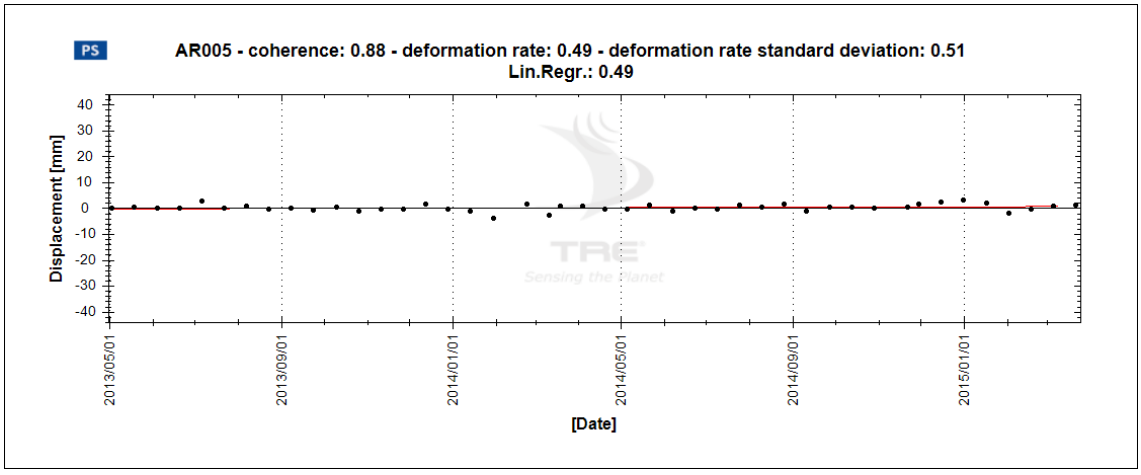

Figure 30: Time series of AR 5.

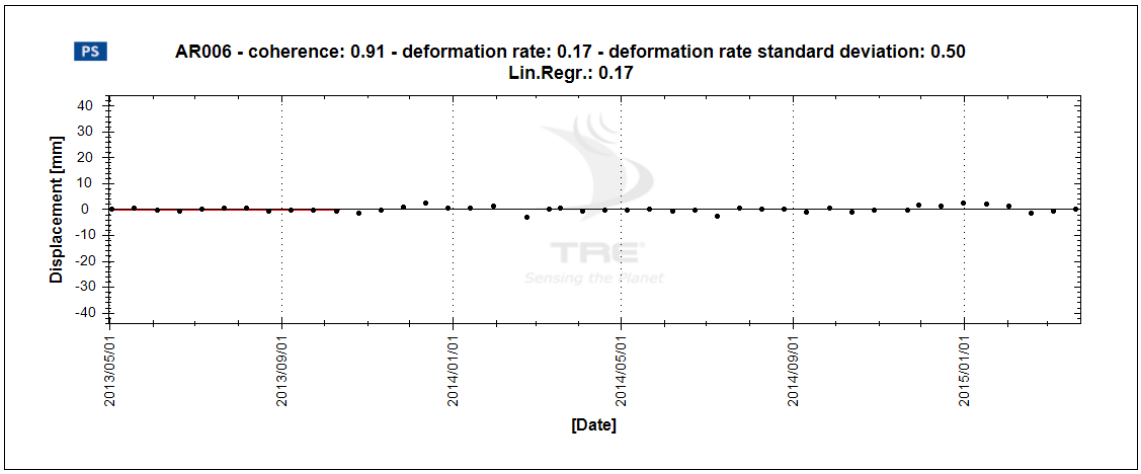

Figure 31: Time series of AR 6.

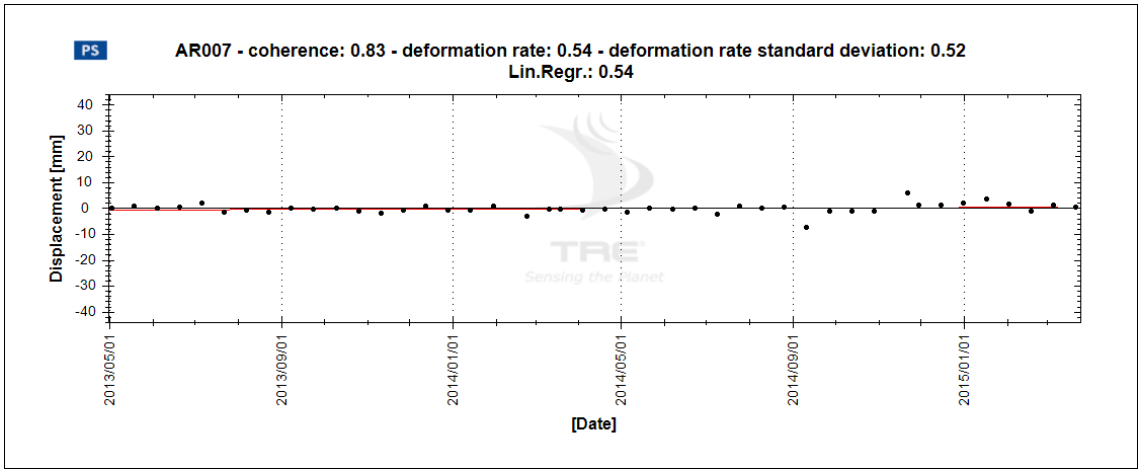

Figure 32: Time series of AR 7.

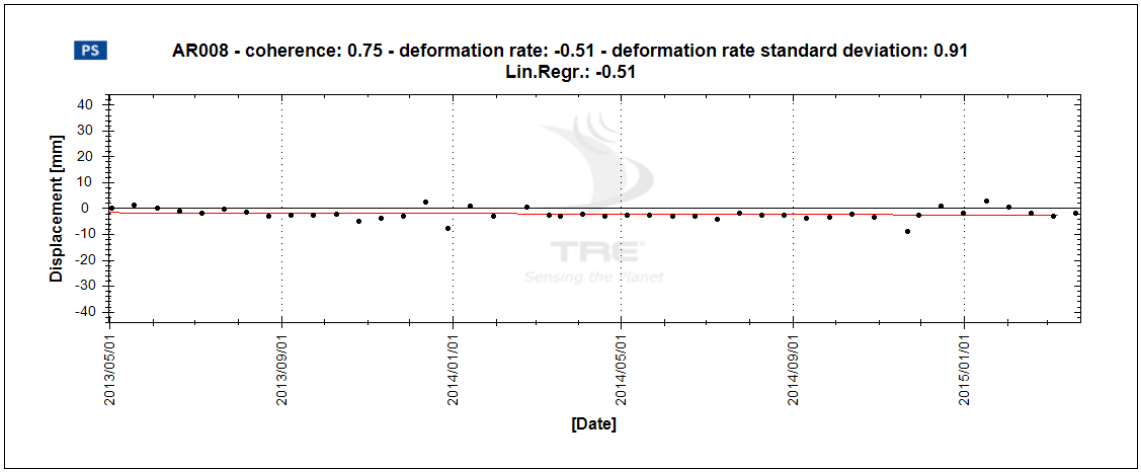

Figure 33: Time series of AR 8.

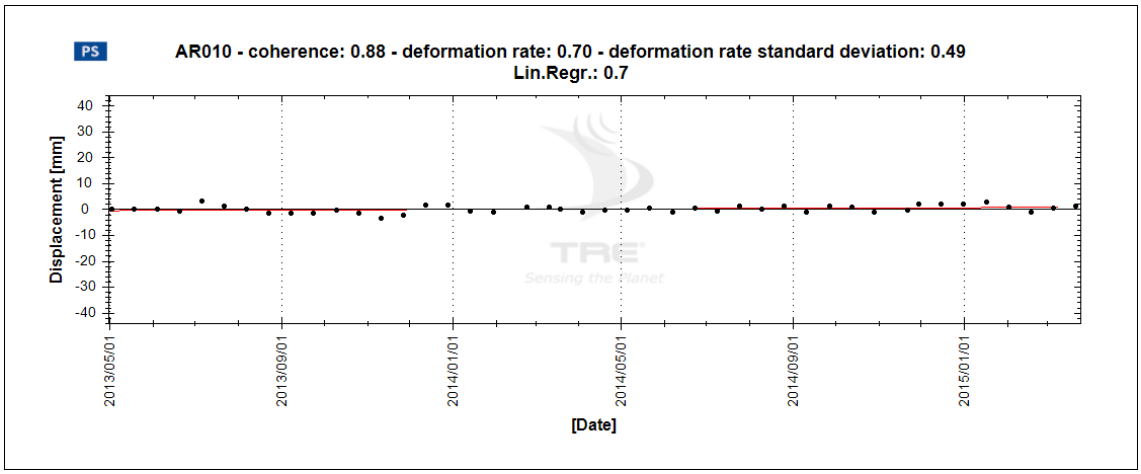

Figure 34: Time series of AR 10.

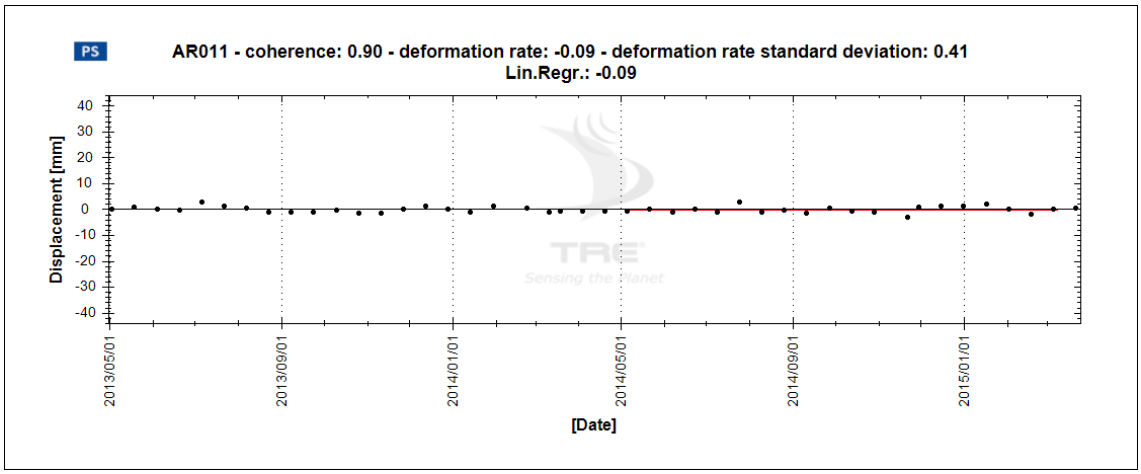

Figure 35: Time series of AR 11.

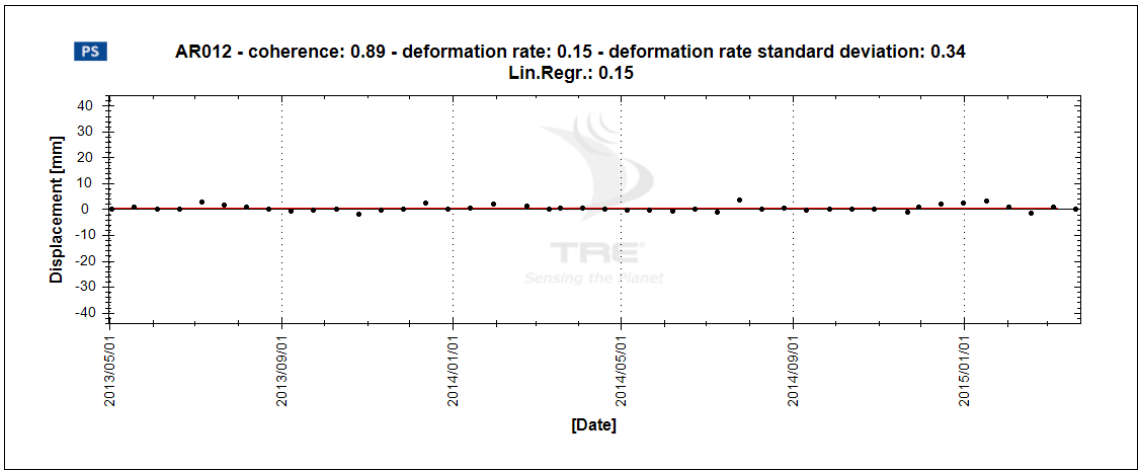

Figure 36: Time series of AR 12.

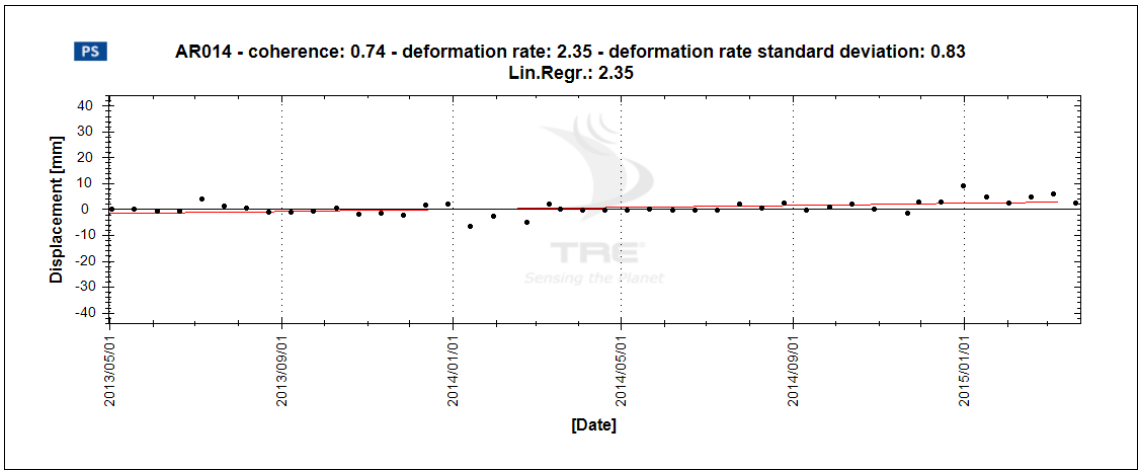

Figure 37: Time series of AR 14.

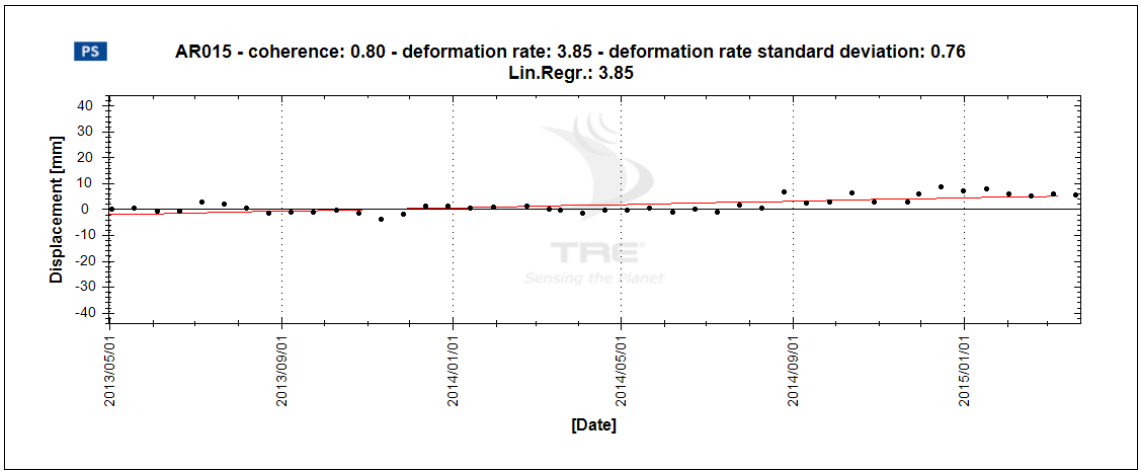

Figure 38: Time series of AR 15.

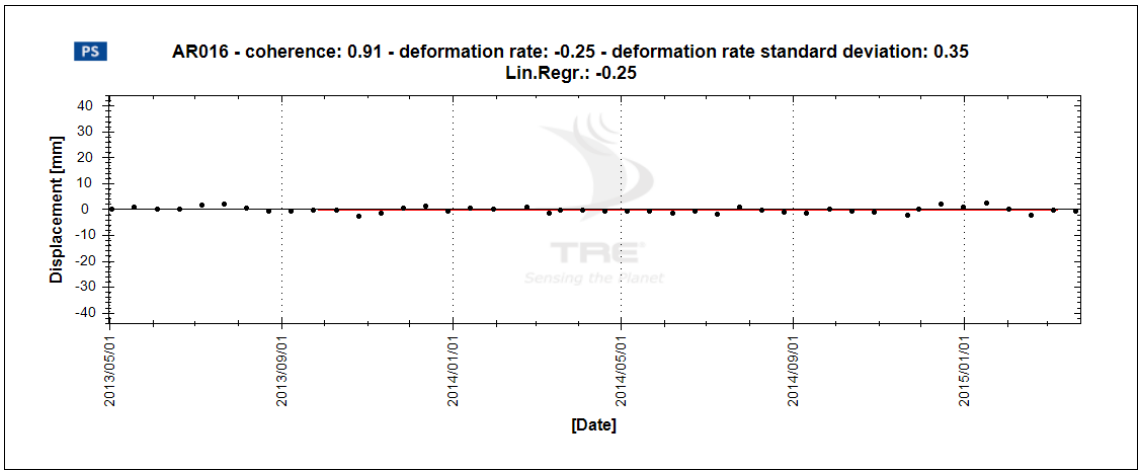

Figure 39: Time series of AR 16.

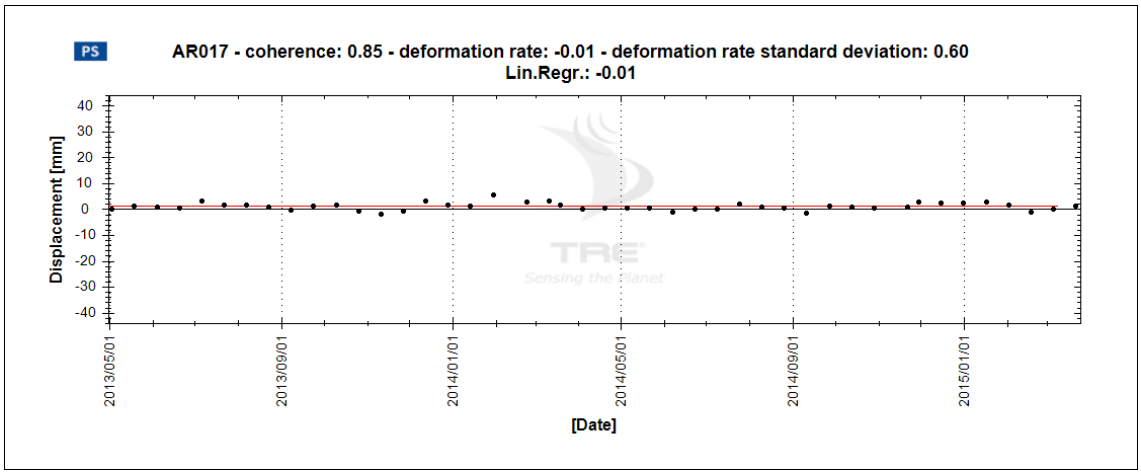

Figure 40: Time series of AR 17.

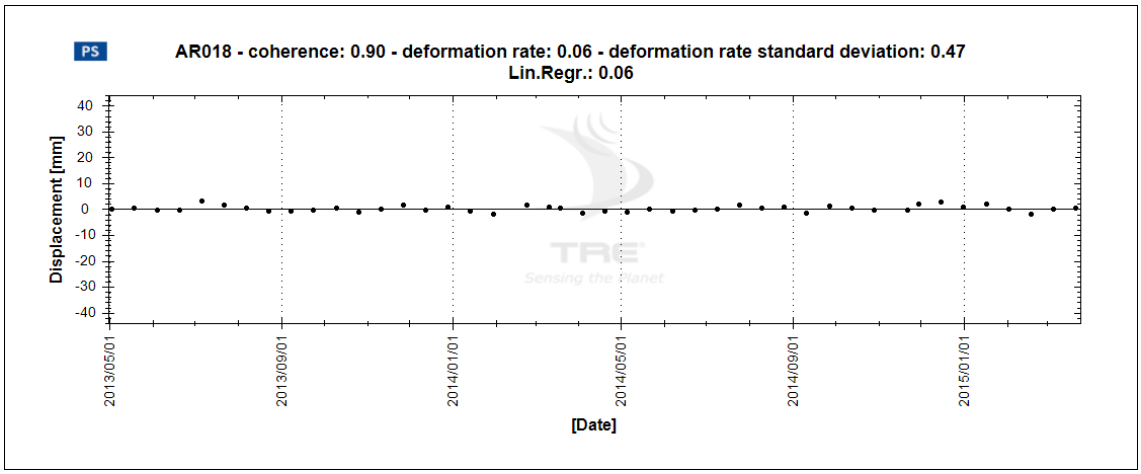

Figure 41: Time series of AR 18.

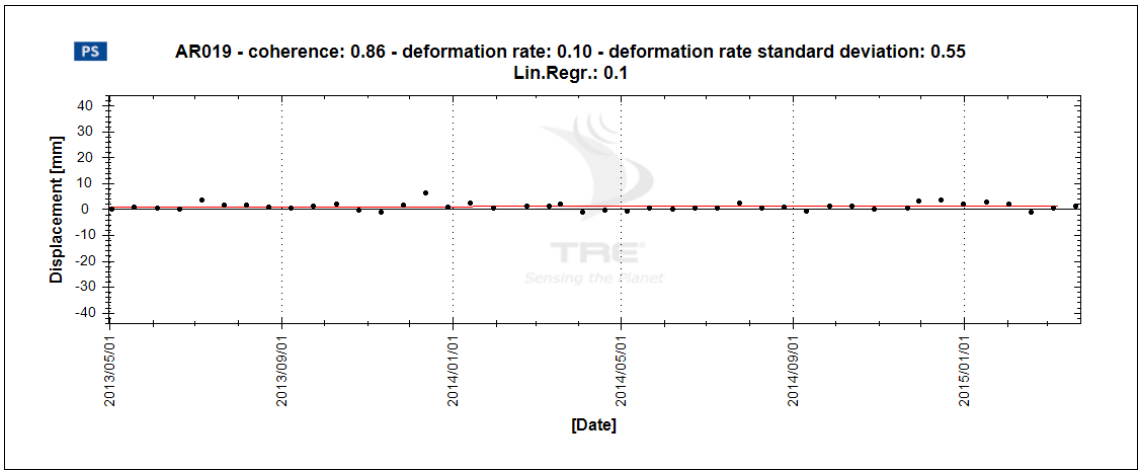

Figure 42: Time series of AR 19.

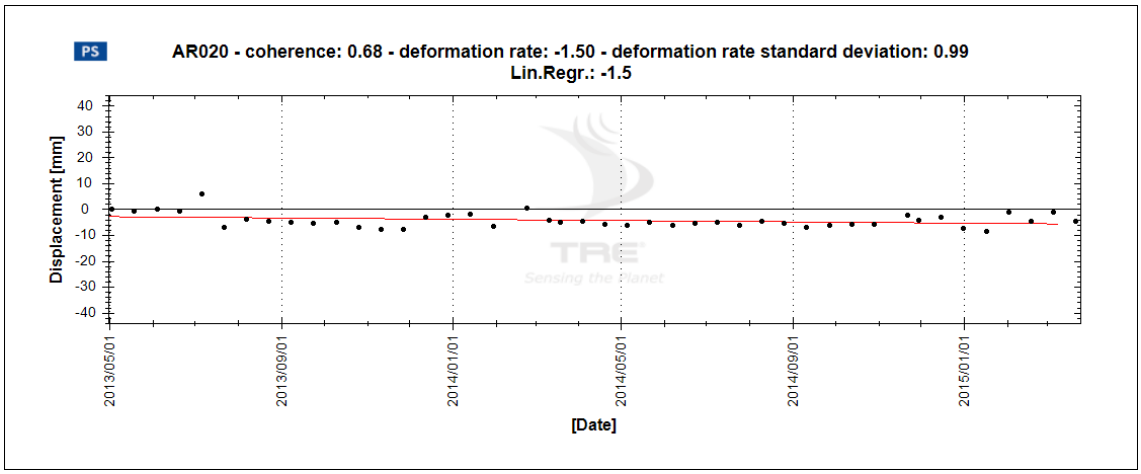

Figure 43: Time series of AR 20.

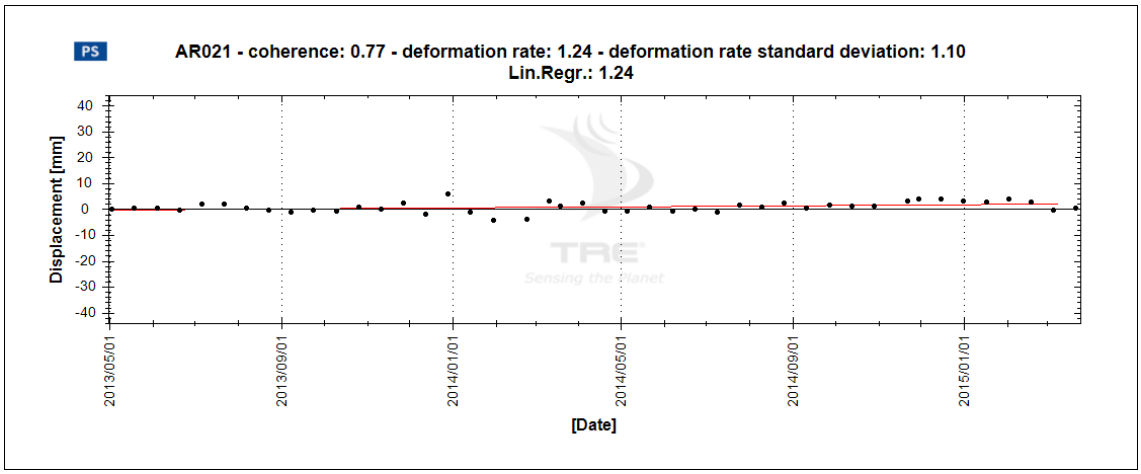

Figure 44: Time series of AR 21.

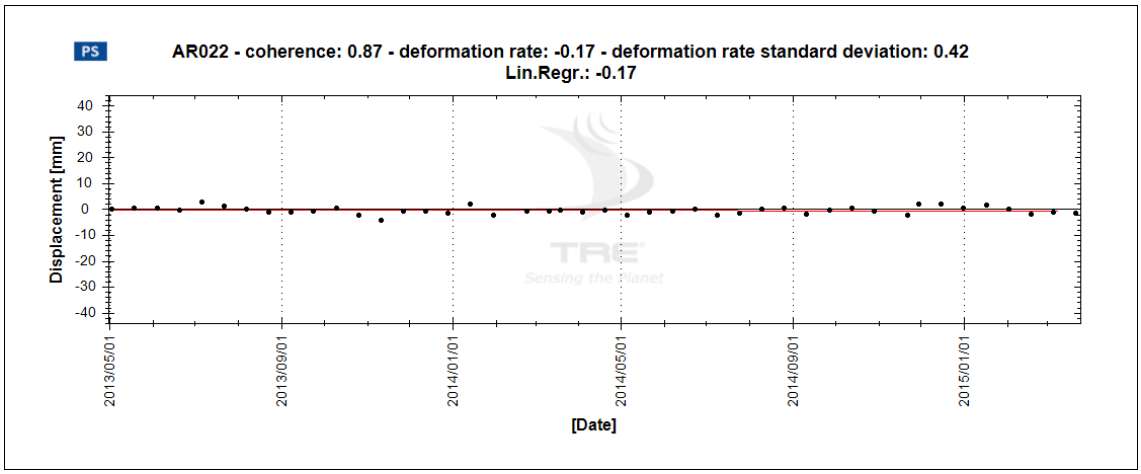

Figure 45: Time series of AR 22.

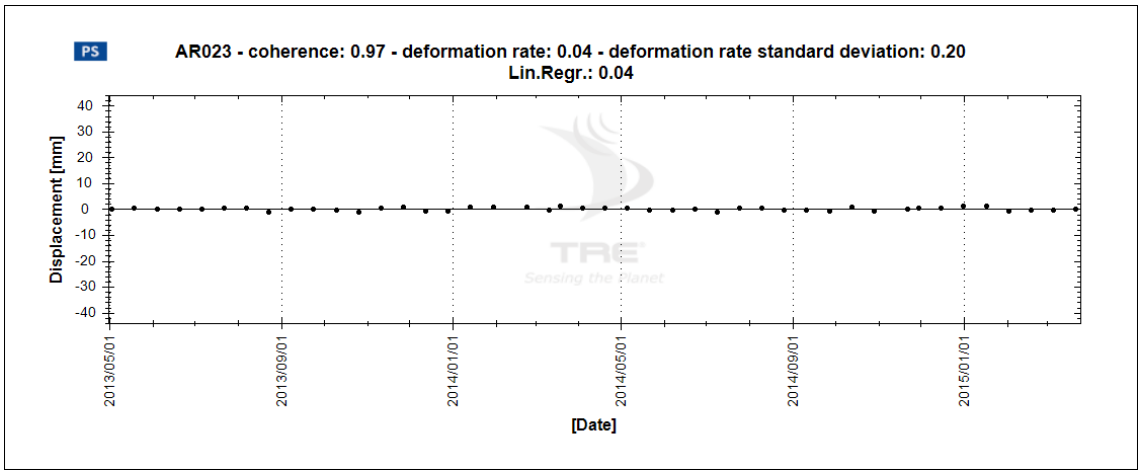

Figure 46: Time series of AR 23.

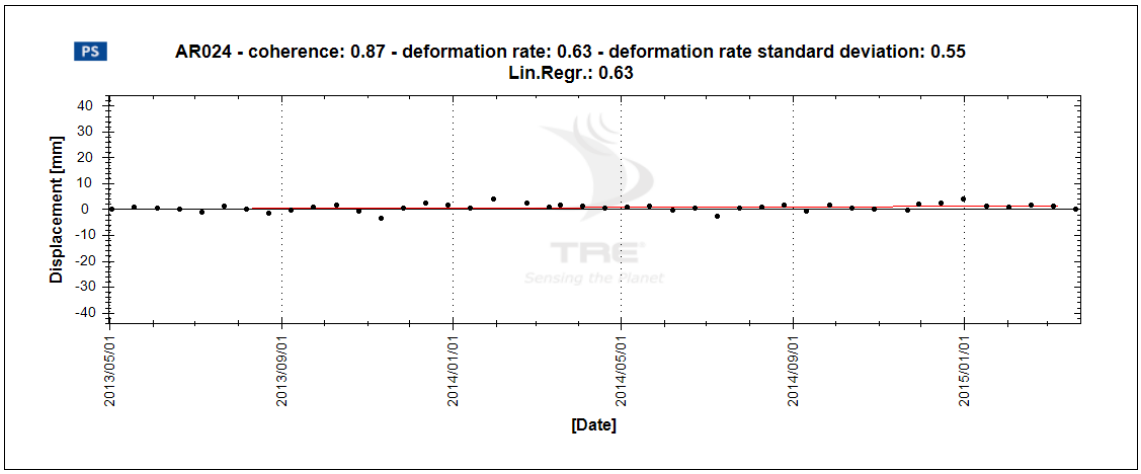

Figure 47: Time series of AR 24.

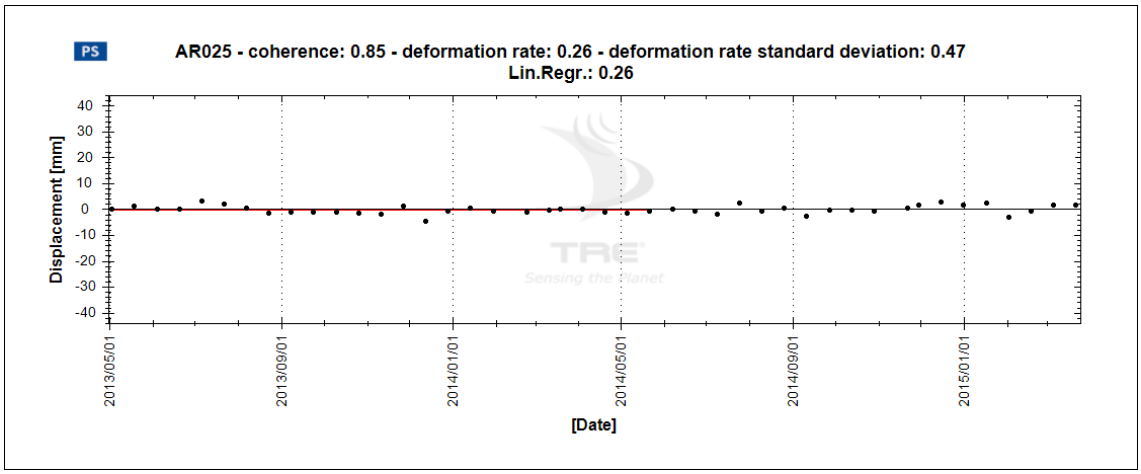

Figure 48: Time series of AR 25.

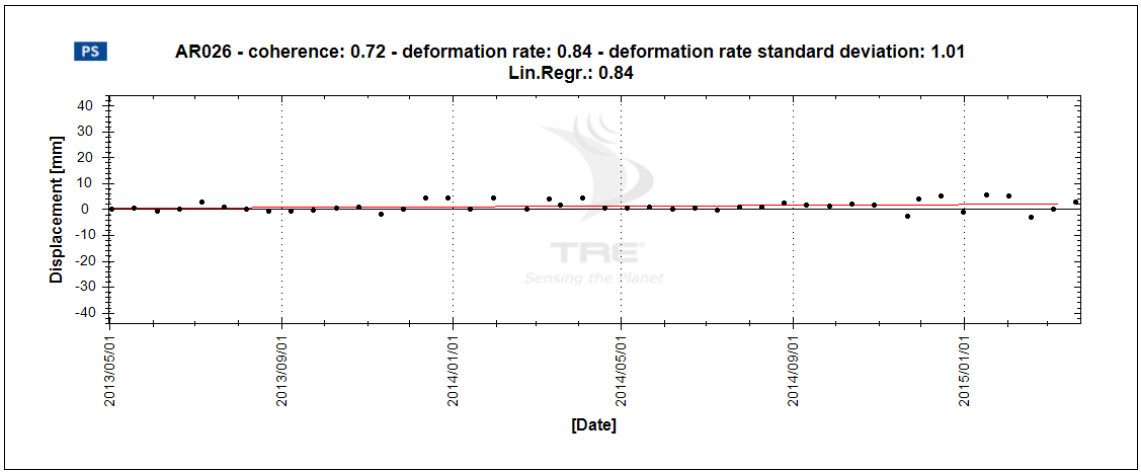

Figure 49: Time series of AR 26.

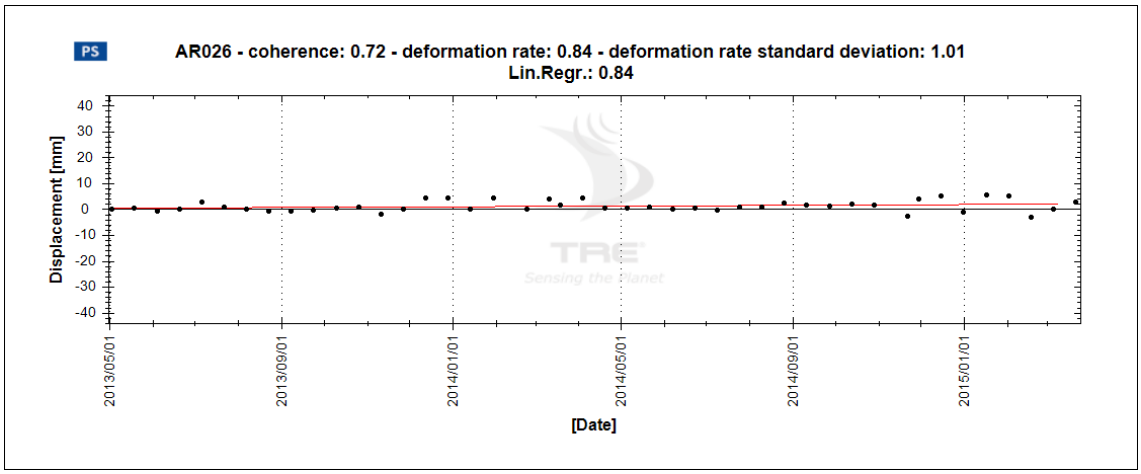

Figure 50: Time series of AR 27.

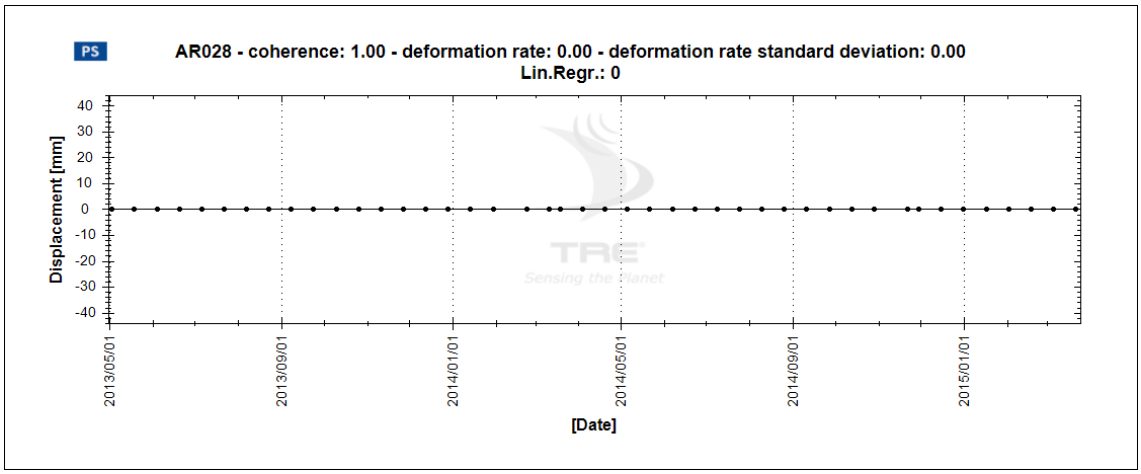

Figure 51: Time series of AR 28.

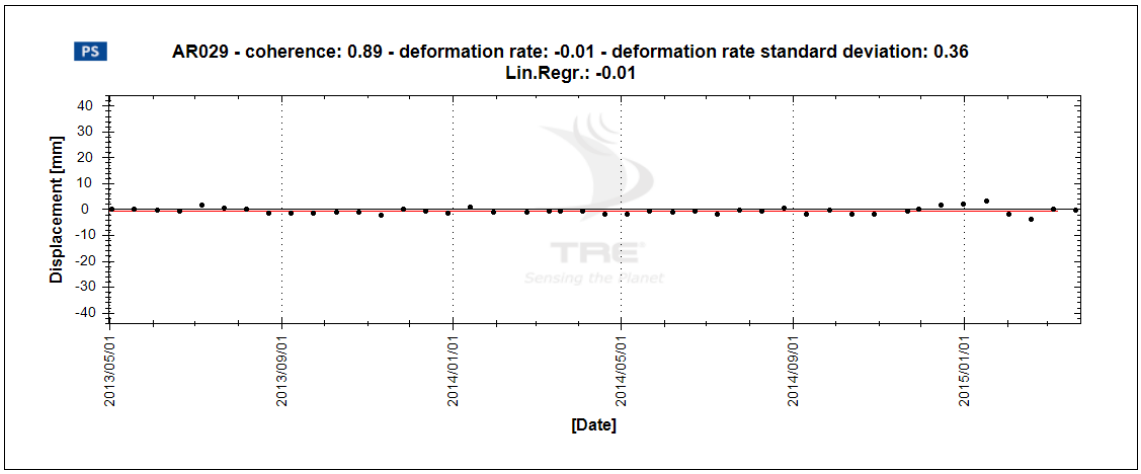

Figure 52: Time series of AR 29.

5.1.3 Comparison to Well Data

To investigate potential correlation between ground movement and CO_2 injection, bottomhole pressures (BHP) and the injected CO_2 volume were compared with displacement results over Dover 33. BHP data was recorded with four-hour frequency for well 1-33 between January 23, 2013 and April 14, 2015. Injected CO_2 volume was recorded daily from February 18, 2013 to April 05, 2014. BHP and CO_2 volume were provided by Battelle.

The results of the analysis are shown in Figure 53 and Figure 55. Ground deformation obtained from the ARs (shown in the top panel of Figure 53) and natural radar targets that cover the full period, as well as the co-injection time period, are included in the graph (shown in the bottom panel of Figure 53). The table below provides descriptions of each data label in Figure 53.

	Data Label		Description
AR results	AR ATS in Dover 33		The average time series derived from ARs within Dover 33.
	AR ATS out Dover 33		The average time series derived from ARs outside of Dover 33.
	AR 10		The closest AR to the injection well.
Natural radar target co-injection results	ATS in Dover 33 (Post-Inj)		The average time series derived from natural radar targets from the co-injection period within Dover 33.
	ATS in AOI (Post-Inj)		The average time series derived from only natural radar targets in the AOI for the co-injection period.
Natural radar target full data results	ATS in Dover 33 (Full)		The average time series derived from natural radar targets within Dover 33 for the full data.
	ATS in AOI (Full)		The average time series derived from natural radar targets in the AOI for the full data.
	ATS1 (Full)		The average time series of natural radar measurements within 100 metres (328feet) of the injection well for the full data.

Table 5: Description of data labels in Figure 53.

While the magnitude of BHP increased from zero to over 3,000 PSI and over 244,000 tons of CO_2 were injected, ground deformation in the ARs and natural radar targets stayed within ±5 mm throughout the 35-month monitoring period (April 2012 to March 2015). Oscillations greater than -5 or +5 mm (but below ±10 mm) were only observed in the winter, likely caused by measurement noise related to snowfall. Accordingly, this phenomenon is usually more notable in natural radar targets than in artificial reflectors.

The results indicate that surface displacement within and outside of Dover 33 are similar. No discernable surface deformation response to variations in bottomhole pressure and injected CO_2 volume was observed.

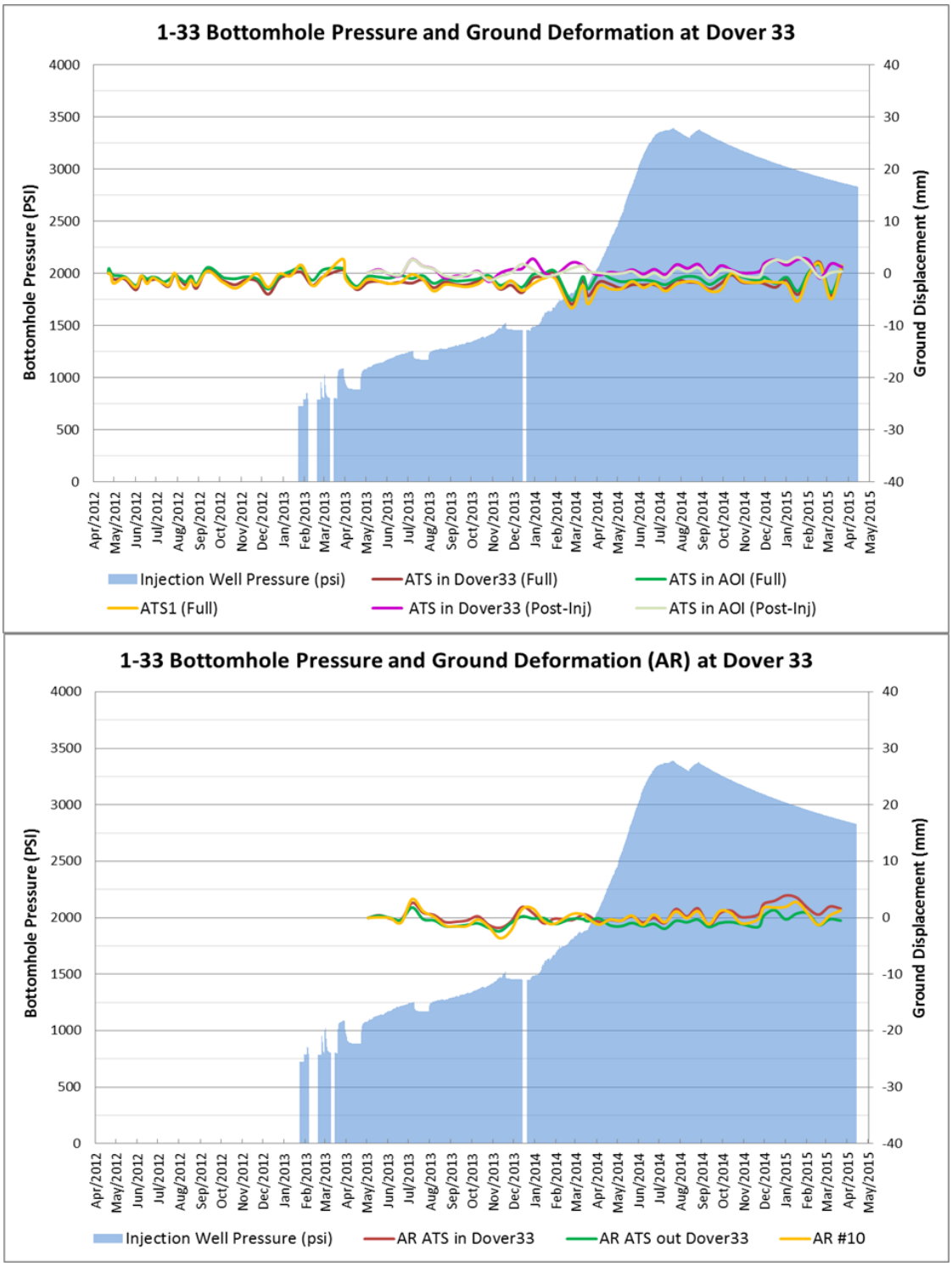

Figure 53: BHP and ground deformation results obtained at Dover 33. The top panel represents ground deformation results obtained from the ARs, while the bottom panel shows ground deformation results obtained from natural radar targets for both the full and co-injection data.

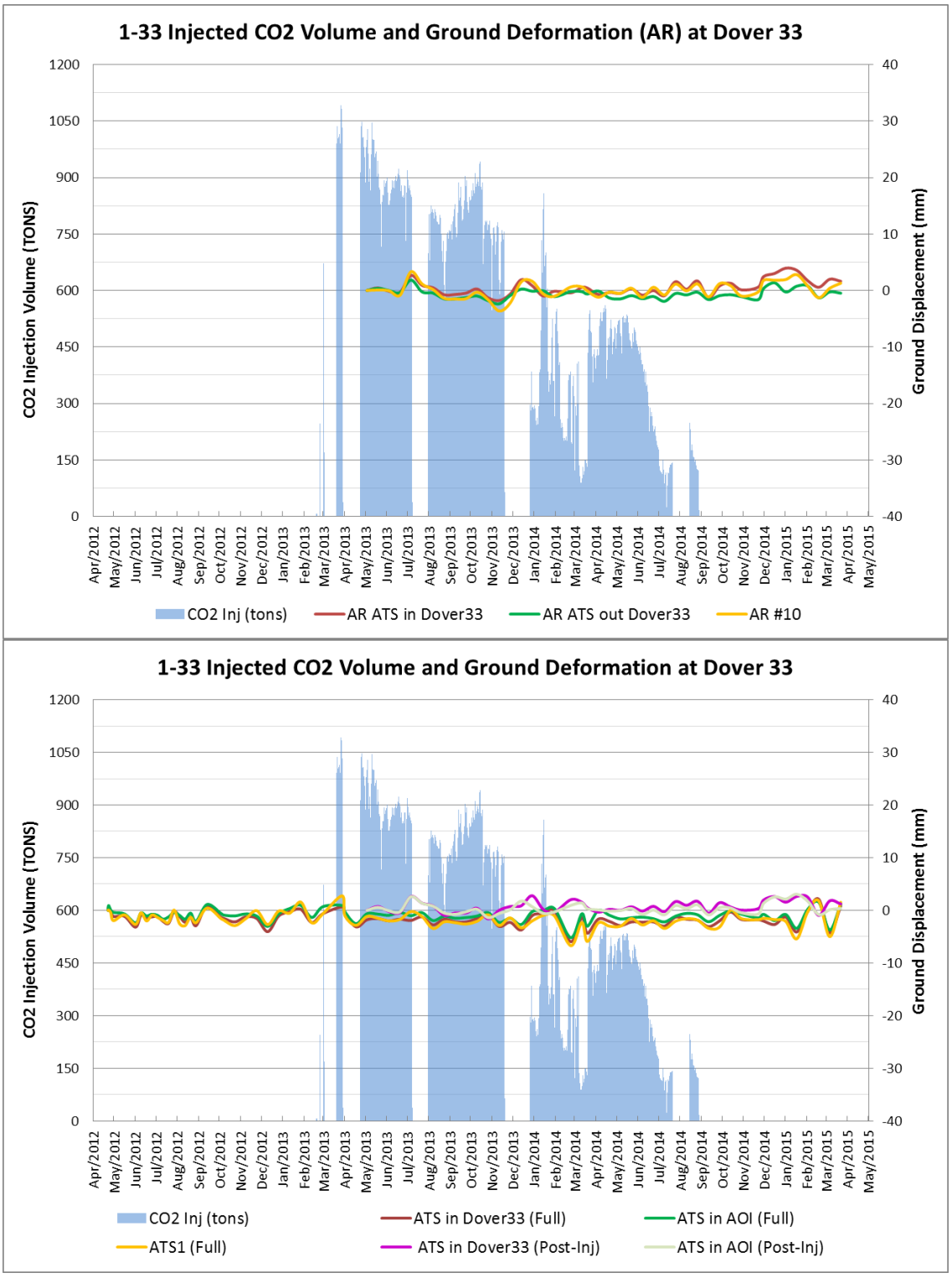

Figure 54: Injected CO_2 volume and ground deformation results obtained at Dover 33. The top panel represents ground deformation results obtained from the ARs, while the bottom panel shows ground deformation results obtained from natural radar targets for both the full and co-injection data.

5.2 Ground Deformation over the Remaining Reefs

Results obtained over the remaining eight reefs located across the northern portion of the AOI were also examined (Figure 55). Average time series were generated for all measurement points contained within each reef and are shown in Figure 56 to Figure 63, inclusive. All average displacement rates in the reefs are within -1.8 to +1.6 mm/yr, and no discernible ground deformation was observed within the nine reefs in the AOI.

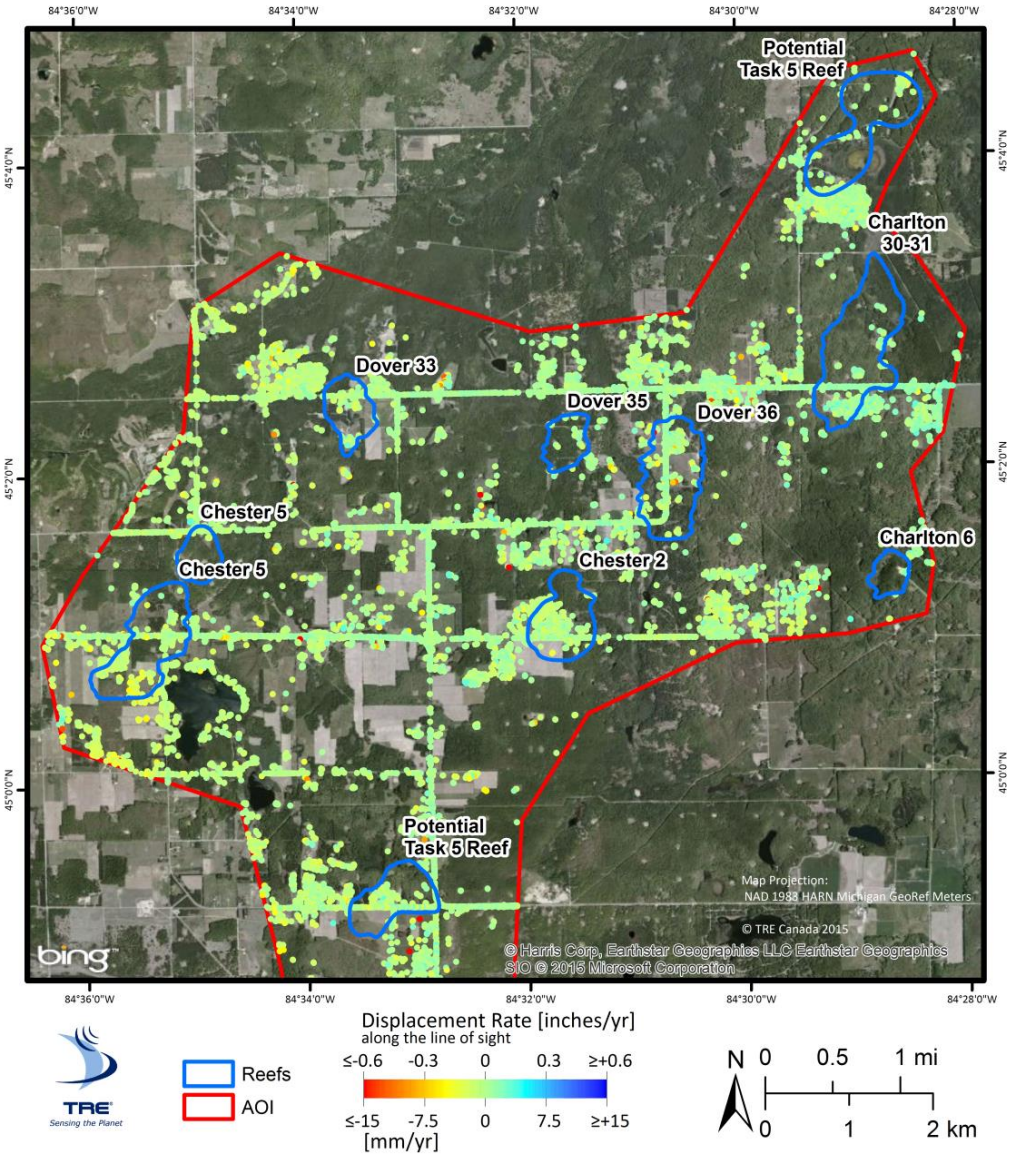

Figure 55: Surface displacement results over eight reefs located in the northern portion of the AOI.

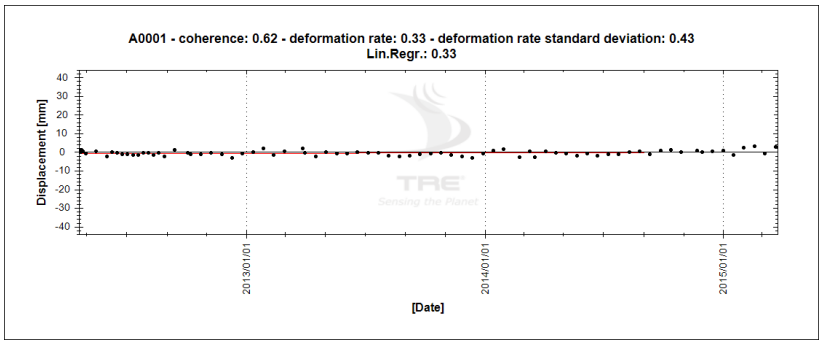

Figure 56: Average time series of all measurement points identified within the Dover 35 reef.

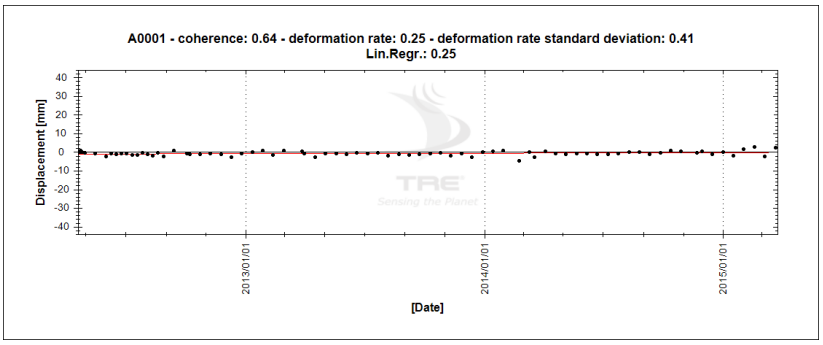

Figure 57: Average time series of all measurement points identified within the Dover 36 reef.

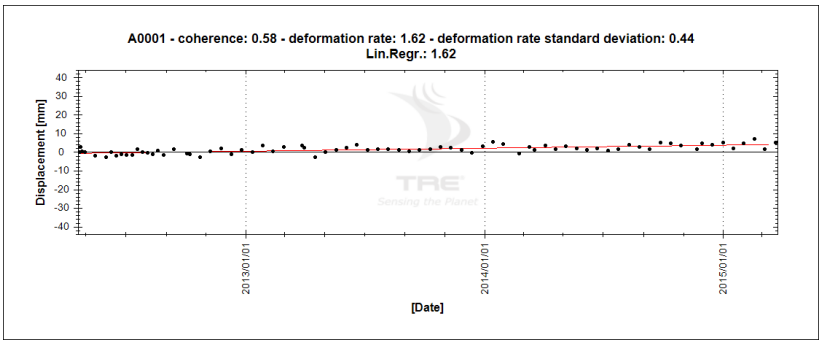

Figure 58: Average time series of all measurement points identified within the Charlton 6 reef.

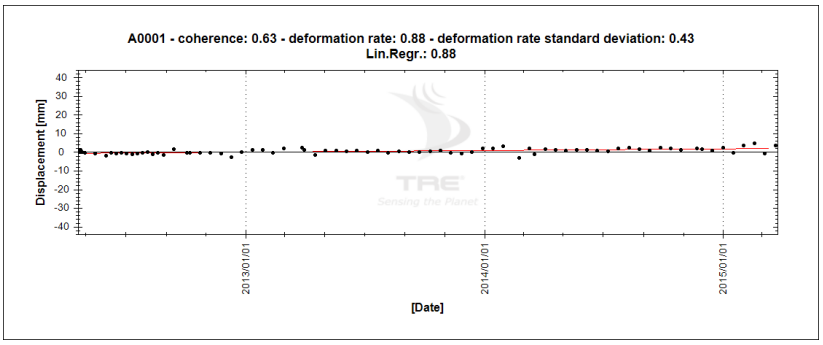

Figure 59: Average time series of all measurement points identified within the Charlton 30-31 reef.

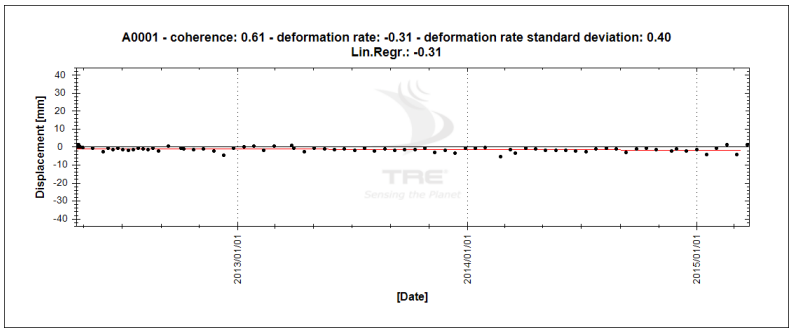

Figure 60: Average time series of all measurement points identified within the Chester 2 reef.

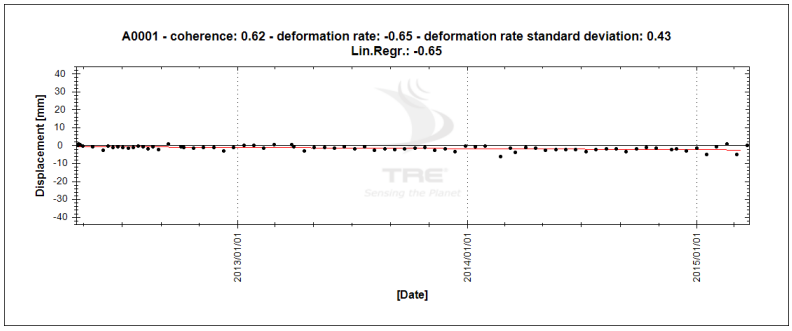

Figure 61: Average time series of all measurement points identified within the Chester 5 reef.

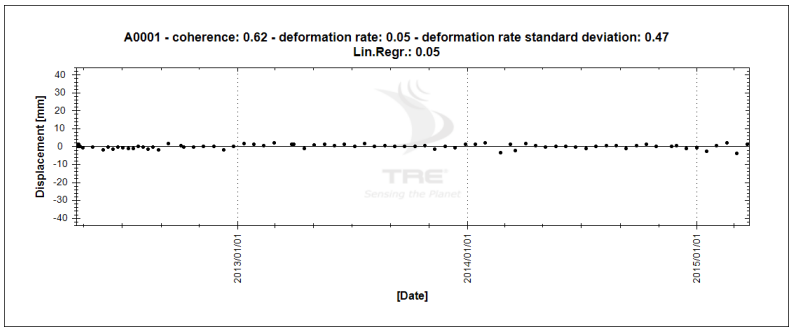

Figure 62: Average time series of all measurement points identified within the potential Task 5 reef in the northeast of Figure 55.

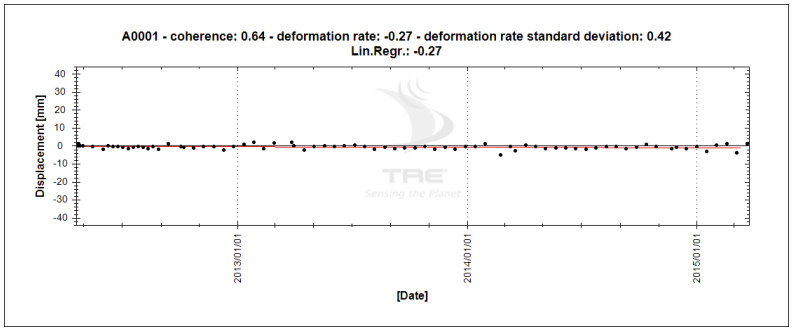

Figure 63: Average time series of all measurement points identified within the potential Task 5 reef in the south of Figure 55.

5.3 Ground Deformation over Different Well Types

Well type and location information was provided by Battelle in order to analyze any movement trends occurring in close proximity to oil and gas operations. Measurement points identified within a 150 meter (500 foot) buffer of each well were used to calculate an average displacement rate for each well (Figure 64). A summary of the results is shown in Table 6. Results were compared to a random sample of measurements taken from areas where no wells were present, as well as the average displacement value of the entire data set.

Ground deformation rates identified between April 2012 and March 2015 were within ± 2 mm/year for all different well types, random areas with no wells, and the entire AOI. No observable differences between well types were identified.

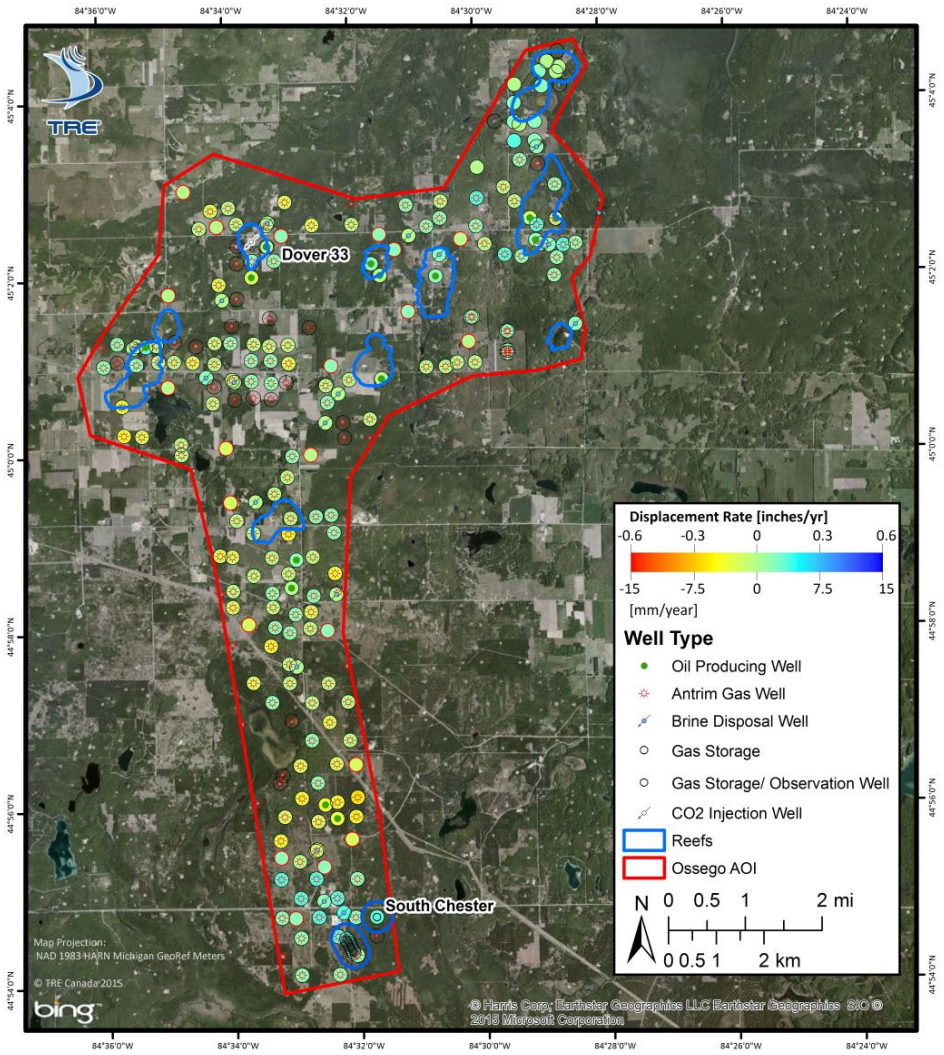

Figure 64: Surface displacement results identified within a 500 foot (150 meter) buffer around all wells included in the files provided by Battelle.

Well Type	Average Displacement Rate (mm/yr)	Standard Deviation (mm/yr)	Cumulative Deformation (mm)	Number of Samples
GS/GSO	1.3	0.5	4.9	10
Oil	-0.5	0.4	0.3	18
Gas	-0.4	0.4	0.5	146
BDW	0.01	0.4	2.0	19
Random Sample (No Wells within 150 m)	-0.3	0.4	1.1	21
All Measurement Points (PS and DS)	-0.2	0.4	1.3	22,309

Table 6: Summary of the average displacement rates identified within a 150 meter (500 foot) buffer around all wells within the AOI, a random sample of areas with no wells within 150 meter (500 foot), and the entire AOI.

5.4 Comparisons with other CCS projects

TRE has monitored ground deformation response for numerous CCS/EOR projects worldwide, including several where distinct surface deformation was observed. One well-known example is that of In Salah, in Algeria. In this case, although no ground deformation was expected, uplift was detected around the three injection wells within a month of the start of CO_2 injection and exceeded 20 mm after three years (Figure 65). The deformation around the wells had a distinct form, with the areas of uplift centered on the wells and uplift magnitude decreasing with distance from the well (Figure 66). It was also possible to correlate ground movement with the volume of CO_2 injected (Figure 67).(Ringrose et all, 2009, Vasco D. W. et al., 2010, Rucci et al., 2013).

The behaviour observed at In Salah contrasts with the lack of ground response observed at Dover 33. No deformation is identified in the area of the injection well and there is no apparent correlation with the injected CO_2 volume nor with bottomhole pressure. Although unexciting, the lack of deformation at Dover 33 is a positive development as it provides an indication that CO_2 has not strayed from the reef and that no anomalous behaviour can be observed from the surface.

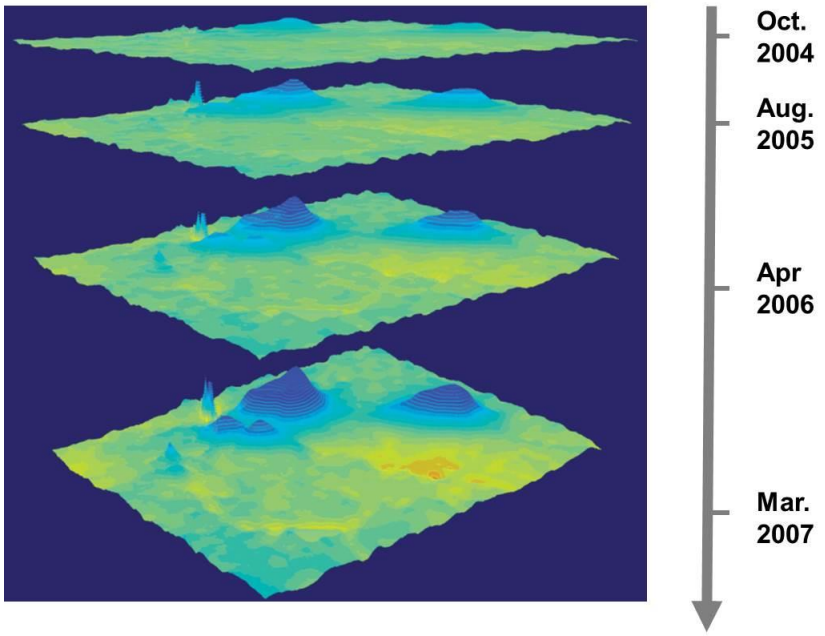

Figure 65: 3D view of measured ground deformation (with vertical exaggeration) at In Salah.

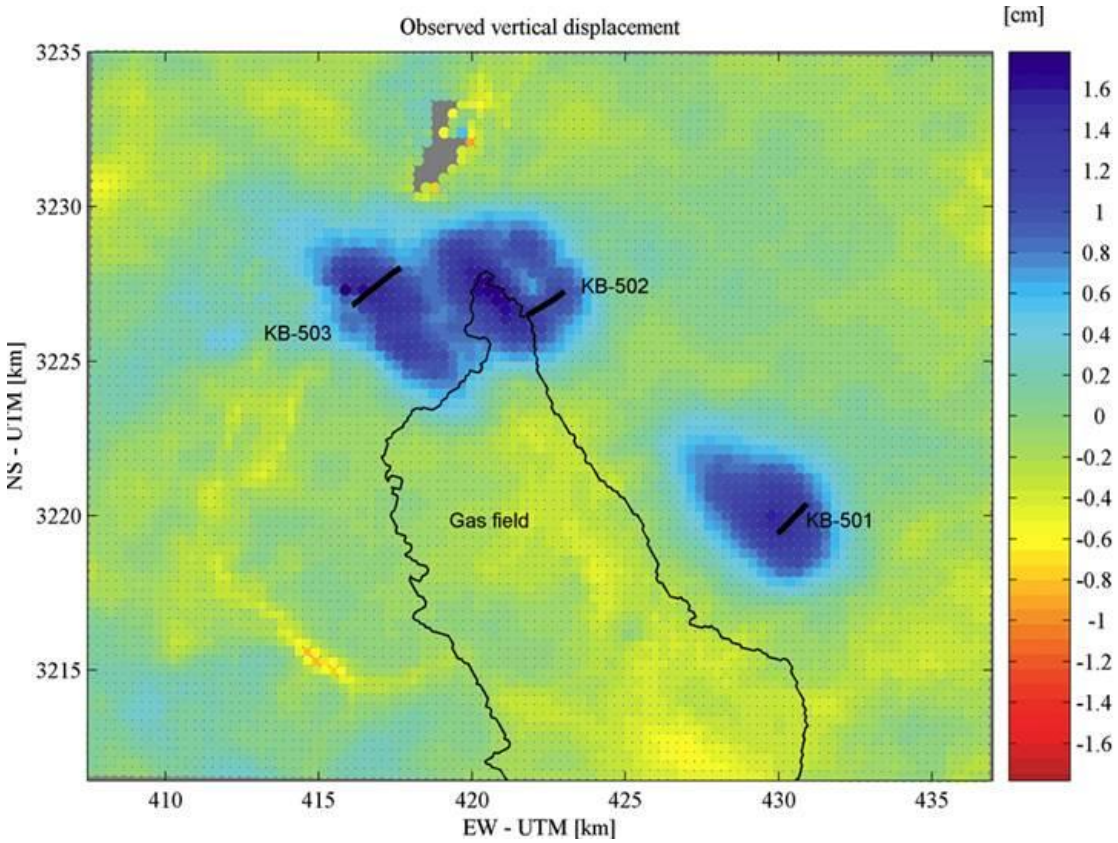

Figure 66: Surface deformation at In Salah measured between 2004-08 (from Rucci et al, 2013).

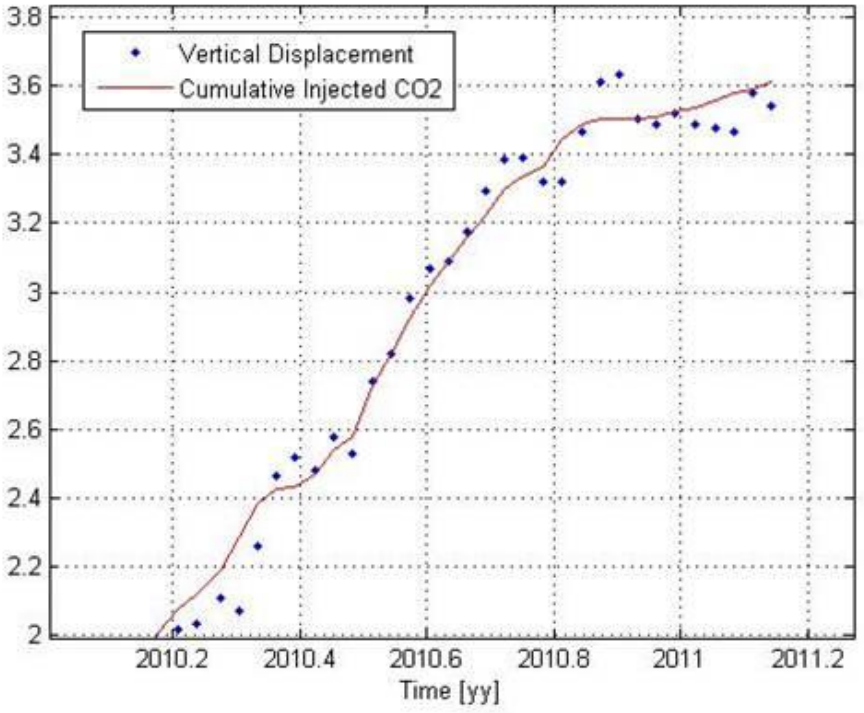

Figure 67: Correlation between the volume of injected CO_2 and ground movement at In Salah between 2010-11.

6 Summary and Recommendations

InSAR was used to monitor ground deformation over Dover 33 during CCS operations in three stages. An initial historical analysis covering 1992 to 1999 using the ERS satellite provided an overview of natural ground deformation over the AOI in the past. A second analysis consisted of baseline monitoring over a period of six months (April 2012 to October 2012) prior to the start of CO_2 injection. Further processing focused on continuous monitoring during CO_2 injection with 16-day revisit satellite data from April 2012 to March 2015.

The results of the current monitoring analysis indicate no discernible response to CO_2 injection within Dover 33, both from natural radar targets and artificial reflectors. Deformation trends remain similar those observed in the baseline results. This is confirmed both in the spatial domain (Dover 33 vs AOI) and the temporal domain (co-injection vs full processing data sets). Finally, no correlations were observed in the comparison of ground deformation against the bottomhole pressure and injected CO_2 volume.

29 Artificial Reflectors (AR) were installed to supplement the distribution of natural measurement points within and around Dover 33. The ARs exhibit average displacement values of 1.1 mm/yr within Dover 33 and 0.01 mm/yr outside the reef. However, no clear ground deformation in response to the CO_2 injection can be observed.

The signature of the ground movement observed at In Salah was contrasted with the lack of uplift observed at Dover 33. The comparison highlights the completely different behaviour of ground surface response between the two sites.

To conclude, all results collected to investigate ground deformation in relation to CO_2 injection have not shown movements in response to CCS operations. Although this is the final scheduled InSAR data processing over Dover 33, imagery is continuing to be acquired over the site until March 2016, which allows the possibility of additional processing in the future.

Along with this report, a technical appendix is included, which contains the list of delivered files, AR visibility check results and additional information regarding the InSAR processing.

7 Reference

- Ringrose P., Atbi M., Mason D., Espinassous M., Myhrer Ø., Iding M., Mathieson A., and Wright I. report on the lessons learned so far from early phase monitoring of the pioneering In Salah CO2 storage project in Algeria by joint venture partners BP, Sonatrach, and StatoilHydro which has a planned operational lifetime of more than 20 years. Plume development around well KB-502 at the In Salah CO2 storage site. *First break,* Vol. 27, Jan 2009.
- Vasco D. W., Rucci A., Ferretti F., Bissell R. C., Ringrose P. S., Mathieson A. S., Wright I. W. Satellite-based measurements of surface deformation reveal fluid flow associated with the geological storage of carbon dioxide. *Geophysical Research Letters*, Vol. 37, Feb. 2010.
- Rucci A., Vasco D. W., Novali F. Monitoring the geologic storage of carbon dioxide using multicomponent SAR interferometry. *Geophysical Journal International,* Jan 2013.

8 Delivery of Data

8.1 List of Delivered Files

The deliverables of the SqueeSAR™ analysis include the present report, the PS/DS data files and a software tool for assisting with the loading, viewing and interrogation of the data in ESRI ArcGIS 10.1. Table 7 and Table 8 list the files contained on the accompanying CD.

Data type	Description
.shp	ESRI Shapefile for displaying the database file (dbf) geospatially in a GIS environment.
.dbf	Table containing the height, velocity, velocity standard deviation, acceleration, coherence and time series of all the PS/DS identified.
.xml	An encoding document for each -TSR.shp, VERT.shp, EAST.shp file. This file contains metadata for data processing and provides information for the TRE customer toolbar application.
.mxd	An ESRI ArcGIS 10.1 project file containing the results.

Table 7: List of delivered types.

	File Name
Full Data	MICHIGAN_CSK_H404_D_T191_Mar15
Co-injection Data	MICHIGAN_CSK_H404_D_T191_POST_INJ_Mar15
AR	MICHIGAN_CSK_T191_D_AR_Mar15

Table 8: List of delivered files.

The ESRI ArcGIS 10 project file is included to make it easier to view the data. Once the data on the CD has been saved to the user's hard drive, it will be sufficient to open the project file with ArcGIS and update the links to indicate the new locations of the data.

8.2 The Structure of the Database Files

Table 9 below describes the attributes of each PS/DS within the database.

Field	Description
CODE	Unique identification code.
SHAPE	Indicates type of geometry (point).
HEIGHT (m)	Elevation above sea level of the PS.
H_STDEV (m)	Standard deviation of PS elevation value.
VEL (mm/yr)	PS movement rate. Positive values correspond to movement toward the satellite (uplift); negative values correspond to motion away from the satellite (subsidence).
V_STDEV (mm/yr)	Standard deviation of PS deformation rate.
ACC (mm/yr^2)	PS acceleration rate.
A_STDEV (mm/yr2)	Standard deviation of PS acceleration value.
COHERENCE	Quality measure [between 0 and 1].
EFF_AREA (m^2)	Size of the area belonging to the PS. For PS EFF_AREA = 0, for DS EFF_AREA > 0.
D(year/month/day) (mm)	Following the EFF_AREA column are a series of fields that contain the displacement values of successive acquisitions relative to the Master, expressed in mm.

Table 9: Description of the fields contained in the Shapefile.

8.3 TREmaps™

The SqueeSAR data are also available on TREmaps™ (Figure 68), a web-based portal accessed via a secure client login (only authorized users have access to the results) for viewing and interrogating deformation data online. The SqueeSAR data is superimposed on a Google Maps background and the individual time-series of each point can be viewed by pointing-and-clicking.

Data can be visualized on any device with an internet connection, including portable tablets. User credentials (username and password) will be provided via email.

TREmaps link: https://tremaps.treuropa.com/tremaps.

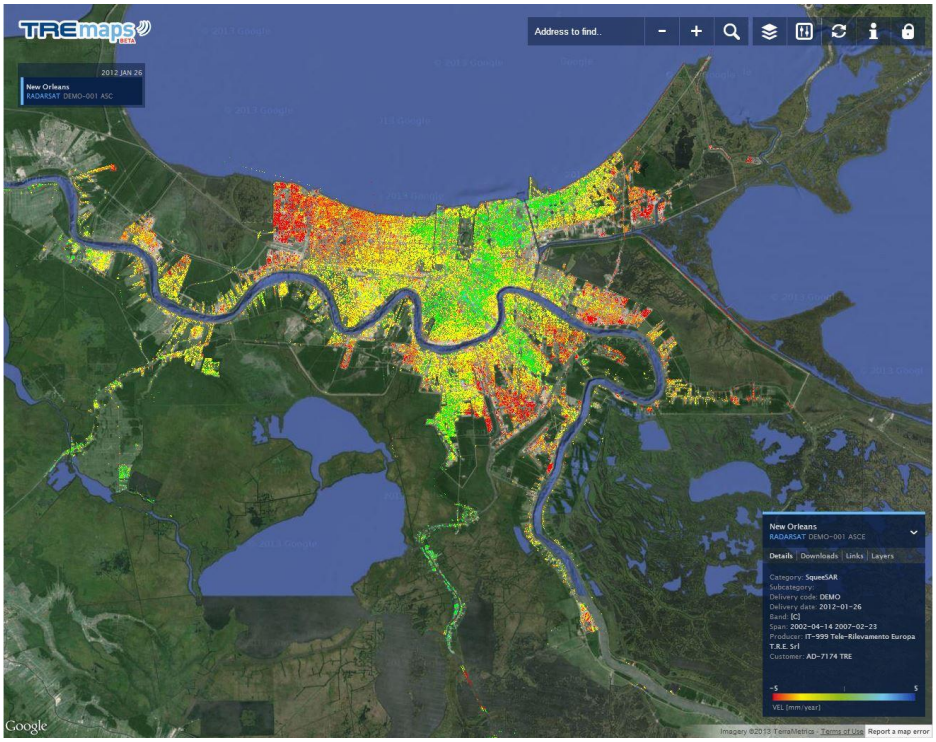

Figure 68: Example of SqueeSAR data within TREmaps.

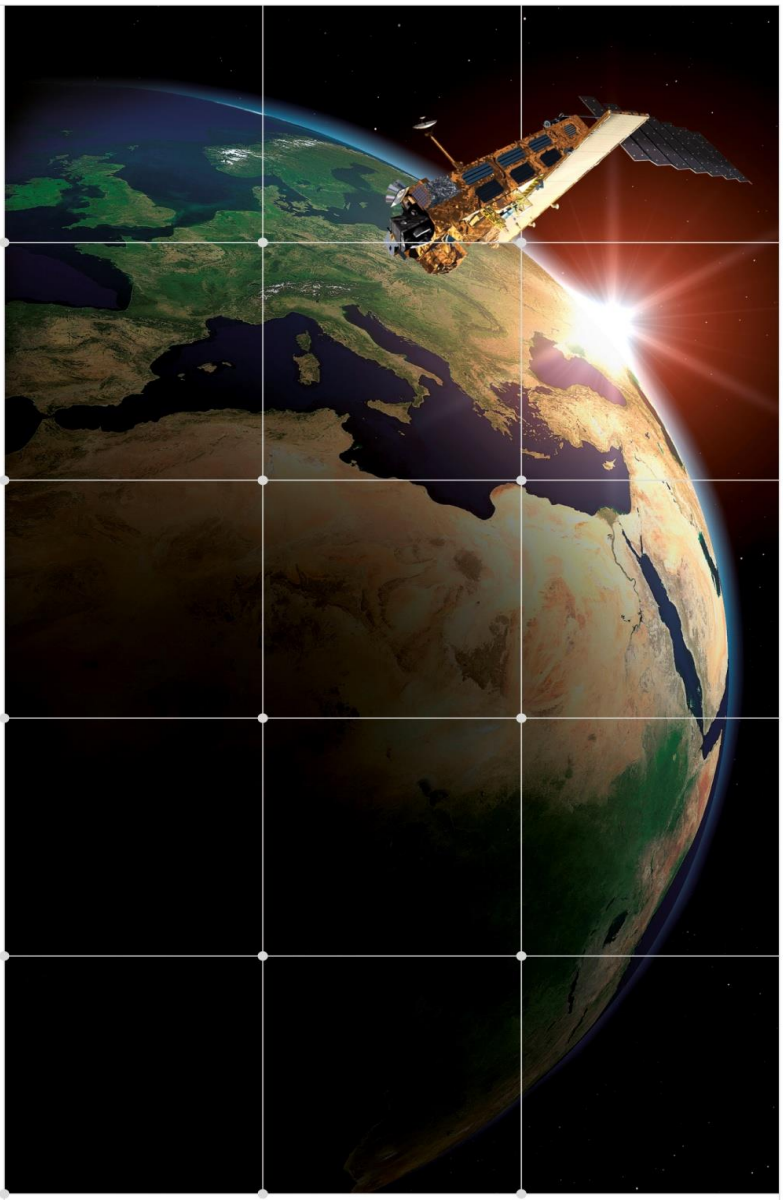

TRE®
Sensing the Planet

Tele-Rilevamento Europa T.R.E. s.r.l.
Ripa di Porta Ticinese, 79
20143 Milano - Italy
Tel. +39.02.4343.121
Fax +39.02.4343.1230

treuropa.com
tre@treuropa.com

TRE Canada Inc.
#410 - 475 West Georgia Street
Vancouver, BC V6B 4M9 - Canada
Tel. +1.604.331.2512
Fax +1.604.331.2513

trecanada.com
info@trecanada.com